Pulsed-Laser Ultrasound Generation in Fiber-Reinforced Composite Material

Mohammad Ali Rezaizadeh

Dissertation submitted to the Faculty of the
Virginia Polytechnic Institute and State University
in partial fulfillment of the requirements for the degree of

Doctor of Philosophy
in
Engineering Mechanics

John C. Duke, Jr., Chair
Kenneth L. Reifsnider
Ronald D. Kriz
Dean T. Mook
D. P. H. Hasselman

November 3, 1998
Blacksburg, Virginia

Keywords: Composite, Laser, Material, NDE, Pulsed, Ultrasound

Pulsed-Laser Ultrasound Generation in Fiber-Reinforced Composite Material

Mohammad Ali Rezaizadeh

(ABSTRACT)

A laser-based ultrasonic technique using a pulsed laser for stimulating ultrasonic waves in fiber-reinforced composite materials is the subject of investigation. For convenience, the material is chosen to be homogeneous transversely isotropic. The study is strictly limited to the laser power regimes that are suitable for nondestructive evaluation. An elastodynamic methodology is presented based on integral formulation in order to develop a representation for the dynamic responses in terms of the characteristics of the source that originated the motion. This requires a computation of elastodynamic Green function which represents the displacement field from the idealized synthetic sources localized precisely in both space and time. A two-dimensional numerical analysis utilizing a finite difference method for computation of the Green function in a finite plate is developed which provides the basis for quantitative nondestructive evaluation of fiber reinforced composite materials. Numerical results are presented for the surface displacement at the epicenter. Prediction based on numerical simulations are compared with experimental results.

ACKNOWLEGEMENTS

The academic pursuits have become my endeavor for almost a life time as I have been emotionally supported by wide circle of family, friends and colleagues.

I would sincerely like to thank Dr. Duke, my mentor, advisor and committee chairman, whose diligent encouragement, constant financial support, unwavering faith and friendship have been an important part of my existence throughout my academic pursuits at Virginia Tech.

I would also like to extend my thanks to the members of committee, Dr. Reifsnider, Dr. Kriz, Dr. Mook, and Dr. Hasselman for their willingness to serve on my committee and for spending their valuable time in reading this manuscript. To Dr. Henneke and Dr. Morris, Head and Assistant Head of the Engineering Science and Mechanics department, many thanks for giving me the opportunity to teach and financial support.

A special thanks to Dr. Mehran Elahi, my very good friend, roommate and enthusiastic running partner. I also extend my special thanks and appreciation to Ms. Linda Painter for emotional support, encouragement and being a good friend. My gratitude to Ms. Edna Danner for her gracious hospitality. To my other friends and colleagues Mr. Mike Horne, Mr. Sanjiv Parikh, Mr. Asghar Moshref-Javadi, Mr. Dara Javadi-Pourafsari, Mr. Karim Pazhoohi, Mr. Mostafa Ehtesham-Daftari, Mr. Rasoul Azimi-Abdoljabbar and Mr. Kayvan Elahi, I am grateful for their advice, suggestions and friendship.

Last but not the least, I extend my deepest thanks and appreciation to my family: my mother, Mrs. Hajyeh Rezaizadeh, my late father, Mr. Gholam Rezaizadeh, my sister and brothers, Nazereh, Mohammad Ebrahim and Mohammad Hossein. All of whom without their continuous encouragement, emotional and financial support, as well as unselfish sacrifices would not have made my life and future possible.

TABLE OF CONTENTS

LIST OF FIGURES

LIST OF TABLES

CHAPTER 1

INTRODUCTION

1.1 Motivation

In recent years, the increasing use of newly engineered materials such as fiber-reinforced composite materials and high temperature alloys in aerospace and energy-related applications has highlighted the need to nondestructively evaluate, characterize and test these material, as well as to accurately predict the fitness for service and the remaining useful life of components or structural systems. The development of reliable test methods for the nondestructive evaluation (NDE) of composite material is a challenging task. However, one technique that has shown great potential in this area is based on ultrasonics.

Ultrasonics has traditionally been a contact technique. The conventional ultrasonic technique employs piezoelectric transducers as emitters and receivers which are placed directly on the workpiece surface or else coupled through liquid couplant. The scanning operations are performed by immersion of components into various liquids to form a coupling medium between the transducers and the workpiece. However, the use of couplants is not allowed for some composite materials that can absorb or can be contaminated by these substances. In addition, it is difficult to inspect composite structures that

possess complex geometries with difficult to reach locations. The electromagnetic acoustic transducer (EMAT) does not suffer from these couplant problems. The EMAT is known as a non-contact technique where electromagnetic acoustic phenomena is used for generation and detection of ultrasound. However, the EMAT is restricted to conducting materials.

Because of the limitations of conventional ultrasonic techniques, a method of non-contact optical generation and detection of ultrasound is of great practical importance for NDE of composite materials. Recent advances in laser technology have made remote optical testing more practical and shows great promise as an NDE tool.

Pulsed-laser ultrasound generation (PLUG) together with laser-based ultrasound reception offers many advantages over conventional contact techniques. Here, the important characteristics of using PLUG as opposed to any of the other conventional ultrasound generators such as piezoelectric transducers or EMAT are summarized.

- PLUG is a completely non-contact, remote source of ultrasound where energy is transferred to the sample without couplant. This permits the generation of ultrasound on hot or rough samples and in hostile or extreme environments such as nuclear plants or outerspace that are either electrical conductors, semiconductors, or insulators.
- The laser beam can be focused to a very small spot which may be used to generate ultrasound on very small or thin samples.
- PLUG can be used for inspecting complex geometries and difficult to access areas.
- PLUG is not affected by variation of distance between sample and laser unit (i.e. the laser beam can be aimed at a sample from a great distances).
- PLUG also is not affected by laser beam angle of incidence directed on sample (i.e. the laser beam can be directed at the sample over a large range of angles of incidence).

- PLUG generates broad band ultrasonic waves.
- All types of elastic waves can be generated simultaneously or distinctly.

The ever-increasing demand for remote ultrasonic methods for nondestructive testing and material evaluation has given attention, not surprisingly, to the development of laser ultrasonic techniques which combine the physics of both laser optics and ultrasonics. The laser light serves as a heat source that raises the temperature, within the near-surface region of the sample, rapidly to just below the threshold for damage. Because of thermoelastic coupling, the heat source is transformed into an intense source of ultrasound. The ultrasound source may excite different types of elastic waves including surface and guided wavemodes, in addition to bulk longitudinal and shear wavemodes for elastic media.

Although PLUG has been carried out extensively on metallic samples, its use for composite materials is of growing interest. The majority of work on composite materials has used conventional piezoelectric sources, other sources such as PLUG are possible and can be used to perform the same type of measurements. The development of PLUG has been particularly useful in developing a new tool for NDE of composite materials.

1.2 Objectives

The objective of the study presented herein is: to develop knowledge required for mechanistic modeling of PLUG in fiber-reinforced composite materials for NDE applications; to demonstrate the feasibility of remotely generating acoustic (mechanical, ultrasonic) waves in fiber-reinforced composite material specimens by impacting its surface with a laser pulse; to theoretically simulate and characterize the laser pulse as an ultrasonic source accompanied by developing a numerical simulation to predict the ultrasonic wave propagation in the fiber-reinforced composite plates; and finally to verify

that the measured displacements are accurately described by the predicted ones.

1.3 Approach

The objectives will be addressed through a combined experimental and analytical investigation to characterize laser generated ultrasonic waves in a unidirectional fiber-reinforced graphite/epoxy composite plate. The study is limited to thermoelastic laser generation mechanisms suitable for NDE applications. Within the frequency range normally used in ultrasonic NDE, the unidirectional graphite/epoxy composite can be assumed to be linearly elastic, homogeneous, and transversely isotropic with a symmetry axis parallel to the fiber direction. The use of an ultrasonic point-source and point-receiver system is proposed to determine the characteristics of elastic waves propagating in unidirectional graphite/epoxy composite specimens with a plate geometry. For experiments, the proposed system will consist of a pulsed laser for stimulation of an ultrasonic pulse in the specimen and a piezoelectric NIST conical transducer for reception of the response from the opposite parallel side (i.e. epicenter) of the plate.

To fully explore the experimental features of laser generated ultrasound, an analytical model that predicts acoustic displacements will be developed. The analytical model will incorporate two distinct aspects, the description of the source of ultrasound, and the description of the medium response from that source. A Green's function formulation will be employed which provides a mathematical separation of these two problems.

1.4 Literature Review

The optical generation of acoustic waves by modulated sunlight was first proposed by Alexander Graham Bell [1]. The absorption of alternating heat

caused an audible signal to be emitted at the frequency of modulation. In 1960, the laser was discovered and it is probably the most important, scientifically, of all artificial light sources. The laser is a unique source of radiation and a convenient way of producing a high energy light beam over a small area. The introduction of laser sources has revolutionized experimental techniques and has led to a remarkable increase in the interest shown in the application of optical methods for generation and detection of acoustic and ultrasonic waves.

The generation of acoustic waves by a laser pulse was first suggested independently by White [2] on a solid and by Askar'yan et. al. [3] on a liquid. The former has predicted that when the surface of a body is subjected to transient heating elastic waves are produced as a result of surface motion due to thermal expansion. This process is analyzed by treating the one dimensional problem in which the heating takes place over an infinitely large area of the specimen. If the input flux is uniformly distributed there will be a temperature gradient normal to the surface. If the input flux is non-uniformly distributed there will be a temperature gradient parallel to the surface in addition to temperature gradient normal to the surface. The formation of these temperature gradients produce, as a result of thermal expansion, strains in the body and lead to the generation of stress waves which propagate into the body from the heated surface. The amplitude of the stress waves depends on the constraints at the heated surface. The stress wave amplitude for a constrained surface is much larger than that for a stress free surface. Other authors [4-7] have carried out studies along similar lines and reported the generation of stress wave by rapid thermal expansion utilizing different high power laser systems and/or modifications to the metal surface. A general feature, however, was that little distinction was made between the various wave modes likely to be generated in the solid and that the use of a high energy laser beam must have resulted in substantial damage to the specimen surface.

Henceforth, there has been a steady growth of interest in understanding the details of the generation processes involved, the distinction between the

generation of different wave modes, the elimination of surface damage, and identification of potential applications of the technique in the field of nondestructive evaluation.

Solid media are capable of supporting various modes of vibration. A sudden disturbance which produces a change in stress in a region of a solid, such as caused by laser irradiation, acts as a source of elastic stress waves which then propagate the stresses throughout the solid. Stress wave propagation in solids is more complex than in liquids. In liquids, the longitudinal acoustic mode is of interest. In elastic solids, however, bulk waves and surface waves are expected. The generation of surface (Rayleigh) waves using a Q-switched ruby laser was first demonstrated by Lee and White [8]. Later, the simultaneous generation of longitudinal, shear, and Rayleigh type surface waves in an aluminum plate using a Q-switched Nd:glass laser operating at a wavelength of 1.06 μm was reported by Ledbetter and Moulder [9].

Considerable effort has been expended in laser/material interaction studies ranging from metal scribing at low laser energy to laser fusion at very high energy. It is important to note the terms laser energy and laser energy density are used frequently by many authors either by their exact definitions or interchangeably. In order to avoid any confusion, the laser energy by itself is defined as the amount of energy the laser device supplies and its unit is denoted by units of energy. However, the energy density is defined as the amount of energy which is supplied by the laser device over the area that the beam is focused at, and the units are energy per unit area.

At moderate energy level, Calder and Wilcox [10,11] described the generation mechanism by interaction of laser energy with a metal. Several applications of noncontact testing of metal such as the measurement of two elastic constants of an isotropic material and flaw detection were explained. The principle of the mechanism is based on purely plasma blowoff where the energy density is very high raising the temperature of the irradiated site way

above the melting point of the material. The rapid deposition of energy produces rapid vaporization and ejection of the material from the small irradiated area of the surface skin of a sample. The combined effect of both strong pressure build-up by the recoil from blowoff of the vapor and the momentum transfer from the ejected material induces compressive stress pulses normal to the sample surface. These stress pulses cause the stress waves that propagate in the metal.

This mechanism of plasma blowoff by laser energy deposition actually removes some material which results in damage to the surface of the metal. The material mass removed by Q-switched Nd:glass laser deposition was measured for four samples including iron, aluminum, tantalum, and nickel by Calder and Wilcox [10,11]. The mass removed depends on many parameters including: melting and vaporization temperature, specific heat, heat of fusion, heat of vaporization, coefficient of absorption, and reflectance.

At low energy level (i.e. < 60 mJ), extensive research was conducted by several authors [12-15] to identify the generation mechanisms. Acoustic pulses can be generated in two principal regimes. The first is in the nonplasma (thermoelastic) regime, where the optical energy density is only sufficient to raise the temperature, of the small irradiated area of metal surface, below the melting point of the material. The rapid temperature rise at the irradiated site leads to a rapid expansion of the metallic substrate, producing thermal strains which results in the radiation of acoustic waves. Under such conditions, damage to the surface through laser irradiation does not occur at all. The second is in the plasma regime, where the optical energy density is high enough to raise the temperature of the small irradiated area slightly above the melting point of the material. Thermal expansion, melting, and evaporation induce parallel and normal compressive stress on the surface. Under such conditions, insignificant surface damage occurs in some cases but in most cases the surface appear colorless and slightly scorched. The important

property of the generation process is that the acoustic waves are reproducible from excitation to excitation.

Aindow et. al. [16] found that laser energies as low as 3 mJ were sufficient to produce ultrasonic pulses in various metals including aluminum, brass, and a range of steels in the nonplasma regime. The multimode Q-switched Nd:YAG laser operating at 1.06 μm, produced single shot pulses of 17 ns half width. The generated longitudinal, shear, and Rayleigh pulses were readily detected by conventional piezoelectric transducers at various frequencies within the 1-10 MHz range. A study of variation of generation efficiency with laser energy density was carried out. In the nonplasma regime, the amplitudes of the longitudinal and shear pulses were proportional to the laser energy, whereas the relationship for the Rayleigh mode was inconclusive. The shear pulse exhibited larger amplitude. In the plasma regime, enhancement of the longitudinal pulse and a decease in generation efficiency of shear pulses was observed. Rayleigh pulses exhibited a complex behavior.

Surface modification and constraint are known to greatly influence the amplitude and duration of the stress pulse induced in the sample. The experimental study by Fairand and Clauer [17] described how liquid water overlay in combination with paint coatings could be used to generate high amplitude pressure waves in solids by high and low energy levels. Gutfeld and Melcher [18] demonstrated the enhancement of the generated acoustic amplitude by the use of mechanically constrained energy absorbing surfaces. A comparison of detected acoustic signals for constrained and free surfaces showed an increase of up to 46 dB at 20 MHz. A quantitative investigation of the effect of surface modification including both a rigid constraining layer and liquid overlay on epicentral displacement waveforms was done by Dewhurst and colleagues [19]. An unfocused 9 mJ laser pulse was used to irradiate 10 mm thick aluminum disks. In all cases, the amplitude of longitudinal mode increased substantially and the shear mode did not receive any significant enhancement.

Ultrasonic source modeling and ultrasonic wave propagation theory have been studied in order to link measured surface displacement waveforms to the properties of the ultrasonic source formed by laser irradiation. The method which was presented by Scruby et. al. [20] represents the thermoelastic source as a center of expansion or dilatation at the metal surface. This is done by assuming that the absorption of energy from the incident laser pulse occurs instantaneously and uniformly throughout a volume of metal near the surface. The deposition of energy is equivalent under this model to instantaneous insertion of volume of material in the metal. The inserted volume is independent of the dimensions of the deposition volume, and depends only on the total energy absorbed. Because the irradiated volume is at the metal surface, the stress free boundary condition is imposed. Thus the point of dilatation becomes equivalent to the sudden appearance of force dipoles parallel to surface. In order to calculate the epicentral acoustic displacement at the far side of the metal specimen, it is necessary to determine the Green's function for the desired specimen. Sinclair [21] calculates the Green's functions for a generalized point multipolar source at the surface of a half space. This approach can be extended to a parallel plate, by including the effect of the second boundary. Using this approach most of the features of the measured waveforms can be predicted by modeling the thermoelastic source as the instantaneous expansion of a point volume of metal at the surface but differs primarily in not predicting the small positive pulse at the longitudinal arrival. A subtle difference is that the measured shear arrival has a greater temporal width than the calculated arrival. Rose [22] has complimented the above theoretical analysis by presenting a comprehensive treatment of the thermoelastic generation process at both constrained and free surfaces. Rose [22] modeled the appropriate point source representation of laser pulse as a Dirac delta function in time. Equations of motion predicting the resultant displacement waveforms at the epicenter of either a half space or a plate are derived following the application of rigorous boundary conditions. A formal

solution for the double transform of the displacement potentials is obtained for the source lying within the surface. The Cagniard-de Hoop technique is used to invert these double transforms. To compare the absolute value of the displacement steps measured experimentally with the theoretical prediction, it is found that there exists good agreement between theory and experiment for the thermoelastic source if the pulse like precursor in the longitudinal arrival is not considered. Wadley et. al. [23] used a capacitance transducer to measure about half the epicentral waveform and generally found excellent agreement. The exception was the appearance at the first arrival of a small positive pulse like spike in the longitudinal arrival. Dewhurst et. al. [19] indicated that this discrepancy with the experiment in not producing the positive pulse at the longitudinal arrival can be accounted for by including thermal diffusion and the finite size of source and detector in the calculation. Doyle [24] has also addressed this problem, and has found the same conclusions. However, they did not give any details of the method by which thermal diffusion was incorporated theoretically.

It might be expected that when the optical energy density is increased to form a plasma at the free metal surface, normal forces or normal force distributions would tend to increasingly dominate the acoustic source, which would also contain horizontal forces from thermal expansion. To test this hypothesis, Dewhurst et. al. [19] formulated a theoretical simulation in which the source is modeled as a combination of these forces. The epicentral waveforms were calculated by adding together the epicenter displacements that would have resulted from each source type taken separately. Good agreement with experiment can be obtained, provided the time dependence of the ablative force is allowed to vary. It was necessary to use a short force pulse to obtain a good fit with the experimental data at lower power densities, implying that the plasma did not persist much after the optical pulse had finished. However, just the opposite occurred at relatively high power densities where the force pulse in the model had to be progressively lengthened to fit experiment, implying

that ablation persists for a long time after the end of the incident optical pulse. The increase in power density drastically reduced the expansion component until it was too small to be measured. This decrease in dilatation must mean that, an increasing proportion of the absorbed optical energy is being used to vaporize metal and generate plasma. The variation of normal force, at first increasing rapidly and then decreasing made the interpretation difficult. These effects were thought to be due to shielding of the metal surface from the optical pulse by the plasma, which is extremely rapidly established. Further theoretical study by Aussel et. al. [25] has shown that the pulse shape varies as a function of the density of incident power under ablation conditions. These studies in the plasma regime appeared to confirm the hypothesis made from experimental observation and to show good agreement of experimental and theoretical epicentral waveforms.

Application of laser ultrasonics has received considerable attention in the field of nondestructive testing of structures. Keck and Mommertz [26] discuss the use of laser for both generation and detection of ultrasound to measure the wave velocity on a steel plate heated up to 900^{o}C in a furnace, to find flaws on the plate and to measure a tube wall thickness. Bar-Cohen [27] presented ultrasonic testing of microwelds in which the ultrasonic source is generated by a pulsed laser. Microwelds are minute welds used for the welding of thin sheet materials where conventional ultrasonic techniques using piezoelectric transducers do not provide the required pulse duration and the required beam cross section.

Calder and Wilcox [28,29] developed a simple experimental arrangement for accurate measurement of the elastic constants of eleven materials by laser energy deposition. These materials are: 1100 aluminum, 6061 aluminum, 304 stainless steel, copper, 1018 steel, brass, phenolic, canvas, nylon, tantalum, tungsten. Each material formed into rod or bar has been subjected to laser deposition, and its elastic constants is found by the measurement of the

velocities of the stress waves generated. The measured constants were in close agreement with published values.

Aharoni et. al. [30] introduced a laser induction and detection technique to measure the surface acoustic waves time of flight on rough surfaces. This noncontact technique was implemented to alleviate the uncertain nature of the contact between the conventional mechanical transducer and the rough test surface and to improve on the time of flight resolution on such materials. Jen et. al. [31] used laser ultrasonic to characterization of piezoelectric ceramics at various fabrication stages. A Nd:YAG laser, producing 15 ns, 0.5 J pulses, is focused through a lens of conical cross section on the surface of the material to be inspected where it produces an annular section. The surface acoustic waves is produced by thermoelastic stresses. The waves converging toward the center of the annulus is detected by an He-Ne laser Michelson interferometer with a probing beam focused on the center of the annular. By measuring the time of flight of the surface pulse, the surface wave velocity in the PZT is obtained.

In recent years the combination of laser generation with reception is given more attention for application to flaw and delamination detection and materials characterization of composite material structures. McKie and Addison, Jr. [32] have developed a laser ultrasonic C-scanning system for nondestructively inspecting metallic and composite structures for defects. Short duration pulses from a Q-switched Nd:YAG laser with wavelength 1.06 mm incident on the test specimen generates ultrasonic pulses which propagate through the specimen. A continuous wave (CW) Argon-Ion laser interferometer is used to probe either the same or the opposite side of the specimen to receive the signal. Laser C-scan was conducted on i) an aluminum plate containing a number of artificially drilled holes and ii) a graphite/epoxy panel which was manufactured to have a simulated delamination. The received C-scan images displays the location of flaws in the metallic specimen and the size and shape of the delamination in composite panel. However, the signal to noise ratio and

hence resolution of these images are poor. Cielo [33] and Cielo et. al. [34] discussed a point by point scanning technique for detection of disbond in layered materials. A pulsed, Nd:YAG, laser is focused on the surface of an aluminum to aluminum, aluminum to honeycomb adhesively bonded laminate, or a metallurgically coated substrate. If the layer is locally disbonded, the incident beam sets up the thermoelastic stresses in the heated region of first layer and eventually leads to local thermal buckling. The surface displacement is monitored with laser interferometer and delamination can be found quickly. The essential feature of this technique is the possibility of thermally loading a surface area smaller than the unbond diameter. This provides a lifting mechanism which could not be obtained with holographic techniques.

The use of optical fibers in laser ultrasonics is reported by several authors which provides the basis for a safe and portable laser-based ultrasonic inspection system. Sarrafzadeh et. al. [35] who directed the laser beam to the sample surface by fiber optic cables. The laser beam was focused by a lens into the multimode multifiber optical guide for generation and single mode fiber is used for the interferometric detection laser. A four foot railroad beam containing several large surface defects was inspected. The presence and absence of flaws were identified successfully by scanning the surface. Burger et. al. [36] is also among those authors who transmitted the laser beam through optical fibers to the sample surface for excitation and detection of ultrasound.

CHAPTER 2

LASER-SOLID INTERACTION

2.1 Introduction

Laser radiation from the ultraviolet to the infrared interacts primarily with the electrons of an atom or molecule, and sometimes with a particular set of atomic vibrations. Furthermore, we also know that the frequencies and energies associated with this reasonably extensive band of electromagnetic radiation do not induce nuclear disturbances or even affect the energy levels of the inner core electrons of an atom. These photons do however readily interact with the outer bound or free valence electrons of the atom. Clearly then the optical properties of any material will be mainly affected by the nature of its outermost electrons and consequently we can generally predict typical optical characteristics of most materials by knowing their electronic configurations and/or their present state. Moreover, the behavior of the optically excited system after absorbing the laser radiation will also depend on the atomic arrangement as well as the nature of any other nearby species [37].

Laser-beam interactions with materials can be based on several fundamentally different microscopic mechanisms. In the following we shall classify reactions into those which are governed by mainly photothermal or photochemical processes [38-42].

2.2 Photothermal Process

In the photothermal process, the laser serves as a heat source and gives rise to temperature within the surface of the solid material. For irradiation of solids by laser frequencies corresponding to energies less than chemical bond strengths, it is obvious that one photon is incapable of directly forcing the atoms to undergo an electronic transition such that a bond is broken. Thus, it seems plausible that the photon energy excites vibrations within the molecules. This is basically a heating process. Photothermal process can be based on vibrational modes of the atom, which are located in the infrared spectral region [38-42].

2.3 Photochemical Process

The photochemical process is initiated by direct photonic stimulation of a particular bond, after which a reaction will occur either as a result of the disruption of the bond or simply as a consequence of the atom being in an excited state. Thus, photochemical bond breaking can be based on dissociative electronic excitations with frequencies that are in the ultraviolet spectral region [38-42].

2.4 Absorption of Laser Light

Laser light in order to cause any lasting effect on a solid must first be absorbed. Absorption very often turns out to be the most critical and involved step in laser-solid interaction.

The light emitted by a laser is electromagnetic radiation. The term electromagnetic radiation includes a continuous range of many different types of radiation whose wavelength may be in the infrared, visible, or ultraviolet

part of the electromagnetic spectrum. Electromagnetic radiation has a wave nature. The waves can be characterized by their frequency. The physical nature of the different types of electromagnetic radiation is the same. In all portions of the spectrum it has the same velocity, c, and the same electromagnetic nature. The different regions of the spectrum are characterized by different ranges of the frequency of oscillation of the wave. There is a relation between the frequency f and wavelength λ valid for all types of electromagnetic radiation,

$$f\lambda = c \tag{2.1}$$

All electromagnetic waves consists of time varying electric and magnetic fields that propagates through any medium at a high velocity which is known as the speed of light, c. The speed of light depends on the medium through which it travels and may be related to the speed of light obtained in a vacuum, c_o, by the formula

$$c = \frac{c_o}{n} \tag{2.2}$$

where n is known as the refractive index of the medium and $c_o = 2.998 \times 10^8$ m/s, is the speed of light in free space. By definition, the refractive index of a vacuum is n=1. Electromagnetic waves travel considerably slower through electrical nonconductors and they hardly penetrate into electrical conductors. When an electromagnetic wave strikes the surface of a solid, the wave may be reflected partially or totally, and any nonreflected part will be absorbed into the solid.

The concept of an energy level is an important idea for absorption of laser radiation in solids. The electron in a given orbit possesses a definite value of energy. The different energy values that an atom can have by virtue of the electron residing in the different quantized orbits are the energy levels of the atom. When radiation interacts with matter, it involves a change from one energy level to another. In a condensed material, solid, the atoms are packed together and the interaction become strong. The energy levels of the individual

atoms broaden and merge into a nearly continuous band, consisting of a large number of closely spaced energy levels. This is the origin of the familiar conduction and valence band electrons in a conductor and semiconductor. Electromagnetic radiation causes electric currents to flow in the conduction band electrons. Some of the energy may be absorbed by resistive losses while the remainder is reflected [43,44].

Absorption of laser radiation by solids is a strong function of wavelength. In the infrared range, absorption arises only from vibrational modes of the crystal lattice or in organic solids by intermolecular vibrations. In this study we shall restrict our attention to laser operating in the infrared region of electromagnetic spectrum where the photothermal process is our concern.

The energy of incident laser radiation on a surface of a non-reflecting, absorbing solid is progressively attenuated as it penetrates into the solid. The well-known exponential form of absorption for normal incidence [43,45] is given by

$$E_a = E_i \, e^{-\gamma z} \tag{2.3}$$

where E_a is absorbed energy, E_i is incident energy, γ is the absorption coefficient. The absorption coefficient γ is a function of k, the light wave damping coefficient, and λ, the optical wavelength, via $\gamma = 4\pi k/\lambda$.

When the radiation impinges from the laser beam onto the plane surface of a finite conducting solid, a part of the electromagnetic wave will penetrate and be absorbed into the solid and the remaining energy will reflect back from the surface. Thus, if the total incident energy is denoted by, E_i, then

$$E_i = E_a + E_r \tag{2.4}$$

and the reflectivity, R,

$$R = \frac{E_r}{E_i} \tag{2.5}$$

where E_a and E_r are the absorbed and reflected energies, respectively [15].

2.5 Depth of Penetration

When electromagnetic radiation from laser light interacts with the surface of a conductor, the combination of electric and magnetic field will affect the distribution of alternating current inside a sample. This causes electric currents to flow in the conduction band electrons near the surface of the sample. These conduction band electrons near the surface shield the interior of the sample from the radiation. The shielding is such that most of the absorption and reflection taken place very close to the surface within what is called the "skin depth" and generally denoted by δ. The penetration and absorption of an electromagnetic field into a solid is attenuated exponentially [45].

In the infrared region of the electromagnetic spectrum, the skin depth can be defined for a conductor as

$$\delta = \frac{1}{\sqrt{\pi f \sigma \mu}} \tag{2.6}$$

where f is the frequency of incident radiation, σ is the electrical conductivity of solid, and μ is the magnetic permeability. This formula is not valid in the visible and ultraviolet region where a quantum mechanical calculation must be made. It is convenient to express the permeability of the solid normalized with respect to the permeability of free space. This is

$$\mu_r = \frac{\mu}{\mu_o} \tag{2.7}$$

where μ_r is the relative permeability and $\mu_o \cong 4\pi \times 10^{-7}$ H/m (henry per meter) is the permeability of free space.

However an "equivalent skin depth" can be defined for a semiconductor in the infrared region of electromagnetic spectrum. This is

$$\delta = \frac{\sigma}{2}\sqrt{\frac{\mu}{\varepsilon}} \tag{2.8}$$

where σ is electrical conductivity, μ and ε are permeability and permittivity respectively. For convenience permittivity of the solid is normalized with respect to permittivity of free space,

$$\varepsilon_r = \frac{\varepsilon}{\varepsilon_o} \tag{2.9}$$

where ε_r is relative permittivity, and $\varepsilon_o \cong 10^{-9}/36\pi$ F/m (farad per meter) is the free space permittivity.

The difference between the equivalent skin depth in a semiconductor and skin depth in a conductor is that in the case of a semiconductor, the wave undergoes few cycles of oscillation in a distance of equivalent skin depth, whereas in the case of a conductor, the wave had completed only one-sixth of a cycle in a skin depth [45].

Using classical electromagnetic theory [46], the reflectivity, R, and absorbed energy, E_a can be expressed in terms of the skin depth, δ,

$$R = \frac{1+(\zeta-1)^2}{1+(\zeta+1)^2} \tag{2.10}$$

where

$$\zeta = \mu_o \sigma c \delta \tag{2.11}$$

Thus the absorbed energy, E_a, is given in terms of skin depth, δ, by

$$E_a = \frac{4\zeta}{1+(\zeta+1)^2} E_i \tag{2.12}$$

where E_i is the total incident energy.

2.6 Mechanism of PLUG in Solid

From the discussions above, it will be seen that electromagnetic radiation from the laser beam with wave length in the infrared region of the electromagnetic spectrum is absorbed in the surface of a sample, causing localize heating. The absorption of electromagnetic radiation and subsequent

heating of the irradiated region can be thought of as a secondary source of energy inside but very close to the surface of the sample. Although driven by the incident laser beam issued by the laser device, it tends to develop its own physical characteristics. Of course, it is this secondary source which determines what happens to the irradiated site and what causes the ultrasonic wave to be generated.

Ultrasonic waves can be generated by a number of different mechanisms depending upon the energy density of the incident laser beam. These mechanisms are categorized as pure thermoelastic effect and ablation/plasma formation. It should be noted that each mechanism may occur independent of one another or both may be present simultaneously. In addition, the effect of radiation pressure is also present in both cases.

Radiation pressure is generated as the laser beam is incident on the sample surface. If we think of radiative energy as photons or massless particles carrying an energy and traveling at the speed of light into a certain direction, then these particles should carry momentum in the amount of energy per speed [15]. Therefore, if photons hit a solid surface a momentum transfer takes place which implies that a stream of photons exerts pressure on the surface. For a laser pulse of incident energy E_i, the radiation pressure is given by

$$p = \frac{(1+R)}{c\,A\,\delta_t} E_i \qquad (2.13)$$

where R is the reflectivity, c is the speed of light, A is the irradiated area, and δ_t is the pulse duration [15].

It is convenient to neglect the effect of radiation pressure for PLUG. Because if an Nd:YAG pulse-laser with characteristics of about 1 mJ energy and 20 ns pulse duration, is being focused to an incident area of about 3 mm^2, it will generate the radiation pressure in the amount of about 100 Pa which subsequently leads to the resulting force of about $3x10^{-4}$ N in magnitude normal to irradiated area in aluminum sample. In graphite/epoxy sample the radiation pressure and the resulting force are about 66 Pa and $2x10^{-4}$ N,

respectively. In comparison the resulting forces from the radiation pressure on the sample surface are generally much smaller than those due to thermoelastic effect.

We now briefly discuss the effect of high and intermediate laser energy densities. The latter mechanism, ablation/plasma formation, occurs at high laser energies. These high energy densities can be reached either by increasing the energy per pulse or by focusing a constant energy onto a smaller surface area using a converging lens. The surface of the irradiated area becomes superheated instantaneously above the boiling point of the material cause a change in phase to occur. Melting and evaporation, or ablation and plasma formation, will result in the removal of material from the sample surface. For the purpose of ultrasonic generation, momentum transfer from the ablating and subsequent ejected material produces an impulsive recoil force normal to the surface as shown schematically in Figure 2.1. It is also interesting to note that at intermediate energy densities simultaneously occurrence of both ablation/plasma formation and thermoelastic effect results. However, both high and intermediate laser energy densities produce substantial damage to the surface of the sample which is not suitable for the field of nondestructive evaluation and testing and they are not of interest to us for more discussion.

Therefore, attention is restricted to the purely thermoelastic generation mechanism at low laser energy densities only. It is this mechanism that produces no damage and is most likely to be suitable for NDE application.

2.7 Thermoelastic Generation Mechanism

For low energy densities, the rapid deposition of energy onto the surface of a sample causes localize heating of a small volume very close to the surface within the skin depth. The sudden rise in temperature of the irradiated volumetric region must be accomplished by rapid thermal expansion in all

directions. This thermal expansion introduces the following orthogonal thermoelastic strains locally:

$$\begin{aligned} \varepsilon_1 &= \alpha_1 \Delta T \\ \varepsilon_2 &= \alpha_2 \Delta T \\ \varepsilon_3 &= \alpha_3 \Delta T \end{aligned} \tag{2.14}$$

where α_1, α_2, and α_3 are the linear coefficients of thermal expansion in 1, 2 and 3 directions respectively and ΔT denotes temperature rise. The heated material wants to expand but is restrained initially by the bulk of material, setting up localized stresses. At a free unconstrained surface of the sample there exist no restraint so that the material is free to expand. Therefore no stress is produced normal to the surface. However, the principal stresses caused by thermal expansion act laterally in the plane of the surface causing lateral force distributions. Indeed these lateral force distributions may be approximated by two orthogonal force dipoles to simulate the thermoelastic source as shown schematically in Figure 2.2.

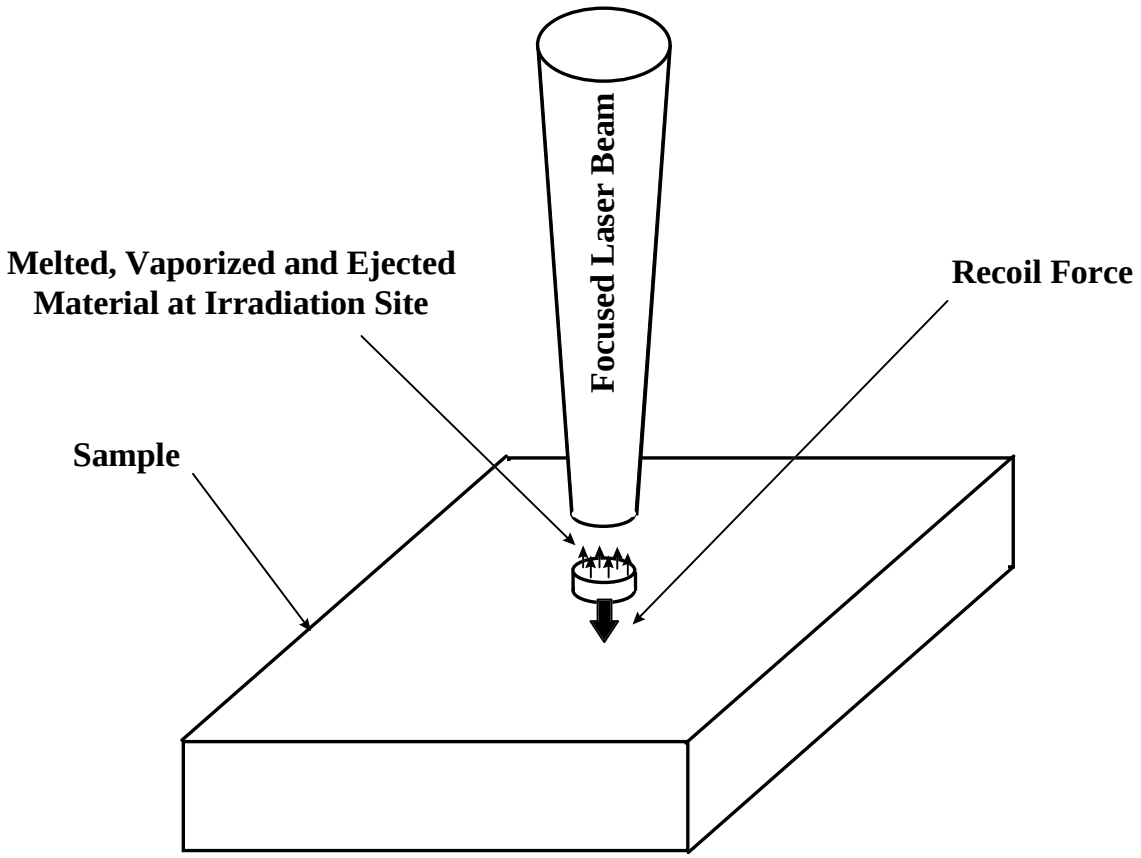

Figure 2.1. Schematic diagram of the PLUG source, mechanism of ablation/plasma formation at high energy density.

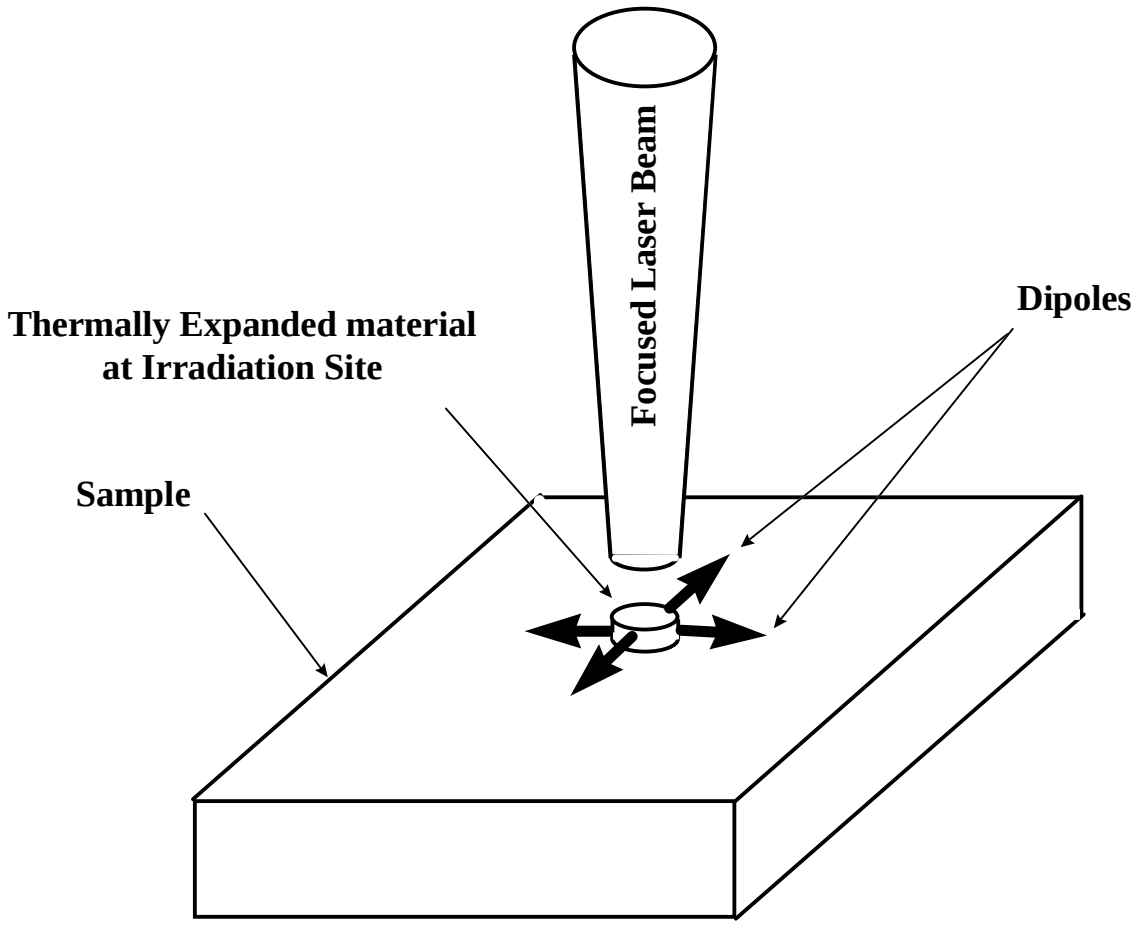

Figure 2.2. Schematic diagram of the PLUG source, mechanism of thermoelastic at low energy density.

CHAPTER 3

THE ELASTODYNAMIC MODEL

3.1 Introduction

An analytical framework for studying PLUG in solids must incorporate the following three components: a description of pulsed-laser ultrasonic source excitation, equations for the acoustic motion that can propagate once acoustic motion has been initiated and a theory coupling the pulsed-laser ultrasonic source description into the particular solution sought for the equations of motion. Nondestructive acoustic techniques are largely an observation, an interpretation and an identification of information between two points of a medium. For this reason we need to know what information about the motion at one point of a medium is sufficient to determine uniquely the motion that may be observed at another point. This may be accomplished by the development of a representation for the displacement in terms of the quantities that originated the motion.

In the early part of this chapter we shall begin with basic equations in linear dynamic elasticity in three dimensional anisotropic media, introduce the discussion of uniqueness and the concept of dynamic reciprocity [47]. The dynamic reciprocity relation for elastic waves offers a simplified means of computing the radiation of body waves from various forms of sources and

disturbances. Then we extend the discussion to the elastodynamic Green function where it can be used together with dynamic reciprocity relation to obtain a representation for displacement. This shall be accomplished by the representation theorem [48-51]. Later a complete description and formulation of the laser source as a point thermo-mechanical disturbance is given. Finally the corresponding structural responses will be computed numerically by employing a finite difference numerical method.

3.2 Equations of Motion

Suppose a linear elastic body occupies a volume, V, in space bounded by a boundary, S. If $u_i = u_i(\underline{x}, t)$ denote the displacement at point $\underline{x} = (x_1, x_2, x_3)$ and time t, then the system of equations governing the motion of a homogeneous linear elastic body with body force f_i consist of the equations of motion, constitutive equations, the strain-displacement relations, and stress vector/traction:

$$\sigma_{ij,j} + f_i = \rho \ddot{u}_i \tag{3.1}$$

$$\sigma_{ij} = C_{ijkl}\varepsilon_{kl} \tag{3.2}$$

$$\varepsilon_{ij} = \frac{1}{2}\left(u_{i,j} + u_{j,i}\right) \tag{3.3}$$

$$\sigma_i = \sigma_{ji}\, n_j \tag{3.4}$$

where C_{ijkl} is the elasticity stiffness tensor and n_j is the outward unit normal to surface S.

3.3 Uniqueness Theorem

Consider a linear elastic body, with volume, V, and boundary, S, of either finite or infinite extend that is subjected to body force $f_i = f_i(\underline{x})$ throughout V. The displacement $u_i = u_i(\underline{x}, t)$ is uniquely determined by the initial conditions (i.e. the initial values of displacement and particle velocity

at time t = 0) provided that the suitable boundary conditions (i.e. the displacement $u_i(\underline{x}, t)$, or the stress vector $\sigma_i(\underline{n})$, or a linear combination of the two) is specified over boundary S. The proof of uniqueness is based on energy considerations [47].

3.4 Reciprocal Theorem

Suppose that $u_i = u_i(\underline{x}, t)$ is the displacement at one point due to a body force $f_i = f_i(\underline{x}, t)$ applied at another point of the elastic body and initial conditions at time t = 0 and boundary conditions on S. Let the $\sigma_i = \sigma_i(\underline{u}, \underline{n})$ be the stress vector due to the displacement u_i where $\underline{n}$ is the unit vector normal to the boundary S. Then suppose $g_i = g_i(\underline{x}, t)$ is another body force parallel to u_i and applied at the same point u_i was measured, and $v_i = v_i(\underline{x}, t)$ is the corresponding displacement at the point of application of f_i. Similarly let $\sigma_i = \sigma_i(\underline{v}, \underline{n})$ be the stress vector due to displacement v_i. In general the initial conditions at t = 0 and boundary conditions for v_i are different from the condition for u_i. The reciprocal theorem states that v_i will be parallel to f_i. Thus f_i and u_i are interchangable. In physical term this means if a linear elastic body is subjected to two different sets of forces, the work done by the first system of forces in moving through the displacements produced by the second system of forces is equal to the work done by the second system of forces in moving through the displacements produced by the first system of forces.

The mathematical form of reciprocal relationship between a pair of displacements and a pair of forces through a 3-D linear elastic body without involvement of any initial conditions is given by Betti's reciprocity theorem [48].

$$\begin{aligned} &\iiint_V v_i(f_i - \rho\ddot{u}_i)\, dV + \iint_S v_i\sigma_i(\underline{u}, \underline{n})\, dS \\ &= \iiint_V u_i(g_i - \rho\ddot{v}_i)\, dV + \iint_S u_i\sigma_i(\underline{v}, \underline{n})\, dS \end{aligned} \tag{3.5}$$

Furthermore, equation (3.5) holds even if the quantities u_i and v_i are expressed at different time. Let the quantities u_i and f_i be expressed at time $t_1 = t$ and the quantities v_i and g_i be expressed at a different time $t_2 = \tau - t$. Then by integrating equation (3.5) over all time and prescribing an undisturbed initial state of rest, the acceleration terms combine on integration by parts reduces to terms depending only on the initial and final values where the convolution

$$\iiint_V dV \int_{-\infty}^{\infty} \rho\left\{\ddot{u}_i(\underline{x}, t)\, v_i(\underline{x}, \tau - t) - u_i(\underline{x}, t)\, \ddot{v}_i(\underline{x}, \tau - t)\right\} dt = 0 \tag{3.6}$$

is zero. This leads to the following

$$\begin{aligned} &\int_{-\infty}^{\infty} dt \iiint_V \left\{u_i(\underline{x}, t) g_i(\underline{x}, \tau - t) - v_i(\underline{x}, \tau - t)\, f_i(\underline{x}, t)\right\} dV \\ &= \int_{-\infty}^{\infty} dt \iint_S \left\{v_i(\underline{x}, \tau - t)\sigma_i(\underline{u}, \underline{n}) - u_i(\underline{x}, t)\sigma_i(\underline{v}, \underline{n})\right\} dS \end{aligned} \tag{3.7}$$

which is the modified form of Betti's reciprocity theorem [48] for displacement with quiescent past.

3.5 The Green's Function Approach

Green's function is an advanced technique for solving differential equations that are more complicated and/or for developing approximate solutions to the problems for which no exact solution may be obtained. If it is applied to simple problems, it will merely provide an alternate procedure for recovering results. The technique uses the notion of superposition of solutions. This means, the solution of problem involving complicated sources can be expressed in terms of a superposition of solutions of a problem due to collection of highly localized sources. The Dirac delta function (δ-function) is a mathematical artifice for representing these highly localized sources in both space and time. In essence the physical significance of Green's functions can be interpreted as the response of a system to a unit impulsive input and its elastodynamic counterpart is defined as the elastodynamic Green's function

which is the elastic response to an impulsive point force of unit strength [50,51].

In elastodynamics both force and displacement are vectors. Therefore the elastic response which relates them will be a higher order tensor. If a unit impulsive force is applied in the n-direction at the point $\underline{\varsigma} = (\varsigma_1, \varsigma_2, \varsigma_3)$ and time τ, then the elastic response will be denoted by $G_{in}(\underline{x}, t; \underline{\varsigma}, \tau)$ as the i-th component of displacement at point $\underline{x} = (x_1, x_2, x_3)$ and time t. The elastic response, $G_{in}(\underline{x}, t; \underline{\varsigma}, \tau)$, depends on both source and receiver coordinates, $\underline{\varsigma}$ and $\underline{x}$ respectively, and satisfies the equation of motion throughout volume V, [48]

$$\rho \frac{\partial^2}{\partial t^2} G_{in}(\underline{x}, t; \underline{\varsigma}, \tau) = \delta(\underline{x} - \underline{\varsigma})\, \delta(t - \tau)\, \delta_{in} + \frac{\partial}{\partial x_j}\left(C_{ijkl} \frac{\partial}{x_l} G_{kn}(\underline{x}, t; \underline{\varsigma}, \tau) \right) \tag{3.8}$$

and initial conditions:

$$G_{in}(\underline{x}, t; \underline{\varsigma}, \tau) = \frac{\partial}{\partial t} G_{in}(\underline{x}, t; \underline{\varsigma}, \tau) = 0 \quad \text{if } t \le \tau \text{ and } \underline{x} \ne \underline{\varsigma} \tag{3.9}$$

and homogeneous boundary conditions on the boundary S are given by either S as a rigid boundary where the displacement is zero, i.e.

$$G_{in} = 0 \tag{3.10}$$

or S as a free boundary where the traction is zero, i.e.

$$C_{ijkl}\left(\frac{\partial}{\partial x_l} G_{kn} \right) n_j = 0 \tag{3.11}$$

We apply the modified form of Betti's reciprocity theorem equation (3.7) where $u_i(\underline{x}, t)$ becomes $G_{im}(\underline{x}, t; \underline{\varsigma}_1, \tau_1)$, $v_i(\underline{x}, t)$ becomes $G_{in}(\underline{x}, t; \underline{\varsigma}_2, -\tau_2)$, and f_i and g_i respectively given by

$$f_i(\underline{x}, t) = \delta(\underline{x} - \underline{\varsigma}_1)\, \delta(t - \tau_1)\, \delta_{im} \tag{3.12}$$

$$g_i(\underline{x}, t) = \delta(\underline{x} - \underline{\varsigma}_2)\, \delta(t + \tau_2)\, \delta_{in} \tag{3.13}$$

In view of the homogeneous boundary conditions equations (3.10) and (3.11) the right hand side of the modified form of Betti's reciprocity theorem equation (3.7) will vanish leaving

$$\int_{-\infty}^{\infty} dt \iiint_{v} \begin{Bmatrix} G_{im}(\underline{x}, \tau - t; \underline{\varsigma}_1, \tau_1)\, \delta(\underline{x} - \underline{\varsigma}_2)\, \delta(t + \tau_2)\, \delta_{in} \\ - G_{in}(\underline{x}, \tau - t; \underline{\varsigma}_2, -\tau_2)\, \delta(\underline{x} - \underline{\varsigma}_1)\, \delta(t - \tau_1)\, \delta_{im} \end{Bmatrix} dV = 0 \qquad (3.14)$$

Here the integrals are eliminated due to δ-functions yields the general reciprocity relationship [48] for source and receiver

$$G_{nm}(\varsigma_2, \tau + \tau_2; \varsigma_1, \tau_1) = G_{mn}(\varsigma_1, \tau - \tau_1; \varsigma_2, -\tau_2) \qquad (3.15)$$

Setting $\tau = 0$ in equation (3.15) gives the desired relationship of a space-time reciprocity

$$G_{nm}(\varsigma_2, \tau_2; \varsigma_1, \tau_1) = G_{mn}(\varsigma_1, -\tau_1; \varsigma_2, -\tau_2) \qquad (3.16)$$

Shifting the time origin to zero ($\tau_1 = 0$) gives the space-time reciprocity in the form of

$$G_{nm}(\varsigma_2, \tau_2; \varsigma_1, 0) = G_{mn}(\varsigma_1, 0; \varsigma_2, -\tau_2) \qquad (3.17)$$

3.6 Representation Theorems

The modified form of Betti's reciprocity theorem [48] equation (3.7) in conjunction with a Green's function enables the displacement u_i to be determined from body force f_i and boundary conditions on S. In equation (3.7) we let the body force g_i be a unit point force of the form $\delta_{in}\, \delta(x - \varsigma)\, \delta(t)$ for which the corresponding displacement v_i becomes $G_{in}(\underline{x}, t; \underline{\varsigma}, 0)$ and the corresponding stress vectors $\sigma_i(\underline{v}, \underline{n})$ are replaced by

$$C_{ijkl}\left(\frac{\partial}{\partial x_l} G_{kn}(\underline{x}, t; \underline{\varsigma}, 0)\right) n_j \qquad (3.18)$$

then a representation for the displacement u_i at observation point $\underline{\varsigma}$ and time τ with source at $\underline{x}$ and time t become

$$\begin{aligned} u_n(\varsigma, \tau) = & \int_{-\infty}^{+\infty} dt \iiint_{v} f_i(\underline{x}, t) G_{in}(\underline{x}, \tau - t; \underline{\varsigma}, 0)\, dV \\ & + \int_{-\infty}^{+\infty} dt \iint_{s} \begin{Bmatrix} G_{in}(\underline{x}, \tau - t; \underline{\varsigma}, 0) \sigma_i(\underline{u}, \underline{n}) \\ - u_i(\underline{x}, t) C_{ijkl} n_j \dfrac{\partial}{\partial x_l} G_{kn}(\underline{x}, \tau - t; \underline{\varsigma}, 0) \end{Bmatrix} dS \end{aligned} \qquad (3.19)$$

interchanging the symbols $\underline{x}$ and $\underline{\varsigma}$ and the symbols t and τ permits ($\underline{x}$, t) to be the general position and time at which the desired displacement is sought. Thus

$$
\begin{aligned}
u_n(\underline{x}, t) = & \int_{-\infty}^{+\infty} d\tau \iiint_V f_i(\underline{\varsigma}, \tau)\, G_{in}(\underline{\varsigma}, t-\tau; \underline{x}, 0)\, dV(\varsigma) \\
& + \int_{-\infty}^{+\infty} d\tau \iint_S G_{in}(\underline{\varsigma}, t-\tau; \underline{x}, 0)\, \sigma_i(\underline{u}, \underline{n})\, dS(\varsigma) \\
& - \int_{-\infty}^{+\infty} d\tau \iint_S u_i(\underline{\varsigma}, t)\, C_{ijkl} n_j \frac{\partial}{\partial \varsigma_l} G_{kn}(\underline{\varsigma}, t-\tau; \underline{x}, 0)\, dS(\varsigma)
\end{aligned}
\tag{3.20}
$$

It might seem that in equation (3.20) knowledge of both displacement and stresses are needed everywhere on the boundary S. Obviously this is in contradiction to the earlier statement of the uniqueness theorem as well as the fact that both the function and its derivatives can not be specified in an arbitrary fashion everywhere on the boundary S. However, using the Green's function approach it is always possible to eliminate unwanted quantities.

By way of example, if the Green's function G_{in} is chosen to satisfy stress-free boundary conditions the last surface integral in equation (3.20) vanishes, leaving only the surface integral over applied stresses on the boundary. Furthermore, the reciprocal theorem for Green's function equation (3.17) must be invoked on equation (3.20) to give the displacement representation [48] in the form of

$$
\begin{aligned}
u_n(\underline{x}, t) = & \int_{-\infty}^{+\infty} d\tau \iiint_V f_i(\underline{\varsigma}, \tau)\, G_{ni}(\underline{x}, t-\tau; \underline{\varsigma}, 0)\, dV(\varsigma) \\
& + \int_{-\infty}^{+\infty} d\tau \iint_S G_{ni}(\underline{x}, t-\tau; \underline{\varsigma}, 0)\, \sigma_i(\underline{u}, \underline{n})\, dS(\varsigma)
\end{aligned}
\tag{3.21}
$$

3.7 Volume Source Mechanism

A volume source (an indigenous source) is an internal volumetric region Γ bounded by a closed surface Σ inside an elastic medium V, that undergoes a

sudden change of form (i.e. thermal expansion) resulting from a sudden change in temperature. An indigenous source [49] may be described as an event in the elastic medium V which does not involve forces exerted by bodies outside the medium. Such a source may be described in terms of a so-called transformational or stress-free strain which is a static phenomenon. In order to illustrate this, we shall need to perform a sequence of four imaginary mechanical operations: cutting, straining, restoring, and welding [48].

As Figure 3.1 shows, let's take an elastic medium V enclosed by external surface S to consist of an internal source volume Γ enclosed by surface Σ. 'Cutting', isolate the source medium Γ by imaginary cutting along its surface Σ and removing it from the surrounding medium V in such fashion where the source medium Γ removed is held in its original shape by imaginary forces applied over its surface Σ. Of course, these forces have the same strength over Σ as the forces imposed across Σ by the surrounding medium V before the cutting operation. Concurrently the hole induced in medium V by the cutting process is also held at its original shape and size by applying exactly the same magnitude but oppositely orientated forces imposed on the surface Σ of the source volume Γ. Therefore the stress in the elastic medium V is kept unchanged. 'Straining', raise the temperature of source medium Γ so it undergoes a thermal straining without increasing or decreasing the stress within the source volume. It's this strain that is named as stress-free strain. 'Restoring', apply additional forces over the surface Σ to restore the strained source medium to its original volume and shape. Obviously this third process will generate an additional stress field of

$$\delta\sigma_{pq} = - C_{pqrs}\, \delta\varepsilon_{rs} \tag{3.22}$$

throughout the source volume Γ which leads to restoring forces of

$$\delta f_p = - C_{pqrs}\delta\varepsilon_{rs}\nu_q \tag{3.23}$$

over its surface Σ. The outward unit normal to the surface Σ is represented by ν. 'Welding', place the source volume Γ which is now in its original shape and

size back in its hole, then weld across the cut and release the applied forces on both Σ^+ (surface of the hole) and Σ^- (surface of the source volume). The stress on Σ^- is now greater than that on Σ^+ by the amount of stress given in equation (3.22). These differences in stress over the surfaces Σ^- and Σ^+ lead to the stress discontinuity across Σ in the ν-direction.

The above process of stress-free strain is a static phenomena used in static cases where

$$\delta\sigma_{pq,q} = \frac{\partial}{\partial\varsigma_q}\left(C_{pqrs}\,\delta\varepsilon_{rs}\right) = 0 \tag{3.24}$$

however it can be extended to dynamics cases [48] where a stress-free strain $\delta\varepsilon_{rs}$ can be defined for the medium at any given time and equation (3.24) is still true for each instant. Thus the stress discontinuity across Σ is given by

$$\sigma_p = \left(C_{pqrs}\Delta\varepsilon_{rs}\right)\nu_q \tag{3.25}$$

The displacement representation equation (3.21) obtained from the representation theorem can be modified by taking the surface of medium V to consist of an external surface labeled S and two internal surfaces labeled Σ^+ (surface of the hole) and Σ^- (surface of the source volume) with unit normal ν pointing from Σ^- to Σ^+ [48]. This is

$$\begin{aligned} u_n(\underline{x},\,t) \;=\; & \int_{-\infty}^{+\infty} d\tau \iiint_V f_i(\underline{\varsigma},\,\tau)\, G_{ni}(\underline{x},\,t-\tau;\,\underline{\varsigma},\,0)\, dV(\varsigma) \\ & + \int_{-\infty}^{+\infty} d\tau \iint_S G_{ni}(\underline{x},\,t-\tau;\,\underline{\varsigma},\,0)\,\sigma_i(\underline{u},\,\underline{n})\, dS(\varsigma) \\ & + \int_{-\infty}^{+\infty} d\tau \iint_\Sigma G_{ni}(\underline{x},\,t-\tau;\,\underline{\varsigma},\,0)\,\sigma_i(\underline{u},\,\underline{\nu})\, d\Sigma(\varsigma) \end{aligned} \tag{3.26}$$

The surface of medium V labeled S is not of direct interest if V is assumed large, and in the absence of body force f_i for the displacement u_n, the equation (3.26) gives the displacement representation

$$u_n(\underline{x},\,t) \;=\; \int_{-\infty}^{+\infty} d\tau \iint_\Sigma G_{ni}(\underline{x},\,t-\tau;\,\underline{\varsigma},\,0)\,\sigma_i(\underline{u},\,\underline{\nu})\, d\Sigma(\varsigma) \tag{3.27}$$

or inserting for σ from equation (3.25) gives

$$u_n(\underline{x}, t) = \int_{-\infty}^{+\infty} d\tau \iint_{\Sigma} C_{ijkl} \Delta\varepsilon_{kl} \nu_j G_{ni}(\underline{x}, t-\tau; \underline{\varsigma}, 0)\, d\Sigma(\varsigma) \tag{3.28}$$

The Gauss (divergence) theorem is invoked to convert the surface integral into a volume integral. Then applying equation (3.24) leads to

$$u_n(\underline{x}, t) = \int_{-\infty}^{+\infty} d\tau \iiint_{\Gamma} C_{ijkl} \Delta\varepsilon_{kl} \frac{\partial}{\partial\varsigma_j} G_{ni}(\underline{x}, t-\tau; \underline{\varsigma}, 0)\, d\Gamma(\varsigma) \tag{3.29}$$

The first quantity $C_{ijkl}\Delta\varepsilon_{kl}$ has dimensions of moment (i.e. force x length) per unit volume and is known as the seismic moment density tensor or moment of the dipolar source in seismology [48]. For a finite volume source

$$m_{ij} = \iiint_{\Gamma} C_{ijkl} \Delta\varepsilon_{kl}\, d\Gamma \tag{3.30}$$

where m_{ij} can be physically represented as the strength of the disturbance. In general the moment density tensor, m_{ij}, has nine elements.

$$[m] = \begin{bmatrix} m_{11} & m_{12} & m_{13} \\ m_{21} & m_{22} & m_{23} \\ m_{31} & m_{32} & m_{33} \end{bmatrix} \tag{3.31}$$

These elements are couples at a point produced by three components of force and three moment arm directions as shown in Figure 3.2. The diagonal elements (m_{11}, m_{22}, m_{33}) are special couples with the force and moment arm in the same direction and they are normally known as dipoles (double force without moment). For a source volume undergoing a purely transformational volume expansion under temperature changes, only the diagonal components (dipoles) are nonzero [48].

The second quantity $\partial G_{ni}/\partial\varsigma_j \equiv G_{ni,j}$ can be represented physically as the displacement in n-direction due to couple produced by two equal and opposite forces in the i-direction with moment arm in the j-direction.

3.8 Heat Transfer

The absorption of laser radiation by a solid causes intense heating of the target which is equivalent to a source of heat in or on the solid. Heat conduction is the mode of heat transfer in which energy exchange take place in the source volume region of the sample. The response of a material can be calculated by solving the three dimensional heat conduction equation

$$-\nabla \cdot \vec{q}(\underline{r},\, t) + g(\underline{r},\, t) = \rho C_p \frac{\partial T(\underline{r},\, t)}{\partial t} \tag{3.32}$$

where T is the temperature, q is the heat flux vector pointing in the direction of decreasing temperature, g is the heat generation rate in the medium, ρ is the mass density, and C_p is the specific heat, subject to appropriate initial and boundary conditions.

3.9 Problem Statement: Laser Source and Structure Responses

The physical problem we wish to consider is the structural response of a homogeneous elastic transversely isotropic finite circular plate with thickness h and radius r_o when a single laser beam pulse interacts with the surface of the sample. The laser beam is assumed to be aimed perpendicular to the transverse plane. The geometry of the problem is shown in Figure 3.3. The origin of the coordinate system is set at the bottom surface of the plate and the z-axis is directed upward. The laser beam aimed at the origin O where it heats a finite subsurface volume taken to be a disk shape of diameter d and thickness η. Since the geometry of the problem has axial symmetry it is convenient to use a cylindrical coordinate system. In cylindrical coordinates r, θ, z, with corresponding displacement components u_r, u_θ, u_z, the axial symmetry is characterized by the conditions of $u_\theta = 0$, $\partial/\partial\theta = 0$, and the components u_r, u_z are independent of θ.

$$u_r = u_r(r, z) \tag{3.33a}$$

$$u_z = u_z(r, z) \tag{3.33b}$$

Therefore the stress and strain components are also independent of θ.

The elastic stiffness coefficients, C_{ijkl}, given in the constitutive law have 5 independent elastic coefficients for transversely isotropic elastic materials. The following contracted notation to represent C_{ijkl} in compact form have been introduced for convenience. In this notation, pairs of subscript involving the numbers 1, 2, and 3 are replaced as follows:

$$\begin{gathered} 11 \to 1 \quad 22 \to 2 \quad 33 \to 3 \\ 23 = 32 \to 4 \quad 13 = 31 \to 5 \quad 12 = 21 \to 6 \end{gathered} \tag{3.34}$$

The components of C_{ijkl} in the form of the stiffness matrix [C] in the contracted notation is:

$$[C] = \begin{bmatrix} C_{11} & C_{12} & C_{13} & 0 & 0 & 0 \\ C_{12} & C_{22} & C_{23} & 0 & 0 & 0 \\ C_{13} & C_{23} & C_{33} & 0 & 0 & 0 \\ 0 & 0 & 0 & C_{44} & 0 & 0 \\ 0 & 0 & 0 & 0 & C_{55} & 0 \\ 0 & 0 & 0 & 0 & 0 & C_{66} \end{bmatrix} \tag{3.35}$$

where a transversely isotropic elastic material whose axis of symmetry coincides with the z-axis have:

$$\begin{gathered} C_{22} = C_{11} \\ C_{23} = C_{13} \\ C_{55} = C_{44} \\ C_{66} = (1/2)(C_{11} - C_{12}) \end{gathered} \tag{3.36}$$

The relations between the components of stiffness matrix [C] and the engineering constants can be obtained to be

$$C_{11} = \frac{E_1}{1+\nu_{21}} \frac{1-\nu_{31}^2(E_1/E_3)}{\Delta} \tag{3.37a}$$

$$C_{12} = \frac{E_1}{1+\nu_{21}} \frac{\nu_{21}+\nu_{31}^2(E_1/E_3)}{\Delta} \tag{3.37b}$$

$$C_{13} = \frac{E_1 \nu_{31}}{\Delta} \tag{3.37c}$$

$$C_{44} = G_{13} \tag{3.37d}$$

where

$$\Delta = 1 - \nu_{21} - 2\,\nu_{31}^2 \left(E_1 / E_3\right) \tag{3.37e}$$

The constitutive relation for a three dimensional axisymmetric transversely isotropic solid is given by

$$\begin{bmatrix} \sigma_{rr} \\ \sigma_{\theta\theta} \\ \sigma_{zz} \\ \sigma_{\theta z} \\ \sigma_{rz} \\ \sigma_{r\theta} \end{bmatrix} = \begin{bmatrix} C_{11} & C_{12} & C_{13} & 0 & 0 & 0 \\ C_{12} & C_{11} & C_{13} & 0 & 0 & 0 \\ C_{13} & C_{13} & C_{33} & 0 & 0 & 0 \\ 0 & 0 & 0 & C_{44} & 0 & 0 \\ 0 & 0 & 0 & 0 & C_{44} & 0 \\ 0 & 0 & 0 & 0 & 0 & (1/2)(C_{11} - C_{12}) \end{bmatrix} \begin{bmatrix} \varepsilon_{rr} \\ \varepsilon_{\theta\theta} \\ \varepsilon_{zz} \\ \varepsilon_{\theta z} \\ \varepsilon_{rz} \\ \varepsilon_{r\theta} \end{bmatrix} \tag{3.38}$$

where the strain displacement relationship is

$$\varepsilon_{rr} = u_{r,r} \tag{3.39a}$$

$$\varepsilon_{\theta\theta} = (1/r) u_r \tag{3.39b}$$

$$\varepsilon_{zz} = u_{z,z} \tag{3.39c}$$

$$\varepsilon_{rz} = (1/2)\left(u_{r,z} + u_{z,r}\right) \tag{3.39d}$$

$$\varepsilon_{\theta z} = \varepsilon_{r\theta} = 0 \tag{3.39e}$$

The equations of motion for the system are

$$C_{11} u_{r,rr} + C_{44} u_{r,zz} + \left(C_{13} + C_{44}\right) u_{z,rz} + C_{11} r^{-1} u_{r,r} - C_{11} r^{-2} u_r + \rho F_r = \rho u_{r,tt} \tag{3.40a}$$

$$C_{44} u_{z,rr} + C_{33} u_{z,zz} + \left(C_{13} + C_{44}\right) u_{r,rz} + C_{44} r^{-1} u_{z,r} + \left(C_{13} + C_{44}\right) r^{-1} u_{r,z} + \rho F_z = \rho u_{z,tt} \tag{3.40b}$$

Prior to the application of external disturbances the system is at rest with initial conditions at time t = 0

$$u_r = u_z = 0 \tag{3.41}$$

The stress free boundary conditions are assumed for the surfaces contact with air. These stress free boundaries include the top and bottom surfaces of the plate, z = h and z = 0 respectively,

$$\sigma_{zz} = C_{13}\left(u_{r,r} + r^{-1}u_r\right) + C_{33}u_{z,z} = 0 \tag{3.42a}$$

$$\sigma_{rz} = C_{44}\left(u_{r,z} + u_{z,r}\right) = 0 \tag{3.42b}$$

and the other surface of the plate, r = r_o

$$\sigma_{rr} = C_{11}u_{r,r} + C_{12}\frac{u_r}{r} + C_{13}u_{z,z} = 0 \tag{3.43a}$$

$$\sigma_{rz} = C_{44}\left(u_{r,z} + u_{z,r}\right) = 0 \tag{3.43b}$$

The general response of the system can be written by means of the convolution integral given in the form of equation (3.29) where m_{ij} given in equation (3.30) can be regarded as the impulsive dipolar disturbances and $G_{ni,j}$ are the impulsive responses.

3.9.1 Laser Source

Assume that laser irradiation is used to heat the finite volumetric region, Γ, causing a temperature rise of ΔT. In the absence of any stresses or constraints, this produces the thermoelastic strains which are given in terms of the coefficient of linear thermal expansions, α_i, and ΔT,

$$\Delta\varepsilon_{rr} = \alpha_r\,\Delta T \tag{3.44a}$$

$$\Delta\varepsilon_{\theta\theta} = \alpha_\theta\,\Delta T \tag{3.44b}$$

$$\Delta\varepsilon_{zz} = \alpha_z\,\Delta T \tag{3.44c}$$

where α_r, α_θ, and α_z denote the coefficients of thermal expansion in r, θ, and z directions respectively in the cylindrical coordinate system. Also since the geometry of the problem possesses axial symmetry, the coefficients of thermal expansion in r and θ direction are equal.

$$\alpha_\theta = \alpha_r \tag{3.45}$$

We note that substitution of thermoelastic strains into equation (3.30) yield the components of the moment density tensor where only the diagonal components are nonzero.

$$[m]=\begin{bmatrix} m_{rr} & 0 & 0 \\ 0 & m_{\theta\theta} & 0 \\ 0 & 0 & m_{zz} \end{bmatrix} \tag{3.46}$$

where

$$m_{rr}=\left[\left(C_{11}+C_{12}\right)\alpha_r+C_{13}\alpha_z\right]\iiint_{\Gamma}\Delta T\,d\Gamma \tag{3.47a}$$

$$m_{\theta\theta}=\left[\left(C_{11}+C_{12}\right)\alpha_r+C_{13}\alpha_z\right]\iiint_{\Gamma}\Delta T\,d\Gamma \tag{3.47b}$$

$$m_{zz}=\left(2C_{13}\alpha_r+C_{33}\alpha_z\right)\iiint_{\Gamma}\Delta T\,d\Gamma \tag{3.47c}$$

Prediction of thermal effects produced by a pulsed laser beam impinging on a small surface region of homogeneous elastic transversely isotropic infinite plate with thickness h requires the solution of the three dimensional heat conduction equation over the volumetric region Γ bounded by surface Σ. Since the geometry of this problem too has axial symmetry it is convenient to use cylindrical coordinate system. For simplicity we assume that thermal equilibrium is reached locally which means the thermal properties of the solid are independent of temperature and there is negligible heat lost to the surrounding by radiation or convection. By introducing the expression for the heat flux vector and its divergence in a cylindrical system

$$\nabla\cdot\vec{q}=\frac{1}{r}\frac{\partial}{\partial r}\left(rq_r\right)+\frac{1}{r}\frac{\partial}{\partial\theta}\left(q_\theta\right)+\frac{\partial}{\partial r}\left(q_z\right) \tag{3.48}$$

where

$$\vec{q}=-\left(k_r\frac{\partial T}{\partial r}e_r+\frac{k_\theta}{r}\frac{\partial T}{\partial\theta}e_\theta+k_z\frac{\partial T}{\partial z}e_z\right) \tag{3.49}$$

we find the heat conduction equation with axisymmetry

$$k_r\frac{1}{r}\frac{\partial}{\partial r}\left(r\frac{\partial T}{\partial r}\right)+k_z\frac{\partial^2 T}{\partial z^2}+g(r,z,t)=\rho C_p\frac{\partial T}{\partial t} \tag{3.50}$$

where k_r and k_z are thermal conductivity in r and z direction respectively, C_p is the specific heat, and g(r, z, t) is the heat source per unit volume per unit time. The initial conditions are

$$T(r,\ z,\ 0) = 0 \tag{3.51a}$$

$$\frac{\partial}{\partial t} T(r,\ z,\ 0) = 0 \tag{3.51b}$$

For simplicity the boundary Σ is assumed to be insulated which means no heat lost by conduction through the boundary. This is

$$q_n = \hat{n} \cdot \vec{q} = - \hat{n} \cdot \left(k_r \frac{\partial T}{\partial r} \hat{e}_r + k_z \frac{\partial T}{\partial z} \hat{e}_z \right) = 0 \tag{3.52}$$

By rearranging equation (3.50) and integrating over time gives

$$\Delta T = \frac{1}{\rho C_p} \int_0^t \left[\nabla \cdot \vec{q} + g(r, z, t) \right] dt \tag{3.53}$$

Then combining equations (3.47a,b,c) and (3.53) yields

$$m_{rr} = \left[(C_{11} + C_{12}) \alpha_r + C_{13} \alpha_z \right] \frac{1}{\rho C_p} \int_0^t dt \left\{ \iiint_\Gamma \nabla \cdot \vec{q}\, d\Gamma + \iiint_\Gamma g(r, z, t) d\Gamma \right\} \tag{3.54a}$$

$$m_{\theta\theta} = \left[(C_{11} + C_{12}) \alpha_r + C_{13} \alpha_z \right] \frac{1}{\rho C_p} \int_0^t dt \left\{ \iiint_\Gamma \nabla \cdot \vec{q}\, d\Gamma + \iiint_\Gamma g(r, z, t) d\Gamma \right\} \tag{3.54b}$$

$$m_{zz} = \left(2C_{13} \alpha_r + C_{33} \alpha_z \right) \frac{1}{\rho C_p} \int_0^t dt \left\{ \iiint_\Gamma \nabla \cdot \vec{q}\, d\Gamma + \iiint_\Gamma g(r, z, t) d\Gamma \right\} \tag{3.54c}$$

and applying the divergence theorem and the boundary condition, equation (3.52), gives the moment density as

$$m_{rr} = \left[(C_{11} + C_{12}) \alpha_r + C_{13} \alpha_z \right] \frac{1}{\rho C_p} \int_0^t dt \iiint_\Gamma g(r, z, t) d\Gamma \tag{3.55a}$$

$$m_{\theta\theta} = \left[(C_{11} + C_{12}) \alpha_r + C_{13} \alpha_z \right] \frac{1}{\rho C_p} \int_0^t dt \iiint_\Gamma g(r, z, t) d\Gamma \tag{3.55b}$$

$$m_{zz} = \left(2C_{13} \alpha_r + C_{33} \alpha_z \right) \frac{1}{\rho C_p} \int_0^t dt \iiint_\Gamma g(r, z, t) d\Gamma \tag{3.55c}$$

which it can be thought of physically as the measure of the strength of the disturbance caused by thermal expansion of finite volume due to the heat source of finite spatial dimension releasing its energy spontaneously in a finite time. The spatial and temporal distributions of the strength of the heat source depends on the physical nature of the source. For a laser, the spatial distribution of the energy or the beam profile is not uniform. It depends on the beam focus, however for analysis purposes it may be represented by a Gaussian distribution where the intensity decreases exponentially from the center of the beam with the square of the radial distance. If the power of the laser pulse is able to reach its maximum in the order of nanoseconds, the pulse duration is extremely small and can be represented by the Dirac delta function [52]. We can now express the strength of heat source, g(r, z, t), in terms of the pulsed laser beam parameters consisting of total laser energy E, the reflection coefficient R, spatial Gaussian distribution N(r, z) and temporal δ(t) representation of beam profile.

$$g(r,z,t) = (1-R)\,E\,N(r,z)\,\delta(t) \tag{3.56}$$

where the spatial distribution is defined as

$$\iiint_{\Gamma} N(r,z)\,d\Gamma = 1 \tag{3.57}$$

and the temporal representation is

$$\int_0^{\infty} \delta(t)\,dt = 1 \tag{3.58}$$

By combining equations (3.55) through (3.58) the strength of the disturbance becomes

$$m_{rr} = \left[(C_{11}+C_{12})\alpha_r + C_{13}\alpha_z\right]\frac{1}{\rho C_p}(1-R)\,E \tag{3.59a}$$

$$m_{\theta\theta} = \left[(C_{11}+C_{12})\alpha_r + C_{13}\alpha_z\right]\frac{1}{\rho C_p}(1-R)\,E \tag{3.59b}$$

$$m_{zz} = \left(2C_{13}\alpha_r + C_{33}\alpha_z\right)\frac{1}{\rho C_p}(1-R)\,E \tag{3.59c}$$

The system response may be obtained by combining equations (3.29), (3.30), (3.33a,b) and (3.59a,b). In addition, there is a close relationship between the step response, $G^H(t)$, and the impulse response, G(t), where the step response is the integral of the impulse response.

$$G^H(t) = \int_{-\infty}^{t} G(\tau)d\tau \tag{3.60}$$

Therefore the system response is

$$\begin{aligned} u_r(r,\, z,\, t) = {} & m_{rr}G^H_{rr,r} + m_{r\theta}G^H_{rr,\theta} + m_{rz}G^H_{rr,z} \\ & m_{\theta r}G^H_{r\theta,r} + m_{\theta\theta}G^H_{r\theta,\theta} + m_{\theta z}G^H_{r\theta,z} \\ & m_{zr}G^H_{rz,r} + m_{z\theta}G^H_{rz,\theta} + m_{zz}G^H_{rz,z} \end{aligned} \tag{3.61a}$$

$$\begin{aligned} u_z(r,\, z,\, t) = {} & m_{rr}G^H_{zr,r} + m_{r\theta}G^H_{zr,\theta} + m_{rz}G^H_{zr,z} \\ & m_{\theta r}G^H_{z\theta,r} + m_{\theta\theta}G^H_{z\theta,\theta} + m_{\theta z}G^H_{z\theta,z} \\ & m_{zr}G^H_{zz,r} + m_{z\theta}G^H_{zz,\theta} + m_{zz}G^H_{zz,z} \end{aligned} \tag{3.61b}$$

however, the equations (3.61a,b) in conjunction with equation (3.46) and the condition of axisymmetry give a simplified form of the system responses

$$u_r(r,\, z,\, t) = m_{rr}G^H_{rr,r} + m_{zz}G^H_{rz,z} \tag{3.62a}$$

$$u_z(r,\, z,\, t) = m_{rr}G^H_{zr,r} + m_{zz}G^H_{zz,z} \tag{3.62b}$$

where the strength of the disturbance is

$$m_{rr} = \left[(C_{11} + C_{12})\alpha_r + C_{13}\alpha_z\right] \frac{1}{\rho C_p}(1-R)\, E \tag{3.63a}$$

$$m_{zz} = \left(2C_{13}\alpha_r + C_{33}\alpha_z\right) \frac{1}{\rho C_p}(1-R)\, E \tag{3.63b}$$

The equations (3.62a,b) simply give the general response of the system to two dipoles, given by equations (3.63a,b), applied both in the r-direction and in the z-direction.

However we wish to solve the problem for which the laser source is restricted to thermoelastic generation mechanism and it is assumed to be confined to the surface of the sample. The stress free boundary conditions imposed on the boundaries leaves the material to expand perpendicular to the

surface. This implies that m_{zz} vanishes in the equations (3.62a,b). Therefore, the general response of the system is dominated by dipoles in the r-direction only. This gives the system response

$$u_r(r, z, t) = m_{rr} G^H_{rr,r} \tag{3.64a}$$

$$u_z(r, z, t) = m_{rr} G^H_{zr,r} \tag{3.64b}$$

where the strength of the disturbance is

$$m_{rr} = \left[(C_{11} + C_{12})\alpha_r + C_{13}\alpha_z \right] \frac{1}{\rho C_p} (1 - R)\, E \tag{3.65}$$

3.9.2 Structural Response

The equations (3.64a,b) simply indicate that the general response of the system, $u_r(r, z, t)$ and $u_z(r, z, t)$, due to dipoles in the r-direction with the strength of m_{rr} can be determined if we compute the displacement fields $G^H_{rr,r}$ and $G^H_{zr,r}$ in the r-direction and in the z-direction respectively due to the unit step dipoles in the r-direction. For convenience, let $G^H_{rr,r} \equiv A$ and $G^H_{zr,r} \equiv B$ be the step response of the system. The equations of motion are given by

$$C_{11}\frac{\partial^2 A}{\partial r^2} + C_{44}\frac{\partial^2 A}{\partial z^2} + (C_{13} + C_{44})\frac{\partial^2 B}{\partial r \partial z} + C_{11}\frac{1}{r}\frac{\partial A}{\partial r} - C_{11}\frac{1}{r^2}A + \frac{1}{d}H(t) = \rho\frac{\partial^2 A}{\partial t^2} \tag{3.66a}$$

$$C_{44}\frac{\partial^2 B}{\partial r^2} + C_{33}\frac{\partial^2 B}{\partial z^2} + (C_{13} + C_{44})\frac{\partial^2 A}{\partial r \partial z} + C_{44}\frac{1}{r}\frac{\partial B}{\partial r} - (C_{13} + C_{44})\frac{1}{r}\frac{\partial A}{\partial z} = \rho\frac{\partial^2 B}{\partial t^2} \tag{3.66b}$$

The equations (3.66a,b) with proper initial and boundary conditions given in the equations (3.41), (3.42a,b), and (3.43a,b) are solved numerically to find displacement fields A and B. Then the displacements u_r and u_z are determined by equations (3.64a,b).

3.10 Numerical Analysis

Numerical solution methods for the wave propagation problems frequently offer a convenient, general and flexible way of obtaining solution to an arbitrary body of any shape when the analytic efforts are very tedious or unsuccessful. Today with the development of super computers as well as fast personal computers the use of finite difference techniques have provided, in principle, a solution to the elastic wave equation to any desired accuracy. Finite difference methods are conceptually simple, arising as they do from a simple space-time discretization of the governing partial differential equation and its boundary conditions. To minimize the required memory size and computational time of computer an efficient algorithm needs to be chosen based upon maximum exploitation of symmetry of a given problem, simplification of basic equations and boundary conditions allowable for the intended accuracy. Since for an isotropic homogeneous material the propagation of waves is well understood, the application of the finite difference method is rather inefficient. However, for an anisotropic material it is necessary to consider in detail the changes the wave undergoes through the material as it interacts with the material anisotropy. In such a material, then, the finite difference scheme is ideally suited to simulate the propagation of elastic waves.

In the finite difference scheme it is convenient to introduce at the outset the non-dimensional variables $\bar{r}$ and $\bar{z}$ denote non-dimensional coordinates, $\bar{t}$ denotes non-dimensional time, $\overline{A}$ and $\overline{B}$ denote non-dimensional displacement fields. This doesn't change the functional form of any of the either equations. These non-dimensional quantities are introduced as

$$\bar{r} = \frac{r}{h} \tag{3.67a}$$

$$\bar{z} = \frac{z}{h} \tag{3.67b}$$

$$\bar{d} = \frac{d}{h} \tag{3.67c}$$

$$\bar{t} = \sqrt{\frac{C_{33}}{\rho}}\ \frac{t}{h} \tag{3.67d}$$

$$\bar{A} = C_{33} h^2\ A \tag{3.67e}$$

$$\bar{B} = C_{33} h^2\ B \tag{3.67f}$$

where h is the plate thickness. We use these variables to transform the dimensional equation of motion, equations (3.66a,b), to a non-dimensional form

$$\frac{C_{11}}{C_{33}}\frac{\partial^2 \bar{A}}{\partial \bar{r}^2} + \frac{C_{44}}{C_{33}}\frac{\partial^2 \bar{A}}{\partial \bar{z}^2} + \frac{\left(C_{13}+C_{44}\right)}{C_{33}}\frac{\partial^2 \bar{B}}{\partial \bar{r}\partial \bar{z}} + \frac{C_{11}}{C_{33}}\frac{1}{\bar{r}}\frac{\partial \bar{A}}{\partial \bar{r}} - \frac{C_{11}}{C_{33}}\frac{1}{\bar{r}^2}\bar{A} + \frac{1}{\bar{d}}\ H(t) = \frac{\partial^2 \bar{A}}{\partial \bar{t}^2} \tag{3.68a}$$

$$\frac{C_{44}}{C_{33}}\frac{\partial^2 \bar{B}}{\partial \bar{r}^2} + \frac{\partial^2 \bar{B}}{\partial \bar{z}^2} + \frac{\left(C_{13}+C_{44}\right)}{C_{33}}\frac{\partial^2 \bar{A}}{\partial \bar{r}\partial \bar{z}} + \frac{C_{44}}{C_{33}}\frac{1}{\bar{r}}\frac{\partial \bar{B}}{\partial \bar{r}} + \frac{\left(C_{13}+C_{44}\right)}{C_{33}}\frac{1}{\bar{r}}\frac{\partial \bar{A}}{\partial \bar{z}} = \frac{\partial^2 \bar{B}}{\partial \bar{t}^2} \tag{3.68b}$$

Similarly the non-dimensional boundary conditions along the top and bottom horizontal surfaces $\bar{z} = 0$ and $\bar{z} = 1$ read

$$\frac{\partial \bar{B}}{\partial \bar{z}} = -\frac{C_{13}}{C_{33}}\left(\frac{\partial \bar{A}}{\partial \bar{r}} + \frac{1}{\bar{r}}\bar{A}\right) \tag{3.69a}$$

$$\frac{\partial \bar{A}}{\partial \bar{z}} = -\frac{\partial \bar{B}}{\partial \bar{r}} \tag{3.69b}$$

and along the vertical surface $\bar{r} = \frac{r_o}{h}$ read

$$\frac{\partial \bar{A}}{\partial \bar{r}} = -\frac{C_{12}}{C_{11}}\frac{1}{\bar{r}}\bar{A} - \frac{C_{13}}{C_{11}}\frac{\partial \bar{B}}{\partial \bar{z}} \tag{3.70a}$$

$$\frac{\partial \bar{B}}{\partial \bar{r}} = -\frac{\partial \bar{A}}{\partial \bar{z}} \tag{3.70b}$$

The non-dimensional initial conditions at $\bar{t} \le 0$ read

$$\bar{A} = \bar{B} = 0 \tag{3.71a}$$

$$\frac{\partial \overline{A}}{\partial \bar{t}} = \frac{\partial \overline{B}}{\partial \bar{t}} = 0 \tag{3.71b}$$

3.10.1 Finite Difference Formulation

The basis of the finite difference method is the replacement of the differential operator by difference approximations. All the derivatives are approximated by centered finite differences. The centered finite difference approximation is associated with a truncation error of the second order in the increments which increases the order of accuracy. It is convenient to choose a square grid with space increment of $\Delta\bar{r}$ along both r and z axes ($\Delta\bar{z} = \Delta\bar{r}$). Further an increment $\Delta\bar{t}$ is chosen in time. We let $\bar{r} = m\Delta\bar{r}$, $\bar{z} = n\Delta\bar{z}$, $\bar{t} = p\Delta\bar{t}$, where m, n, and p are integers. Also we denote by $\overline{A}(r_m, z_n, t_p)$ and $\overline{B}(r_m, z_n, t_p)$ the approximated components of displacement field, in radial and normal directions respectively, at a grid point $(m\Delta\bar{r}, n\Delta\bar{z})$ at time $p\Delta\bar{t}$. The central difference approximations for the differential operators [53] are:

$$\frac{\partial \overline{A}}{\partial \bar{r}} = \frac{1}{2\Delta\bar{r}}\left[\overline{A}(r_{m+1}, z_n, t_p) - \overline{A}(r_{m-1}, z_n, t_p)\right] \tag{3.72}$$

$$\frac{\partial^2 \overline{A}}{\partial \bar{r}^2} = \frac{1}{(\Delta\bar{r})^2}\left[\overline{A}(r_{m+1}, z_n, t_p) - 2\overline{A}(r_m, z_n, t_p) + \overline{A}(r_{m-1}, z_n, t_p)\right] \tag{3.73}$$

$$\frac{\partial^2 \overline{A}}{\partial \bar{r}\partial \bar{z}} = \frac{1}{4\Delta\bar{r}\Delta\bar{z}}\begin{bmatrix} \overline{A}(r_{m+1}, z_{n+1}, t_p) - \overline{A}(r_{m-1}, z_{n+1}, t_p) \\ -\overline{A}(r_{m+1}, z_{n-1}, t_p) + \overline{A}(r_{m-1}, z_{n-1}, t_p) \end{bmatrix} \tag{3.74}$$

The finite difference grid arrangement is shown in Figure 3.4. Depending on the location of grid points on the plate (i.e. inner, boundary, corner, and source nodes) the finite difference formulation may be different.

3.10.1.1 Inner Nodes

The inner nodes are illustrated by black dots on the solid grid lines in Figure 3.4. The finite difference formulation for interior grid points can be obtained by discretizing the equations of motion, equations (3.68a,b), in explicit forms as

$$\begin{aligned}\overline{A}(r_m,\, z_n,\, t_{p+1}) = &-\overline{A}(r_m,\, z_n,\, t_{p-1}) + \left[2 - \left(2 + \frac{1}{m^2}\right)\gamma_1 - 2\gamma_2\right]\overline{A}(r_m,\, z_n,\, t_p) \\ &+ \left(1 + \frac{1}{2m}\right)\gamma_1\, \overline{A}(r_{m+1},\, z_n,\, t_p) + \left(1 - \frac{1}{2m}\right)\gamma_1\, \overline{A}(r_{m-1},\, z_n,\, t_p) \\ &+ \gamma_2\left[\overline{A}(r_m,\, z_{n+1},\, t_p) + \overline{A}(r_m,\, z_{n-1},\, t_p)\right] \\ &+ \frac{1}{4}\gamma_3\begin{bmatrix}\overline{B}(r_{m+1},\, z_{n+1},\, t_p) - \overline{B}(r_{m-1},\, z_{n+1},\, t_p) \\ - \overline{B}(r_{m+1},\, z_{n-1},\, t_p) + \overline{B}(r_{m-1},\, z_{n-1},\, t_p)\end{bmatrix}\end{aligned} \tag{3.75a}$$

$$\begin{aligned}\overline{B}(r_m,\, z_n,\, t_{p+1}) = &-\overline{B}(r_m,\, z_n,\, t_{p-1}) + \left[2 - 2\gamma_2 - 2\left(\frac{\Delta\bar{t}}{\Delta\bar{r}}\right)^2\right]\overline{B}(r_m,\, z_n,\, t_p) \\ &+ \left(1 + \frac{1}{2m}\right)\gamma_2\, \overline{B}(r_{m+1},\, z_n,\, t_p) + \left(1 - \frac{1}{2m}\right)\gamma_2\, \overline{B}(r_{m-1},\, z_n,\, t_p) \\ &+ \left(\frac{\Delta\bar{t}}{\Delta\bar{r}}\right)^2\left[\overline{B}(r_m,\, z_{n+1},\, t_p) + \overline{B}(r_m,\, z_{n-1},\, t_p)\right] \\ &+ \frac{1}{2m}\gamma_3\left[\overline{A}(r_m,\, z_{n+1},\, t_p) - \overline{A}(r_m,\, z_{n-1},\, t_p)\right] \\ &+ \frac{1}{4}\gamma_3\begin{bmatrix}\overline{A}(r_{m+1},\, z_{n+1},\, t_p) - \overline{A}(r_{m-1},\, z_{n+1},\, t_p) \\ - \overline{A}(r_{m+1},\, z_{n-1},\, t_p) + \overline{A}(r_{m-1},\, z_{n-1},\, t_p)\end{bmatrix}\end{aligned} \tag{3.75b}$$

where the coefficients are

$$\gamma_1 = \left(\frac{C_{11}}{C_{33}}\right)\left(\frac{\Delta\bar{t}}{\Delta\bar{r}}\right)^2 \tag{3.76}$$

$$\gamma_2 = \left(\frac{C_{44}}{C_{33}}\right)\left(\frac{\Delta\bar{t}}{\Delta\bar{r}}\right)^2 \tag{3.77}$$

$$\gamma_3 = \left(\frac{C_{13} + C_{44}}{C_{33}}\right)\left(\frac{\Delta\bar{t}}{\Delta\bar{r}}\right)^2 \tag{3.78}$$

However the inner grid points on the axis of symmetry (z-axis) as shown in Figure 3.4 require special treatments because along the axis of symmetry m takes the value of zero (m = 0). The difference equations (3.75a,b) are no longer defined due to the presence of m in the denominator for those nodes. Thus independent arguments such as continuity and symmetry need to be invoked to obtain valid difference formulation. The argument of continuity of elastic material at grid points along the axis of symmetry forces the radial displacement field $\overline{A}(r_m, z_n, t_{p+1})$ to vanish. Thus the difference equation for radial displacement field when m = 0 is

$$\overline{A}(r_m, z_n, t_{p+1}) = 0 \tag{3.79}$$

For the normal displacement field $\overline{B}(r_m, z_n, t_{p+1})$ the terms causing problems in equation (3.75b) are the ones having m in the denominator where they can be replaced by proper terms using L'Hopital's rule. These troublesome terms are $(1/\bar{r})(\partial\overline{A}/\partial\bar{z})$ and $(1/\bar{r})(\partial\overline{B}/\partial\bar{r})$. They can be replaced by

$$\frac{1}{\bar{r}}\left(\frac{\partial\overline{A}}{\partial\bar{z}}\right) \rightarrow \frac{\partial^2\overline{A}}{\partial\bar{r}\partial\bar{z}} \tag{3.80}$$

$$\frac{1}{\bar{r}}\left(\frac{\partial\overline{B}}{\partial\bar{r}}\right) \rightarrow \frac{\partial^2\overline{B}}{\partial\bar{r}^2} \tag{3.81}$$

By substituting these new terms into the equation (3.75b) and simultaneously considering the following symmetry conditions

$$\overline{A}(r_{m-1}, z_n, t_p) = -\overline{A}(r_{m+1}, z_n, t_p) \tag{3.82}$$

$$\overline{B}(r_{m-1}, z_n, t_p) = \overline{B}(r_{m+1}, z_n, t_p) \tag{3.83}$$

about the z-axis when m = 0 we find the finite difference equation for the normal displacement field at the inner grid points along the axis of symmetry

$$\overline{B}(r_m,\, z_n,\, t_{p+1}) = -\overline{B}(r_m,\, z_n,\, t_{p-1}) + \left[2 - 2\gamma_2 - 2\left(\frac{\Delta\bar{t}}{\Delta\bar{r}}\right)^2\right]\overline{B}(r_m,\, z_n,\, t_p)$$

$$+ 4\gamma_2\, \overline{B}(r_{m+1},\, z_n,\, t_p) + \left(\frac{\Delta\bar{t}}{\Delta\bar{r}}\right)^2\left[\overline{B}(r_m,\, z_{n+1},\, t_p) + \overline{B}(r_m,\, z_{n-1},\, t_p)\right] \qquad (3.84)$$

$$+ \gamma_3\left[\overline{A}(r_{m+1},\, z_{n+1},\, t_p) - \overline{A}(r_{m+1},\, z_{n-1},\, t_p)\right]$$

It is shown in equations (3.75 through 3.84) that the value of the displacement field components can be computed at the time level p+1 if the displacement field components are known at two previous successive time levels (i.e time levels p-1 and p).

3.10.1.2 Boundary Nodes

The boundary grid points must satisfy the stress free boundary conditions given by equations (3.69a,b) and (3.70a,b). Since the treatments of boundary have great influence on both the stability and the accuracy of result and having the source at the boundary is in violation of the stress free boundary condition we adapt the method of fictitious boundary [55]. This method introduces a fictitious plane beyond the actual physical boundary surface where the grid points lying on this fictitious plane just outside the physical medium are called pseudonodes. The fictitious plane and pseudonodes are shown in Figure 3.4. The fictitious boundary is depicted by a dashed line and the pseudonodes are shown by circular rings. It is interesting to note that by introducing the fictitious boundary with pseudonodes, the grid points on the actual physical boundary become part of the interior grid points and the source is now considered acting at the interior grid points as well.

At every pseudonode the components of the displacement field are determined by the relevant boundary conditions equations (3.69) and (3.70) using the central finite difference approximation. In the following the difference equations for the pseudonodes at the bottom horizontal fictitious plane $\bar{z} = 0$ can be stated as

$$\overline{A}(r_m,\, z_{n-1},\, t_p) = \overline{A}(r_m,\, z_{n+1},\, t_p) + \overline{B}(r_{m+1},\, z_n,\, t_p) - \overline{B}(r_{m-1},\, z_n,\, t_p) \tag{3.85a}$$

$$\begin{aligned}\overline{B}(r_m,\, z_{n-1},\, t_p) = \overline{B}(r_m,\, z_{n+1},\, t_p) &+ \frac{C_{13}}{C_{33}}\left[\overline{A}(r_{m+1},\, z_n,\, t_p) - \overline{A}(r_{m-1},\, z_n,\, t_p)\right] \\ &+ \frac{C_{13}}{C_{33}}\left(\frac{2}{m}\right)\overline{A}(r_m,\, z_n,\, t_p)\end{aligned} \tag{3.85b}$$

and for the pseudonodes at the top horizontal fictitious plane $\bar{z} = 1$

$$\overline{A}(r_m,\, z_{n+1},\, t_p) = \overline{A}(r_m,\, z_{n-1},\, t_p) - \overline{B}(r_{m+1},\, z_n,\, t_p) - \overline{B}(r_{m-1},\, z_n,\, t_p) \tag{3.86a}$$

$$\begin{aligned}\overline{B}(r_m,\, z_{n+1},\, t_p) = \overline{B}(r_m,\, z_{n-1},\, t_p) &- \frac{C_{13}}{C_{33}}\left[\overline{A}(r_{m+1},\, z_n,\, t_p) - \overline{A}(r_{m-1},\, z_n, t_p)\right] \\ &+ \frac{C_{13}}{C_{33}}\left(\frac{2}{m}\right)\overline{A}(r_m,\, z_n,\, t_p)\end{aligned} \tag{3.86b}$$

Similarly, for the pseudonodes at the vertical fictitious plane $\bar{r} = \frac{r_\circ}{h}$

$$\begin{aligned}\overline{A}(r_{m+1},\, z_n,\, t_p) = \overline{A}(r_{m-1},\, z_n,\, t_p) &- \frac{C_{12}}{C_{11}}\left(\frac{2}{m}\right)\overline{A}(r_m,\, z_n,\, t_p) \\ &- \frac{C_{13}}{C_{11}}\left[\overline{B}(r_m,\, z_{n+1},\, t_p) - \overline{B}(r_m,\, z_{n-1},\, t_p)\right]\end{aligned} \tag{3.87a}$$

$$\overline{B}(r_{m+1},\, z_n,\, t_p) = \overline{B}(r_{m-1},\, z_n,\, t_p) - \left[\overline{A}(r_m,\, z_{n+1},\, t_p) - \overline{A}(r_m,\, z_{n-1},\, t_p)\right] \tag{3.87b}$$

In addition, the introduction of the fictitious boundary has the advantage of smoothing out the sharp boundary corners and eliminating the ambiguity of nodes sharing both vertical and horizontal boundaries. However the difference equations (3.85) through (3.87) can not be used at the pseudonodes H_B and H_T on the horizontal fictitious planes and the pseudonodes V_B and V_T on the vertical fictitious planes due to smoothing process. Therefore a special difference scheme [55] needs to be adapted for these pseudonodes which assures the same order of accuracy as given to earlier difference equations. These special pseudonodes are also shown in Figure 3.4. The special finite difference scheme [55] adapted for pseudonode H_B is

$$\frac{1}{2}\,\delta_z^o\left[\overline{B}(r_m,\,z_n,\,t_p)+\overline{B}(r_{m-2},\,z_n,\,t_p)\right]= -\frac{C_{13}}{C_{33}}\,\delta_r^o\left[\overline{A}(r_{m-1},\,z_n,\,t_p)\right]-\frac{C_{13}}{C_{33}}\left(\frac{1}{m(\Delta\bar{r})}\right)\overline{A}(r_m,\,z_n,\,t_p) \tag{3.88a}$$

$$\frac{1}{2}\,\delta_z^o\left[\overline{A}(r_m,\,z_n,\,t_p)+\overline{A}(r_{m-2},\,z_n,\,t_p)\right]=-\,\delta_r^o\left[\overline{B}(r_{m-1},\,z_n,\,t_p)\right] \tag{3.88b}$$

where δ_q^o is the centered finite difference operator with respect to the variable q. This is

$$\delta_z^o\left[B(r_m,z_n,t_p)\right]=\frac{1}{2}\left[B(r_m,z_{n+1},t_p)-B(r_m,z_{n-1},t_p)\right] \tag{3.89}$$

Then, the components of displacement field at pseudonode H_B,

$$\overline{B}(r_m,\,z_{n-1},\,t_p)=\overline{B}(r_m,\,z_{n+1},\,t_p)+\overline{B}(r_{m-2},\,z_{n+1},\,t_p)-\overline{B}(r_{m-2},\,z_{n-1},\,t_p) +2\,\frac{C_{13}}{C_{33}}\left(1+\frac{2}{m}\right)\overline{A}(r_m,\,z_n,\,t_p)-2\,\frac{C_{13}}{C_{33}}\left(1+\frac{2}{m}\right)\overline{A}(r_{m-2},\,z_n,\,t_p) \tag{3.90a}$$

$$\overline{A}(r_m,\,z_{n-1},\,t_p)=\overline{A}(r_m,\,z_{n+1},\,t_p)+\overline{A}\,(r_{m-2},\,z_{n+1},\,t_p)-\overline{A}(r_{m-2},\,z_{n-1},\,t_p) +2\left[\overline{B}\,(r_m,\,z_n,\,t_p)-\overline{B}(r_{m-2},\,z_n,\,t_p)\right] \tag{3.90b}$$

In a similar manner the components of displacement field at pseudonode H_T can be obtained.

Finally the special finite difference scheme [55] adapted for pseudonode V_B is given by the following

$$\frac{1}{2}\,\delta_r^o\left[\overline{A}(r_m,\,z_n,\,t_p)+\overline{A}(r_m,\,z_{n+2},\,t_p)\right]= -\frac{C_{13}}{C_{11}}\,\delta_z^o\left[\overline{B}(r_m,\,z_{n+1},\,t_p)\right]-\frac{C_{12}}{C_{11}}\left(\frac{1}{m(\Delta\bar{r})}\right)\overline{A}(r_m,\,z_n,\,t_p) \tag{3.91a}$$

$$\frac{1}{2}\,\delta_r^o\left[\overline{B}(r_m,\,z_n,\,t_p)+\overline{B}(r_m,\,z_{n+2},\,t_p)\right]=-\,\delta_z^o\left[\overline{A}(r_m,\,z_{n+1},\,t_p)\right] \tag{3.91b}$$

Then, the components of displacement field at pseudonode V_B,

$$\overline{A}(r_{m+1},\, z_n,\, t_p) = \overline{A}(r_{m-1},\, z_n,\, t_p) - \overline{A}(r_{m+1},\, z_{n+2},\, t_p) + \overline{A}(r_{m-1},\, z_{n+2},\, t_p) - 2\,\frac{C_{13}}{C_{11}}\left[\overline{B}(r_m,\, z_{n+2},\, t_p) - \overline{B}(r_m,\, z_n,\, t_p)\right] - \frac{C_{12}}{C_{11}}\left(\frac{4}{m}\right)\overline{A}(r_m,\, z_n,\, t_p) \tag{3.92a}$$

$$\overline{B}(r_{m+1},\, z_n,\, t_p) = \overline{B}(r_{m-1},\, z_n,\, t_p) - \overline{B}(r_{m+1},\, z_{n+2},\, t_p) + \overline{B}(r_{m-1},\, z_{n+2},\, t_p) - 2\left[\overline{A}(r_m,\, z_{n+2},\, t_p) - \overline{A}(r_m,\, z_n,\, t_p)\right] \tag{3.92b}$$

In a similar manner the components of displacement field at pseudonode V_T can be obtained.

3.10.1.3 Corner Nodes

The corner nodes P and Q are illustrated in Figure 3.4. Because of the introduction of the fictitious boundaries the corner nodes become part of inner nodes. The finite difference scheme for inner nodes may be employed at corner nodes, except, a special finite difference approximation [53] needs to be adapted for the mixed derivative $\partial\overline{A}/\partial\bar{r}\partial\bar{z}$ in place of the one given in equation (3.74). The adopted scheme eliminate another inaccuracy and instability in the result at corner nodes and provides the same order of accuracy as given to earlier difference equations. The differential operator is given by

$$\frac{\partial\overline{A}}{\partial\bar{r}\partial\bar{z}} = \frac{1}{2\Delta\bar{r}\Delta\bar{z}}\left[\delta_r^+\,\delta_z^+ + \delta_r^-\,\delta_z^-\right]\overline{A}(r_m, z_n, t_p) \tag{3.93}$$

where δ_q^+ and δ_q^- are the forward and backward finite difference operator with respect to the variable q, respectively. These are, for example,

$$\delta_r^+\left[\overline{A}(r_m, z_n, t_p)\right] = \overline{A}(r_{m+1}, z_n, t_p) - \overline{A}(r_m, z_n, t_p) \tag{3.94}$$

$$\delta_r^-\left[\overline{A}(r_m, z_n, t_p)\right] = \overline{A}(r_m, z_n, t_p) - \overline{A}(r_{m-1}, z_n, t_p) \tag{3.95}$$

By substituting the new adapted scheme for the mixed derivative into the difference equations for inner nodes, equations (3.68a,b), we obtain the components of the displacement field for corner node P as

$$\begin{aligned}\overline{A}(r_m, z_n, t_{p+1}) = &-\overline{A}(r_m, z_n, t_{p-1}) + \left[2 - \left(2 + \frac{1}{m^2}\right)\gamma_1 - 2\gamma_2\right]\overline{A}(r_m, z_n, t_p) \\ &+ \left(1 + \frac{1}{2m}\right)\gamma_1\,\overline{A}(r_{m+1}, z_n, t_p) + \left(1 - \frac{1}{2m}\right)\gamma_1\,\overline{A}(r_{m-1}, z_n, t_p) \\ &+ \gamma_2\left[\overline{A}(r_m, z_{n+1}, t_p) + \overline{A}(r_m, z_{n-1}, t_p)\right] \\ &+ \frac{1}{2}\gamma_3\begin{bmatrix}\overline{B}(r_{m+1}, z_{n+1}, t_p) - \overline{B}(r_{m+1}, z_n, t_p) \\ - \overline{B}(r_m, z_{n+1}, t_p) + \overline{B}(r_{m-1}, z_{n-1}, t_p) \\ - \overline{B}(r_{m-1}, z_n, t_p) - \overline{B}(r_m, z_{n-1}, t_p) + 2\overline{B}(r_m, z_n, t_p)\end{bmatrix}\end{aligned} \tag{3.96a}$$

$$\begin{aligned}\overline{B}(r_m, z_n, t_{p+1}) = &-\overline{B}(r_m, z_n, t_{p-1}) + \left[2 - 2\gamma_2 - 2\left(\frac{\Delta\bar{t}}{\Delta\bar{r}}\right)^2\right]\overline{B}(r_m, z_n, t_p) \\ &+ \left(1 + \frac{1}{2m}\right)\gamma_2\,\overline{B}(r_{m+1}, z_n, t_p) + \left(1 - \frac{1}{2m}\right)\gamma_2\,\overline{B}(r_{m-1}, z_n, t_p) \\ &+ \left(\frac{\Delta\bar{t}}{\Delta\bar{r}}\right)^2\left[\overline{B}(r_m, z_{n+1}, t_p) + \overline{B}(r_m, z_{n-1}, t_p)\right] \\ &+ \frac{1}{2m}\gamma_3\left[\overline{A}(r_m, z_{n+1}, t_p) - \overline{A}(r_m, z_{n-1}, t_p)\right] \\ &+ \frac{1}{2}\gamma_3\begin{bmatrix}\overline{A}(r_{m+1}, z_{n+1}, t_p) - \overline{A}(r_{m+1}, z_n, t_p) \\ - \overline{A}(r_m, z_{n+1}, t_p) + \overline{A}(r_{m-1}, z_{n-1}, t_p) \\ - \overline{A}(r_{m-1}, z_n, t_p) - \overline{A}(r_m, z_{n-1}, t_p) + 2\overline{A}(r_m, z_n, t_p)\end{bmatrix}\end{aligned} \tag{3.96b}$$

3.10.1.4 Source Nodes

The source nodes are illustrated in Figure 3.4. Because of the introduction of the fictitious boundary they also become part of the inner nodes. The source dipole is treated as a pair of body forces applied at grid points (m^+ ,n) and (m^- ,n). The finite difference approximation for inner nodes, equations (3.75a,b), may be employed except an additional term to represent the dipole is added to the right hand side of the equation (3.75a).

$$
\begin{aligned}
\overline{A}(r_m,\, z_n,\, t_{p+1}) = -\overline{A}(r_m,\, z_n,\, t_{p-1}) + \left[2 - \left(2 + \frac{1}{m^2}\right)\gamma_1 - 2\gamma_2\right]\overline{A}(r_m,\, z_n,\, t_p) \\
+ \left(1 + \frac{1}{2m}\right)\gamma_1\, \overline{A}(r_{m+1},\, z_n,\, t_p) + \left(1 - \frac{1}{2m}\right)\gamma_1\, \overline{A}(r_{m-1},\, z_n,\, t_p) \\
+ \gamma_2\left[\overline{A}(r_m,\, z_{n+1},\, t_p) + \overline{A}(r_m,\, z_{n-1},\, t_p)\right] \\
+ \frac{1}{4}\gamma_3\left[\begin{array}{l}\overline{B}(r_{m+1},\, z_{n+1},\, t_p) - \overline{B}(r_{m-1},\, z_{n+1},\, t_p) \\ - \overline{B}(r_{m+1},\, z_{n-1},\, t_p) + \overline{B}(r_{m-1},\, z_{n-1},\, t_p)\end{array}\right] + \frac{1}{\overline{\overline{d}}}\, H\left(t_{p+1}\right)
\end{aligned}
\tag{3.97}
$$

3.10.2 Impulse Dipole Stimulus

The physical problem characterization of PLUG presented in section (3.9.1) resulted in a point dipole force whose force-time function was synthesized to be a Heaviside step function.

The Heaviside step function is a very sharply rising force excitation. To avoid discontinuities at t = 0 which might cause oscillation in the numerical simulation, the dipole body force was chosen to be a smoothed version of the Heaviside function with parabolic rise time [56]:

$$
H(t) \Rightarrow \frac{1}{t_r}\left[\frac{t^2}{2} - \left(t - t_r\right)^2\, H\left(t - 2\, t_r\right) + \frac{\left(t - 2\, t_r\right)^2}{2}\, H\left(t - 2t_r\right)\right] \tag{3.98}
$$

where t_r denotes the measure of the rise time increment. The Heaviside step function and its smoothed version are shown in Figure 3.5.

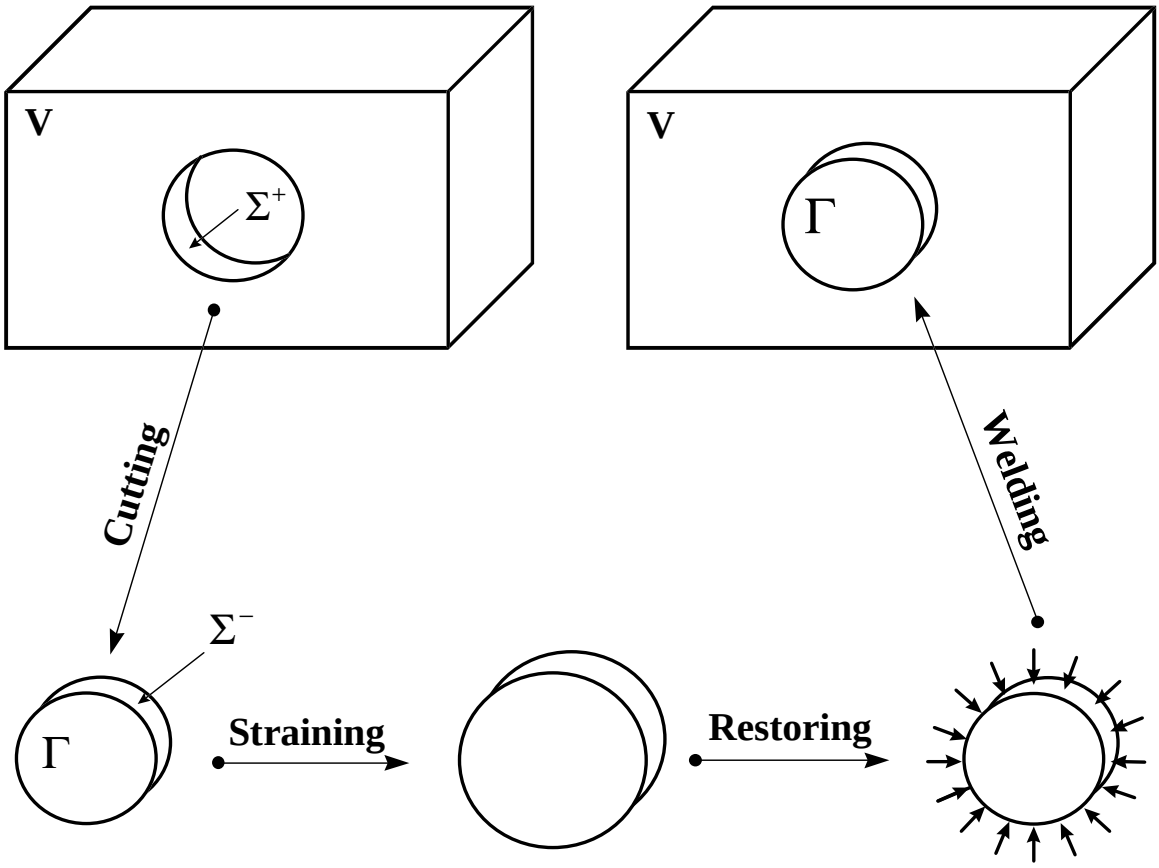

Figure 3.1. Schematic diagram illustrating the transformational-strain/volume-source mechanism.

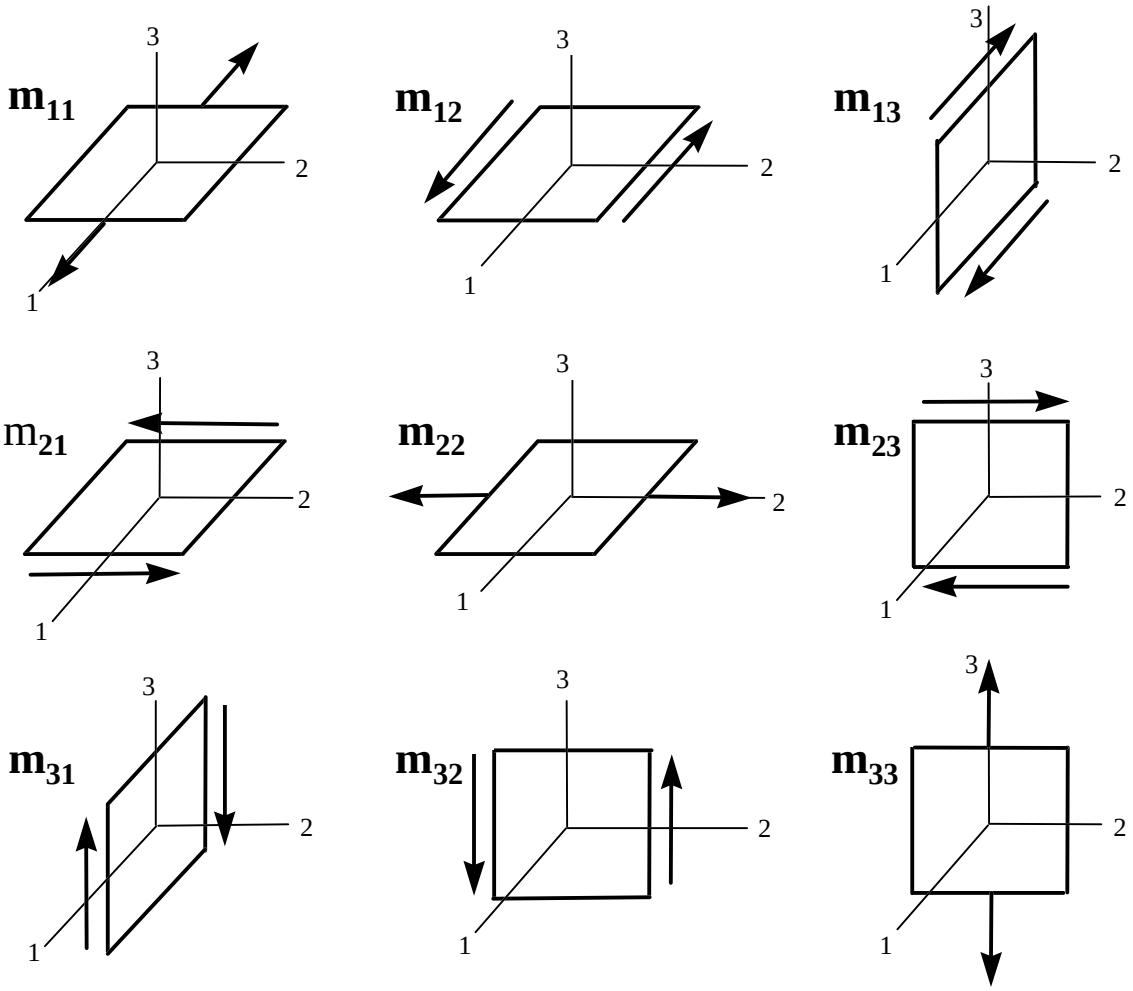

Figure 3.2. Schematic diagram of the moment tensor components.

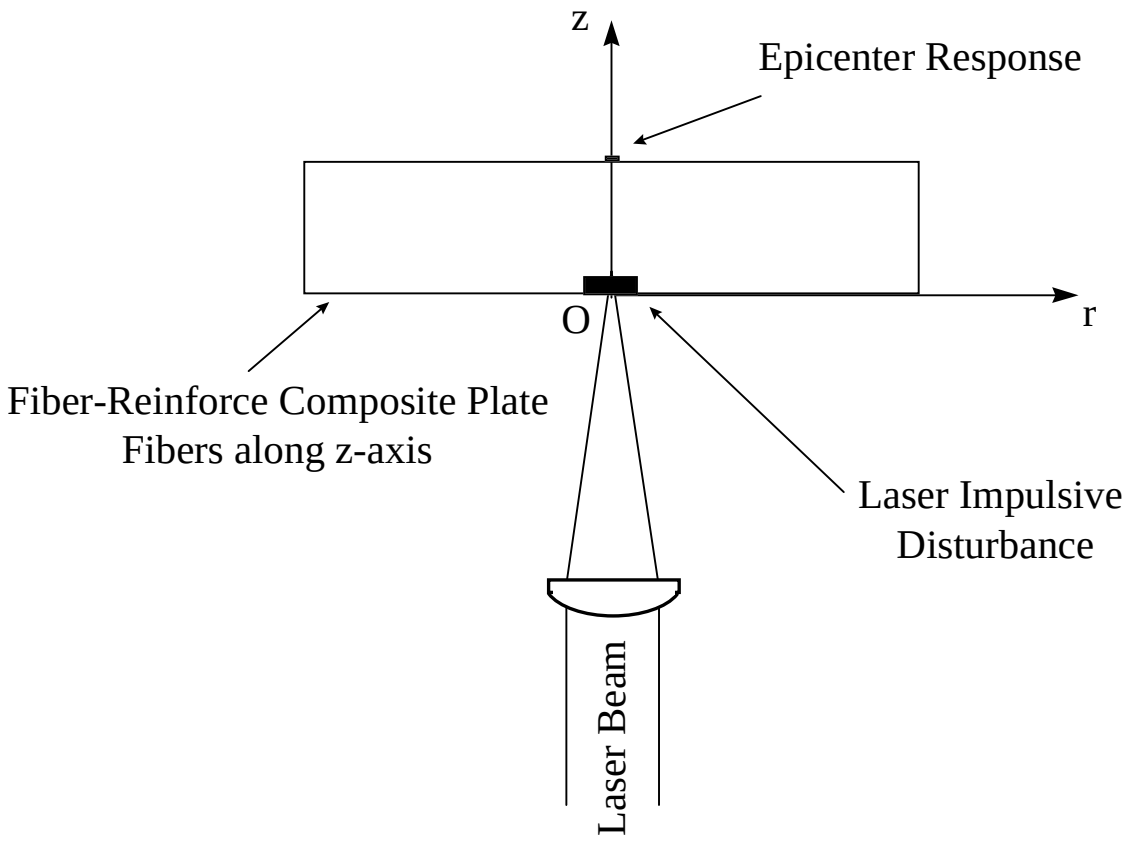

Figure 3.3. Problem geometry.

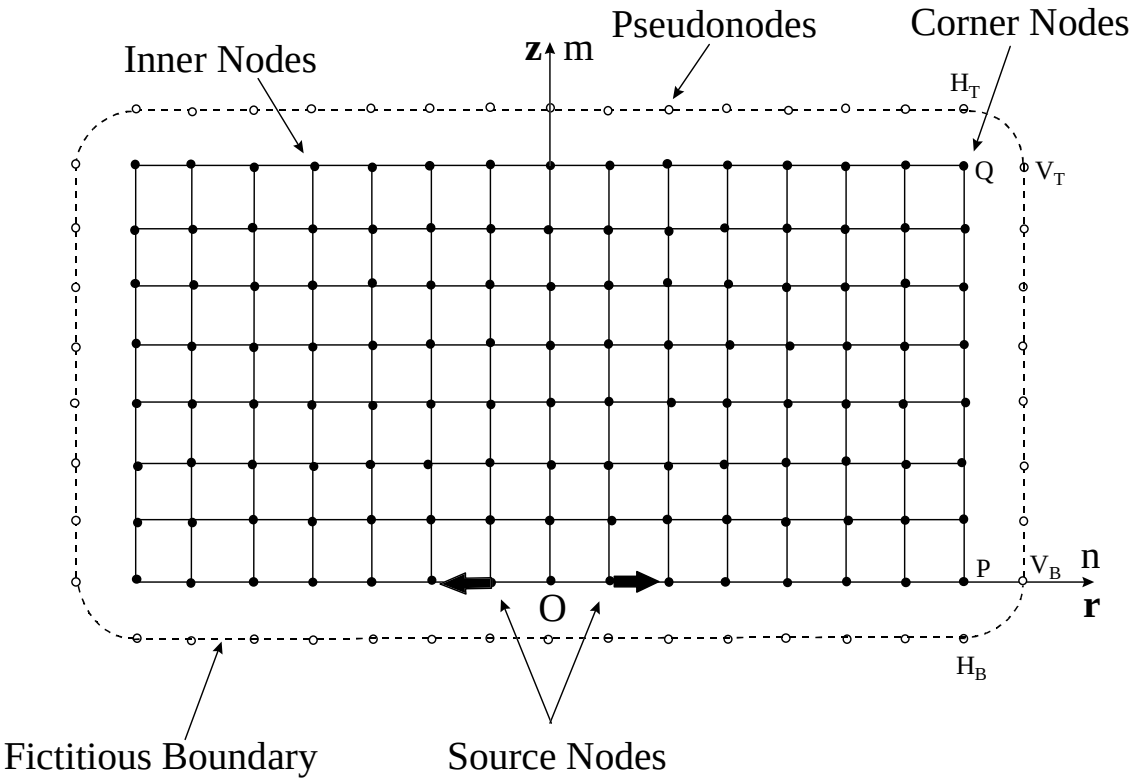

Figure 3.4. Grid arrangement.

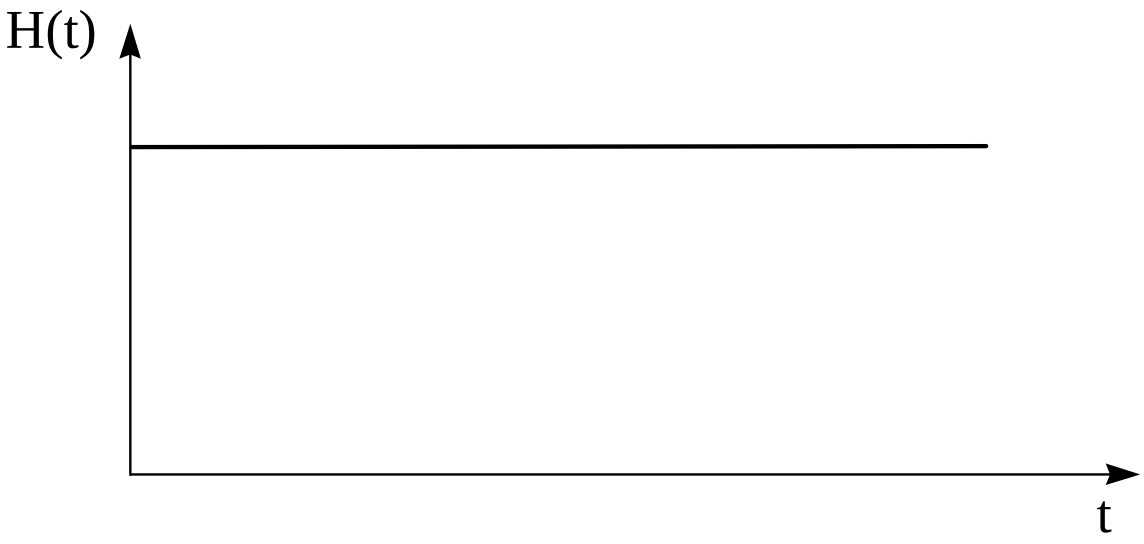

(a) Sharp rise time

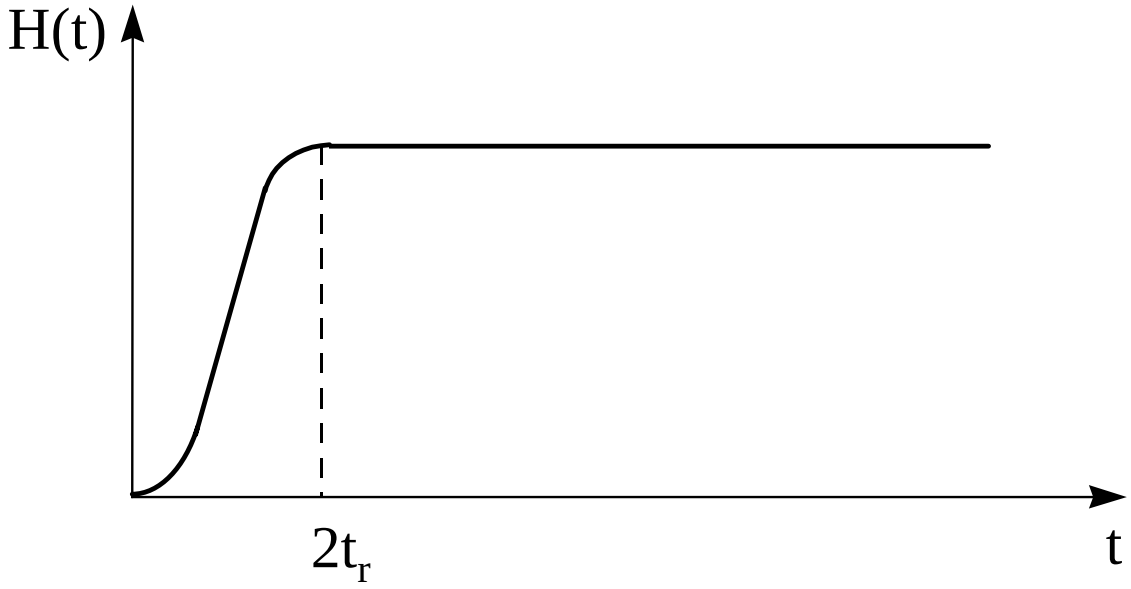

(b) Parabolic rise time

Figure 3.5. The Heaviside step source-time function with (a) sharp rise time, (b) parabolic rise time.

CHAPTER 4

EXPERIMENT

4.1 Introduction

This chapter describes the experimental arrangement including equipment, procedure, and analysis which is used to perform both the out-of-plane displacement measurement and the time-of-flight measurement utilized for this study.

The equipment employed in this experimental investigation consists of a laser system, laser energy monitor, focusing lens, NIST conical transducer, preamplifier, and a 486 IBM-PC compatible equipped with a digital data acquisition system. The brief description of each of these items is given below.

4.1.1 Laser System

The generation of ultrasound in solids in most laboratory research has been carried out with solid state laser systems operated in a pulsed mode under Q-switched conditions. The Q-switching techniques enable the pulses to be produced in the order of 1-100 nanoseconds range which is ideal for ultrasonic generation. The most popular solid state laser now for generation of ultrasound in solids suitable for NDE is the type in which light emitting neodymium

atoms are embedded in a glass or crystalline matrix accompanied with a host, yttrium-aluminum garnet, a brittle crystal known as YAG. The fundamental wavelength for the Nd:YAG laser system is in the infrared region of light spectrum with average wavelength of 1.06 μm (equivalent to 1060 nm). The pulsed Nd:YAG lasers suitable for NDE are commonly deliver energy of typically < 100 mJ with the 4 mm beam diameter having pulse duration of typically < 100 ns.

For the experimental work performed, a Kigre model MK-480 pulsed Nd:YAG Q-switched laser system operating in the infrared part of the electromagnetic spectrum at 1.06 μm wavelength was employed. The unfocused laser beam diameter is 4 mm. This system is capable of delivering maximum nominal output energy of 10 mJ in a single pulse. The pulse width/duration of the system is approximately 20 ns. By convention, pulse duration is defined as the full width of the pulse at half height.

4.1.2 Laser Energy Monitor

The Delta Developments pulsed laser energy monitor near visible version (wavelength range of 200 nm-1100 nm) was employed to monitor some of the characteristics of the laser energy supplied by the laser system. The unit is capable of measuring energy ranging between 0 - 100 mJ with beam diameter in the range of 2 mm to 38 mm. It is also equipped with a number of BNC output sockets providing pulse shape, pulse energy, trigger in and trigger out. The trigger out signal is used to trigger the data acquisition unit.

4.1.3 Focusing Lens

To focus the laser beam into a smaller spot size, a High Power Model laser focusing lens marketed by Oriel corporation was used. The lens was appropriate for pulsed Nd-YAG lasers with damage threshold of 2 GW/cm^2 in

10 ns pulses. It is fabricated from fused silica for higher efficiency and has anti-reflection “W” coatings on both sides for minimum reflection losses. The lens allows maximum input beam diameter of 27.1 mm and the minimum spot size of approximately 0.015 mm may be reached at a nominal focal length of 300 mm.

4.1.4 Transducer

The NIST conical piezoelectric transducer [57] commercially known as Model 501 dynamic surface displacement transducer was used in the experimental study conducted. This point receiver contains a small-aperture, conical, lead-zirconate-titanate piezoelectric element with a large brass backing mass and it is furnished with a shield/preamplifier housing. The shield/preamplifier housing is a large hollow aluminum cylinder with an aluminum cap which provides shielding from electromagnetic interference and a matched battery powered preamplifier is attached on the inside housing wall having unity gain and providing low output impedance of 50 Ω for the transducer. The Model 501 provides measurement of normal (out-of-plane) surface displacement with very high sensitivity and it has flat frequency response over the broad frequency band from some 50 kHz to 1 MHz.

4.1.5 Preamplifier

A battery operated Panametrics ultrasonic preamplifier with selectable 40 dB or 60 dB gain settings was available to amplify the signal from the NIST conical transducer. The preamplifier bandwidth is specified to be from 0.02 MHz to 10 MHz.

4.1.6 Data Acquisition

A PC based SONIX digital data acquisition system was employed to perform ultrasonic signal observation, storage, and analysis. The SONIX STR-8100 2 channel A/D converter board and control software provides high ultrasonic signal capture and data collection of up to 64K record length. The STR-8100 provides a maximum sampling rate of 100 MHz with 8-bit resolution.

4.2 Experimental Details

Figures 4.1 and 4.2 show the photograph view and the schematic diagram of the testing set-up and procedure for PLUG in both the unidirectional fiber-reinforced graphite/epoxy composite sample and aluminum sample. The material properties of both graphite/epoxy sample and aluminum sample are tabulated in Tables 4.1 and 4.2 respectively.

The laser unit with its beam aiming aperture facing vertically up is attached to a mounting plate which is fastened to the vertical height mounting assembly capable of three axes (x, y, z axes) translation. The laser energy monitor is mounted to a fixed platform above the laser unit such that the laser beam enters into the instrument through the bottom circular opening and exits from the top opening. The focusing lens is attached to the same fixed platform right on the top opening of the laser energy monitor where the laser beam exits. An 8 by 12 inch plate with an opening hole on its center is mounted to a laboratory jack positioning stage capable of three axes translation. The sample is placed on the plate opening hole and properly restrained. Finally the NIST conical receiving transducer is placed on the sample and adjusted with a great deal of care and precision such that it sits exactly at the center of sample

where it was marked. Then the NIST conical transducer is properly shielded by the shield/preamplifier housing assembly.

The experimental procedure begins with turning the key switch to the “On” position. The “Laser On” button and “Standby” button will light up simultaneously on the laser control unit. The unit will automatically set itself in the standby mode. The standby mode allows the hand-held “Fire” switch to lock out and eliminates accidental firing. As a preliminary step the laser unit should be kept on the standby mode for 10 to 15 minutes letting both the energy storage unit fully charged up and the laser head assembly reach temperature equilibrium. When the unit becomes fully energized the “Test” button is pushed (eventually the “Test” button lights up) activating the “Fire” switch to fire only the flashlamp while the unit is still unarmed. The purpose of the test mode is to use the flashlamp to align the beam to the desire spot. Thus the flashlamp and the horizontal control knobs on both the vertical height mounting assembly and the laboratory jack positioning stage is used to aim the laser beam to the designated spot on the sample. Then the laboratory jack positioning stage is raised by the vertical control knob to focus the laser beam to a spot size of approximately 2 mm in diameter on the sample.

Table 4.1. Typical room temperature material properties for T300/5208 graphite/epoxy from literature and/or manufacturer details.

Density	ρ	1600	Kg/m^3
Young's Moduli (f)	E_1	137.93	GPa
Young's Moduli (p)	E_2	14.48	GPa
Shear Moduli (12, 13, 23)	G	5.86	GPa
Poisson's Ratio (12, 13, 23)	ν	0.21	
Thermal Expansion (f)	α_1	$-0.3x10^{-6}$	1/K
Thermal Expansion (p)	α_2, α_3	$28.1x10^{-6}$	1/K
Specific Heat	C_p	1000	J/Kg.K
Thermal Conductivity (f)	K_1	25	W/m.K
Thermal Conductivity (p)	K_2	0.59	W/m.K
Thermal Diffusivity (f)	κ_1	$170x10^{-6}$	m^2/s
Thermal Diffusivity (p)	κ_2	$4x10^{-6}$	m^2/s
Wave Velocity(Longitudinal, z)	v_l	9339.63	m/s
Wave Velocity(transverse, z)	v_s	1914.09	m/s

[a] Letter f indicates fiber direction; p perpendicular to the fibers.

Table 4.2. Typical room temperature material properties for aluminum from literature and/or manufacturer details.

Density	ρ	2779	Kg/m^3
Shear Modulus	μ	26.1	GPa
Bulk Modulus	B	75.5	GPa
Lame Constant	λ	58.1	GPa
Poisson's Ratio	ν	0.345	
Young's Modulus	E	70.2	GPa
Thermal Expansion	α	$0.231x10^{-4}$	1/K
Specific Heat	C_p	880	J/Kg.K
Thermal Conductivity	K	240	W/m.K
Thermal Diffusivity	κ	0.94	cm^2/s
Longitudinal Wave Velocity	v_l	6400	m/s
Shear Wave Velocity	v_s	3150	m/s

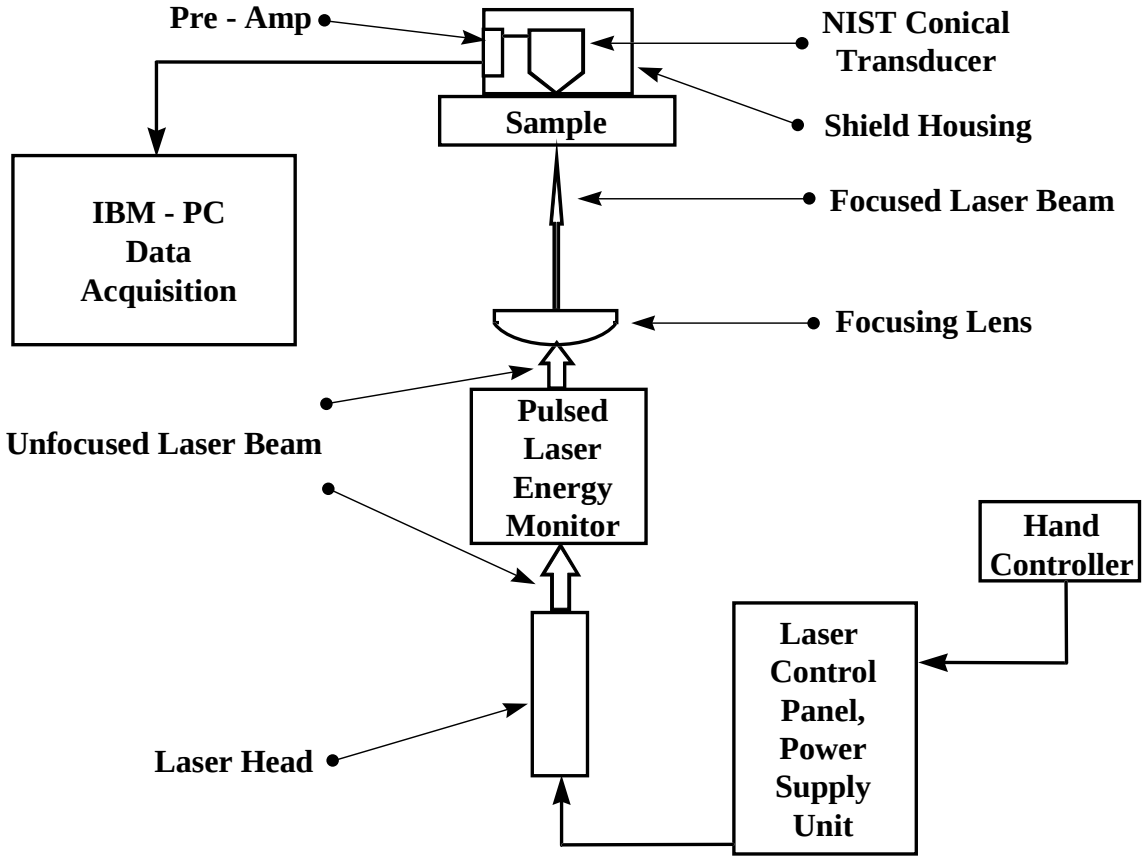

Figure 4.1. Schematic diagram of experimental apparatus.

CHAPTER 5

RESULTS AND DISCUSSION

As discussed earlier, the principal contributions of this study were both the experimental verification and the analytical formulation of a mechanistic model for the PLUG in the unidirectional fiber-reinforced composite plate with axisymmetry (i.e. transversely isotropic material). The laser pulse was characterized and simulated as an ultrasonic disturbance that launches elastic waves in the plate. A numerical simulation (i.e. finite difference scheme) was developed to predict the surface displacement at epicenter to the source in the plate.

The analytical source model presented here, provides a means of simulating the extremely rapid deposition of a single laser pulse beam energy to a finite transient thermoelastic volume source. The analysis approximates the finite volume source to be an effective disk-like source at the plate surface. The source dimensions, diameter and thickness, are equivalent to the incident laser beam aperture and the laser energy penetration depth within the plate surface respectively. The graphite/epoxy composite absorbs about 75 percent of the incident laser energy very near the surface, the absorbed laser energy attenuates exponentially [58] as it penetrates into the material. The thickness of the effective disk-like source was estimated experimentally. A single ply graphite/epoxy composite lamina was placed between the laser unit

and the laser energy monitor. The thickness of a single ply composite lamina is about 0.2 mm. No detectable transmitted pulse energy level was detected by the laser energy monitor through the thickness of the single ply graphite/epoxy composite lamina when it was exposed to the Nd-YAG laser pulse at wavelength of 1.06 μm. Therefore it was revealed that the transmission and absorption of laser energy pulse was confined to a thin surface layer within the surface of the first lamina of the graphite/epoxy composite laminate. The effective disk-like source created by the irradiation of the surface of graphite/epoxy composite plate was simulated physically as an effective point source that acts as a system of dipoles radiating ultrasonic energy. The characteristics of the dipoles were established theoretically by a seismic moment density tensor [48] described in chapter 4. One characteristic of PLUG in graphite/epoxy composite plate was the fact that the plate surface was not loaded. By definition, this free surface was the one at which stresses must be zero. Therefore any contribution to radiation energy from these stresses normal to the surface arose only from thermal expansion at some considerable distance into the plate thickness. However, the estimated thickness of the above effective disk-like source was attained to be sufficiently small confined within the thickness of a single ply lamina (i.e. < 0.2 mm) that appreciable dipoles in the direction normal to plate surface would be absent. Thus it would be expected that the dipoles, radially oriented and parallel to the plate surface were the only source of radiating ultrasonic energy.

In practice, the size of the fiber diameter is far smaller than the laser beam aperture (i.e. the diameter of the above effective disk-like source model). For comparison, the diameter of a fiber is about 6.6 micron and the diameter of the disk-like source model involving thermoelastic generation mechanism is about 2 mm. Therefore it is plausible to ignore beam fiber and beam matrix interactions including different electromagnetic absorption levels for the fiber and matrix, heat transfer, thermoelastic and interface effects between fiber and matrix. This approach significantly simplified the analysis.

The temporal profile of the Nd-YAG laser pulse operating at 1.06 μm wavelength is shown in Figure 5.1. For the nanosecond pulse duration in time the basic assumption of an instantaneous conversion of the absorbed laser radiation into heat energy was justified during laser impact. For low thermal conductivity of graphite/epoxy composite, very little or no heat energy from laser pulse was conducted away. As a result the temperature rise was contained within the well-defined effective volume source dimensions. Subsequently it was expected that the instantaneous expansion of laser heated effective disk-like source at the plate surface constrained laterally by the surrounding material would induce a system of strong radially oriented impulsive force dipoles into the rest of the composite plate. Later, the amount of the impulsive force dipoles from a laser pulse $Q\delta(t)$ resulted in the Heaviside step source-time function $QH(t)$ for the themoelastic volume source when the laser pulse temporal profile was integrated with time.

For the purpose of testing and validating the finite difference program the aluminum plate was selected. In this numerical analysis, we assumed that a 0.9 mJ laser pulse of 20 ns pulse duration, 2 mm incident beam aperture with the estimated incident power density of approximately ≅1.4 MW/cm^2 was aimed at the surface of 10 mm thick aluminum plate. This value for the incident laser power density is considerably below the threshold for damage and it falls within the thermoelastic regime. The estimated damage threshold laser power density for the thermoelastic regime is approximately ≅19 MW/cm^2 for aluminum [16]. The aluminum has the laser energy absorption coefficient of approximately 10 percent [15]. Typical material and thermal properties, at room temperature, of the aluminum in this study are included in Table 4.2.

The characteristics of an ultrasonic waveform predicted by the finite difference program at the epicenter of a 10 mm thick aluminum plate are shown in Figure 5.2. Well defined longitudinal and shear arrival times are exhibited. The first arrival time at approximately ≅1.6 μs corresponds to the direct longitudinal wave. The direction of the displacement is toward the

source. The second arrival time at approximately ≅3.3 μs corresponds to the direct shear wave. The amplitude of the longitudinal wave is considerably shorter compare to the amplitude of shear wave. This suggests that the ultrasonic source created by the thermoelastic generation mechanism in metals [15] contains a large shear wave component.

In comparison, the numerically predicted waveform at the epicenter of the aluminum plate, Figure 5.2, is in reasonable agreement with the experimentally measured waveform, Figure 5.3. These epicenter waveforms are similar to those obtained in the literature [12,14,15,20,22] by other researchers.

The ultrasonic waveform predicted analytically-numerically for the observation point at the epicenter from a laser pulse of 0.9 mJ energy impacted on a 10 mm thick graphite/epoxy composite plate is shown in Figure 5.4. The laser beam characteristics used in the numerical analysis have typical values of 20 ns pulse duration, 2 mm incident beam aperture with the estimated incident energy density of approximately ≅0.028 J/cm^2 and the estimated incident power density of approximately ≅1.4 MW/cm^2. This value for the incident laser energy density is considerably below the threshold for damage and it falls within the thermoelastic regime. The estimated damage threshold laser energy density for the thermoelastic regime is approximately ≅0.070 J/cm^2 for the graphite/epoxy [58]. Typical material and thermal properties, at room temperature, of the graphite/epoxy composite in this study are included in Table 4.1.

While it is tempting to try to simply describe the observed material response it is important to remember that the source does not generate a collection of pure wave modes. Furthermore the disturbance that is created is finite, and is propagating inside a finite piece of oriented material. The predicted ultrasonic waveform in Figure 5.4 exhibits changes at both the longitudinal and shear wave mode arrival times. The disturbance arrival time, at approximately ≅1.1 μs, corresponds to a longitudinal wave mode propagated

directly from the ultrasonic source. The direction of the displacement is negative implying the epicenter surface of the plate is depressed inwards, toward the source. The direct shear arrival time is about five times greater than the direct longitudinal arrival. The arrival time for a shear wave mode propagated directly from the ultrasonic source is approximately ≅5.3 μs. The shear mode is preceded by a simple pulse suspected to be the first reflection of longitudinal wave off the bottom surface then off the top surface of the plate.

Since the path of the wave propagation can be measured on the plate (i.e. plate thickness) and its propagation time from the predicted waveform, one is able to predict the wave speeds for the longitudinal and shear waves of about ≅9091 m/s^2 and ≅1887 m/s^2 respectively. The wave speeds are in accordance with the published ones.

To validate the predicted results, an experimental investigation was undertaken. An experimentally measured ultrasonic waveform is shown in Figure 5.5. The salient features of both the numerically predicted waveform and the experimentally measured waveform at the epicenter are obtained. Changes in features of the experimental waveform occur at times that correspond to those observed in the predicted waveform within 2%.

To examine the reproducibility of the PLUG in fiber reinforced graphite/epoxy composite plate, a sample of 15 wave forms showed almost exact duplicate of one another. The average amplitude of the 15 waveforms versus time, Figure 5.6, when compared to the waveform in Figure 5.5 showed no noticeable differences in the shape and amplitude of the waveform. The r.m.s. error on the ultrasonic amplitude of the 15 waveforms was less than 5 percent. This error was suspected to be from either a combination of digitizing errors or slight shot to shot variation in laser energy, or both.

In a further study, the effect of changing the laser pulse energy on the measured ultrasonic waveform in the graphite/epoxy composite plate was also investigated. Figure 5.7 shows that increasing the laser energy causes the amplitude of the feature appearing to be related to the arrival of a longitudinal

wave mode to increase, however the amplitude of the feature related to the arrival of the shear wave mode is almost unchanged. The variation of the measured amplitude of the feature appearing to be related to the arrival of a longitudinal wave mode as a function of the laser pulse energy is shown in Figure 5.8. It is interesting to note that the data points in Figure 5.8 appear to have rather increasing parabolic trend than linear. However the predicted amplitude of the feature appearing to be related to the arrival of a longitudinal wave mode increases linearly, as shown in Figure 5.9, with the laser energy. The reason for the discrepancy is probably due to the oversimplified assumption in the analytical model. The heat from the thermal source (i.e. the incident irradiated disk-like thermal source) is being conducted away into the bulk even during the extremely short lifetime of the laser pulse. The total incident laser power density depends on both the laser pulse energy and the duration time of the pulse. The laser unit, in general, increases the laser energy and pulse duration simultaneously in order to produce the higher power density. Increasing the pulse width gives more time for the heat to conduct away into the bulk from the heat source. Obviously this causes the temperature of the irradiated surface not to reach the value predicted for ‘no heat conduction’ in both analytical model and experimental analysis.

To further explain the above effects we wish to compute and plot the profile of the rise in temperature at the front surface of the heat source as a function of time. For the purpose of our study here, it is appropriate to consider a 1-D heat conduction equation along z direction. Let I_o be denoted as the absorbed laser heat flux density (i.e. laser power density). The laser pulse here is approximated to be a rectangular pulse switched on at $t = 0$ and off at $t = t_p$ where t_p is denoted as pulse duration width. The temperature profile at any time t, according to Carslaw and Jaeger [59] heat conduction, is derived by Scruby and Drain [15] and Ready [60] for a rectangular pulse,

$$T(z,t) = \frac{2I_o\sqrt{\kappa t}}{K}\,\mathrm{ierfc}\left(\frac{z}{2\sqrt{\kappa t}}\right)u(t) - \frac{2I_o\sqrt{\kappa (t-t_p)}}{K}\,\mathrm{ierfc}\left(\frac{z}{2\sqrt{\kappa (t-t_p)}}\right)u(t-t_p) \tag{5.1}$$

where

$$\mathrm{ierfc}(\xi) = \frac{1}{\sqrt{\pi}}e^{-\xi^2} - \frac{2\xi}{\sqrt{\pi}}\int_{\xi}^{\infty} e^{-\xi^2}\,d\xi \tag{5.2}$$

Letting z = 0 gives the temperature rise at the front surface

$$T(0,t) = \frac{2I_o\sqrt{\kappa t}}{K\sqrt{\pi}}u(t) - \frac{2I_o\sqrt{\kappa (t-t_p)}}{K\sqrt{\pi}}u(t-t_p) \tag{5.3}$$

K and κ are thermal conductivity and thermal diffusivity respectively.

Figure 5.10 shows the temperature profile obtained from equation (5.3) as a function of time for values of laser pulse energy input ranging from 0.5 mJ to 2.5 mJ while the pulse duration is kept constant at 20 ns. The front surface temperature rises almost instantaneously to its maximum during the pulse width and as a result little or no heat is conducted into the bulk. Once the laser pulse ends, the temperature falls as heat is conducted into the bulk. It is shown that increasing the laser energy increases the maximum front surface temperature with no noticeable changes on the temperature profile.

Figure 5.11 shows the different temperature profiles obtained from equation (5.3) as a function of time when the pulse duration is given values ranging from 10 ns to 50 ns while the laser pulse energy input is kept constant at 1 mJ. The front surface temperature requires a longer time to reach its maximum value for a longer pulse width. Thus the heat starts conducting away into the bulk before the maximum temperature is reached. As a result the maximum temperature is considerably lower.

Figures 5.12 and 5.13 show the relationship between the peak temperature, obtained from Figures 5.10 and 5.11 respectively, and the laser pulse power density input. In the case of constant pulse width, there exists a

direct linear relationship between the peak temperature and the laser power density, while the relationship is parabolic for constant laser energy. The shape of the laser pulse (pulse width and amplitude) together determines the peak temperature and the point in time at which it is reached. This peak value and when it occurs affects the amplitude of the stress waves generated.

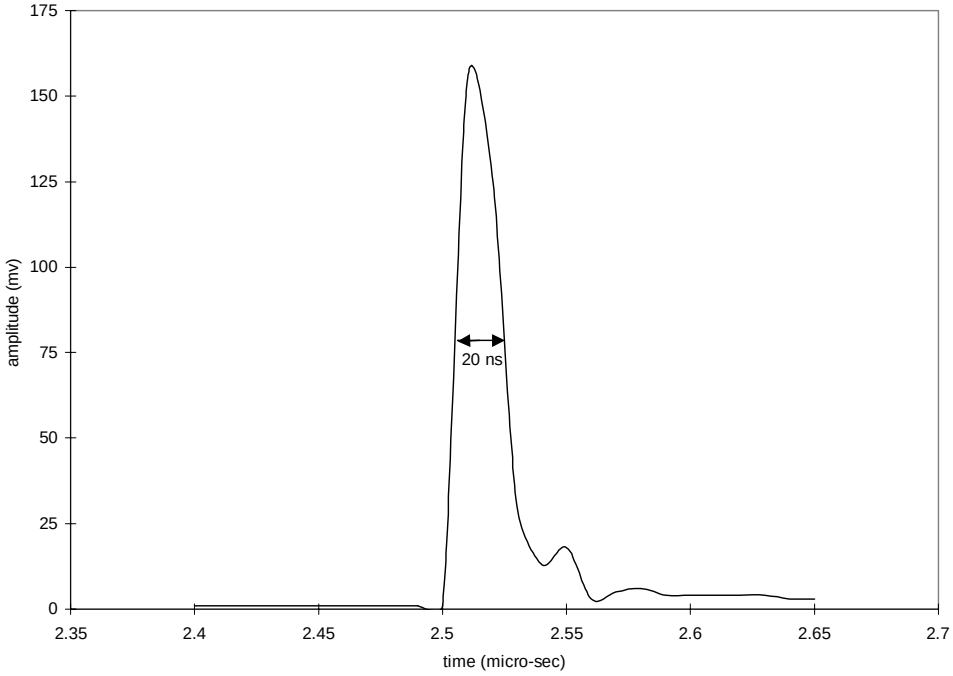

Figure 5.1. Temporal profile of Nd:YAG laser pulse.

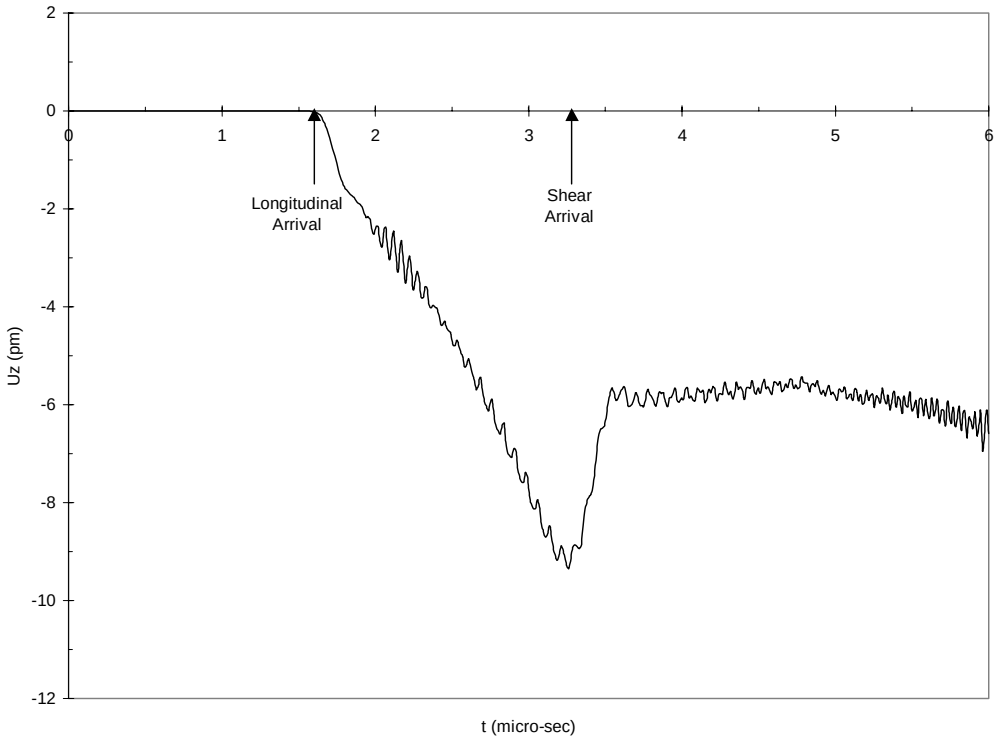

Figure 5.2. Predicted ultrasonic waveform at the epicenter in aluminum sample.

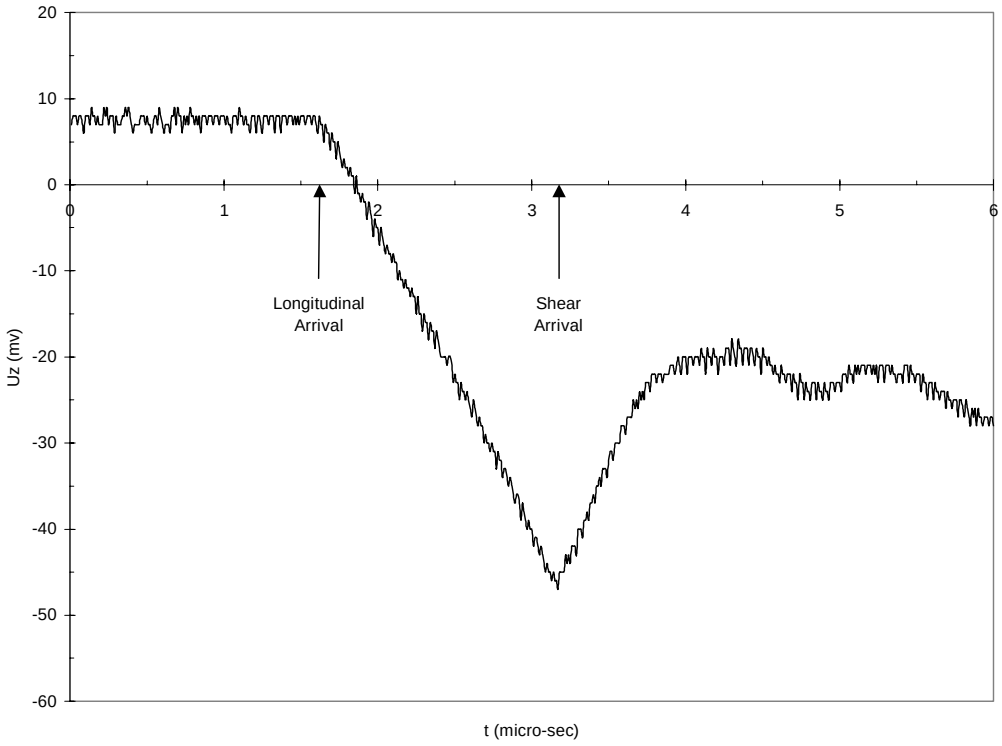

Figure 5.3. Measured ultrasonic waveform at the epicenter in aluminum sample.

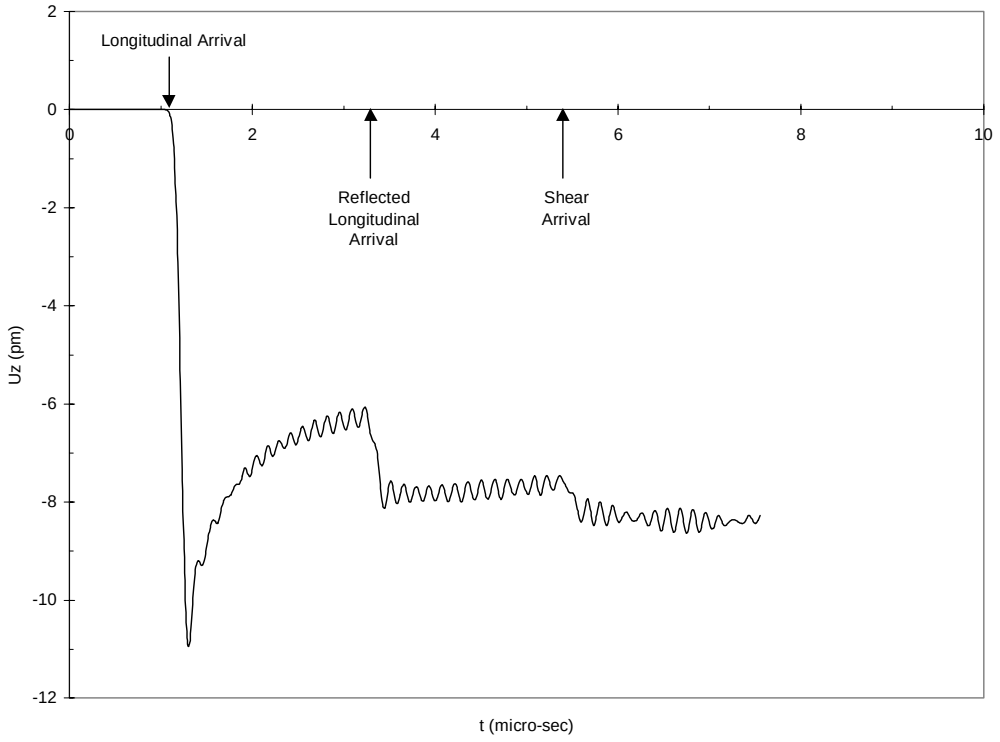

Figure 5.4. Predicted ultrasonic waveform at the epicenter in graphite/epoxy composite sample.

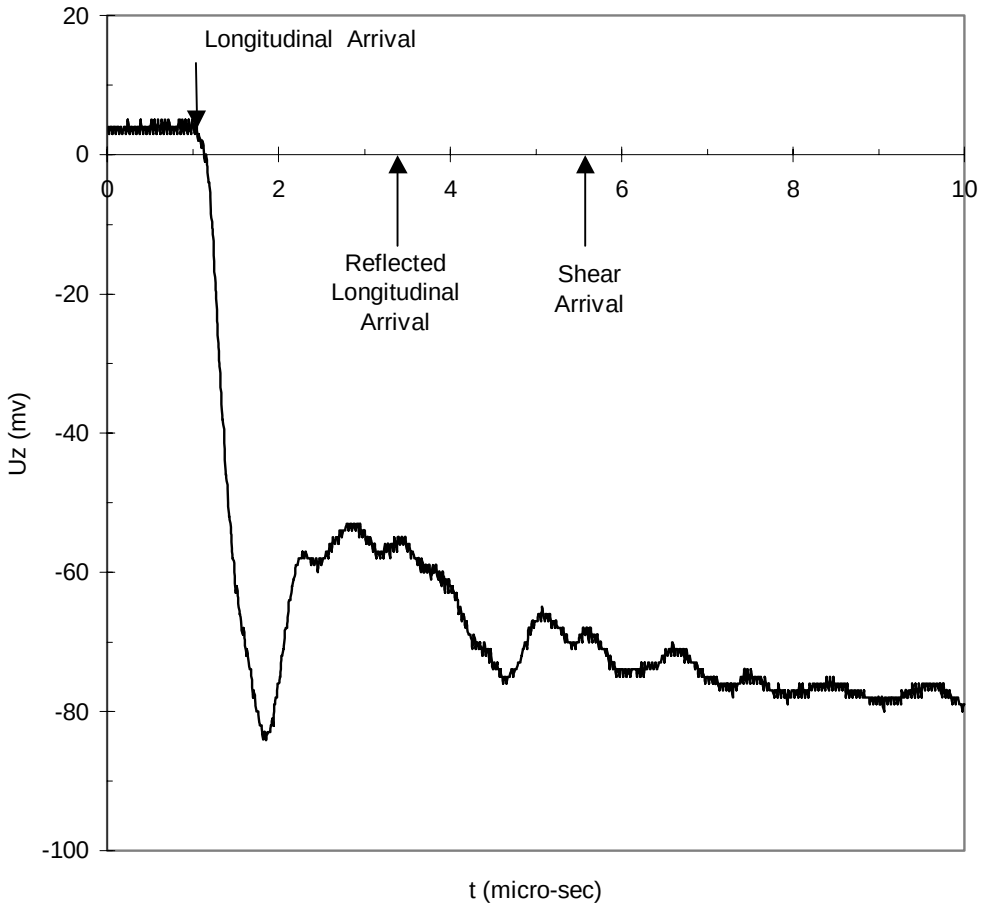

Figure 5.5. Measured ultrasonic waveform at the epicenter in graphite/epoxy composite sample.

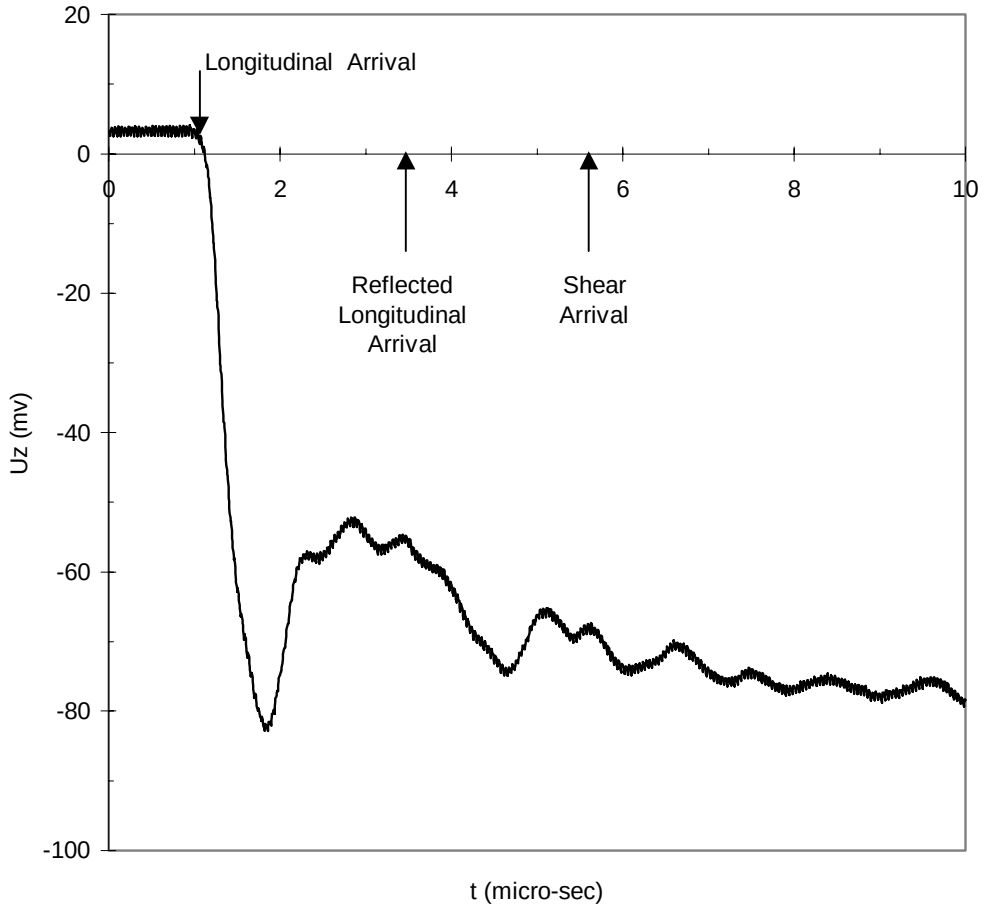

Figure 5.6. Average of 15 measured ultrasonic waveform at the epicenter in graphite/epoxy composite sample.

(a)

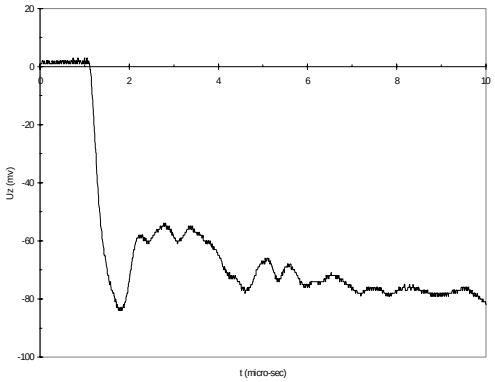

(b)

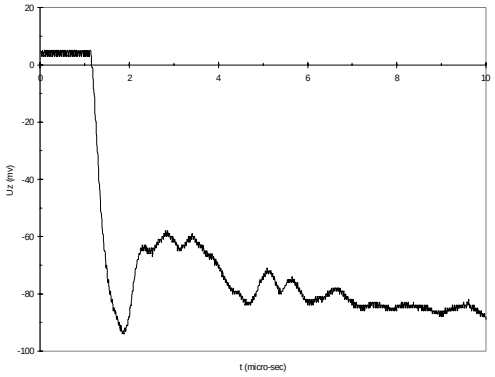

(c)

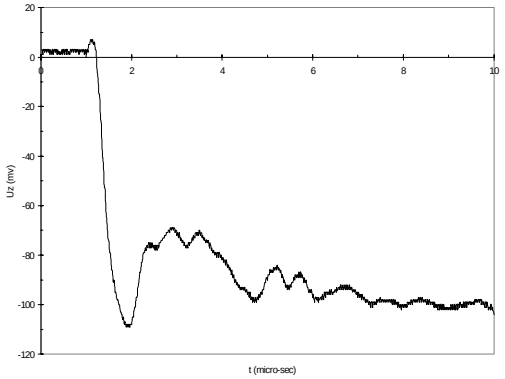

Figure 5.7. Effect of laser energy increase on amplitude of ultrasonic waves in graphite/epoxy composite, (a) 0.9 mJ; (b) 1.2 mJ; (c) 1.8 mJ.

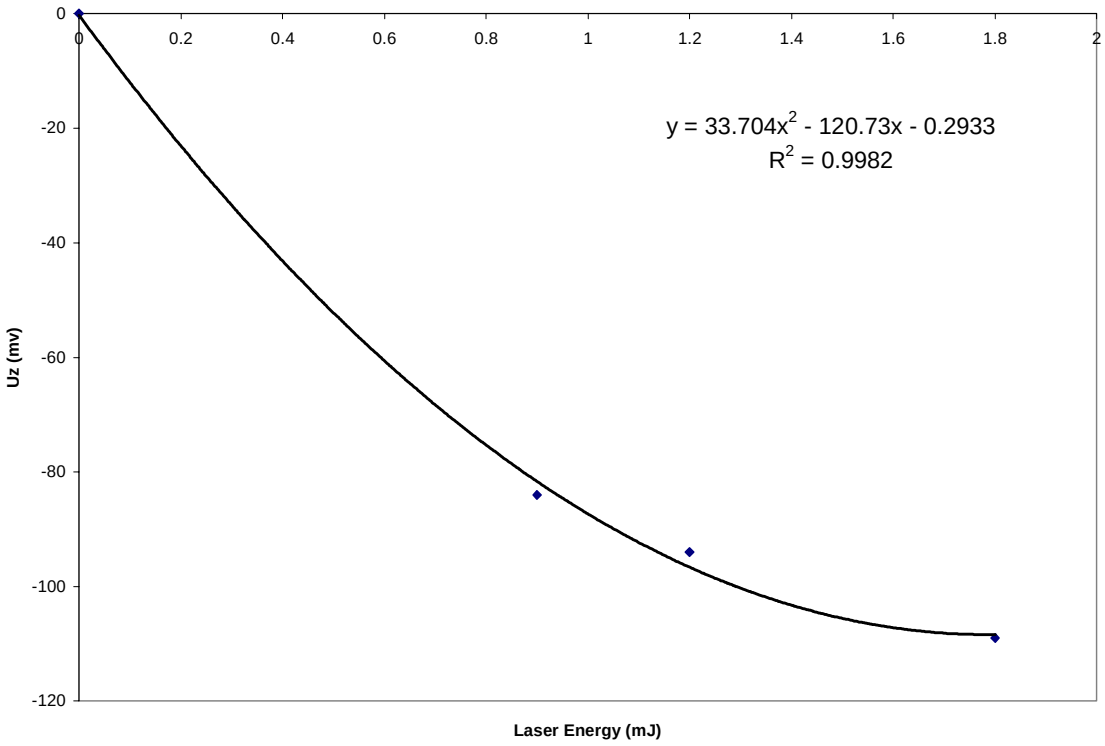

Figure 5.8. Relationship between laser energy and measured amplitude of ultrasonic waves in graphite/epoxy composite.

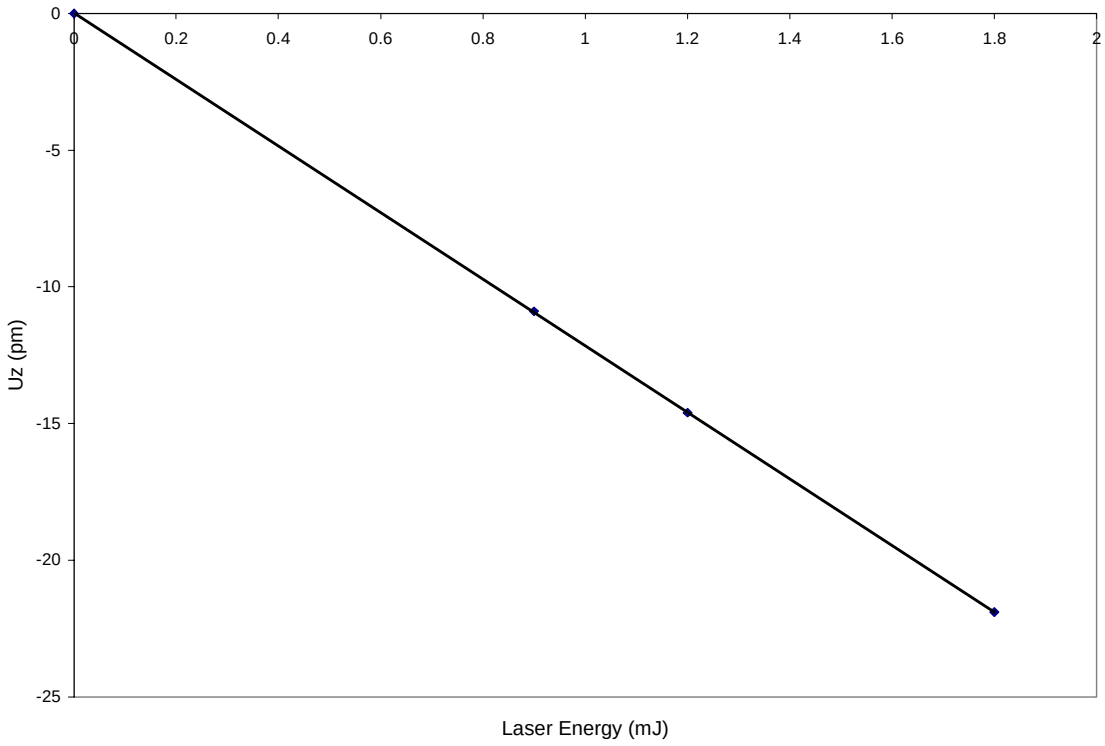

Figure 5.9. Relationship between laser energy and predicted amplitude of ultrasonic waves in graphite/epoxy composite.

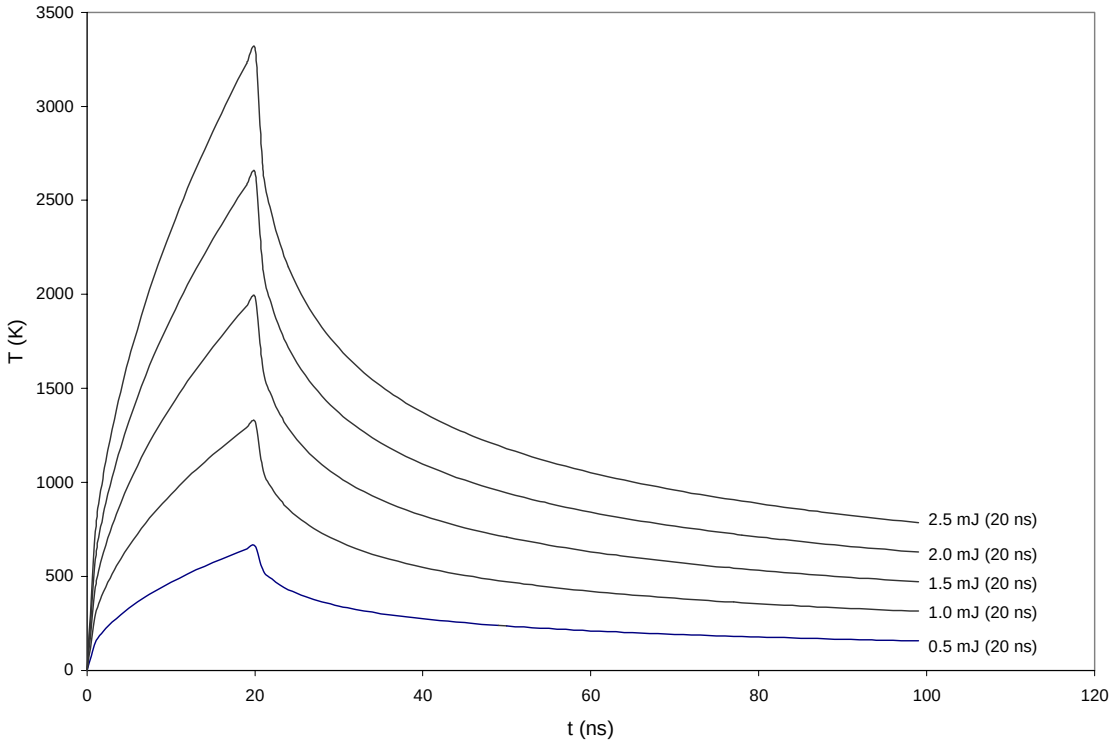

Figure 5.10. Front surface temperature profile of heat source in graphite/epoxy composite in response to an increase in incident laser energy with constant pulse width

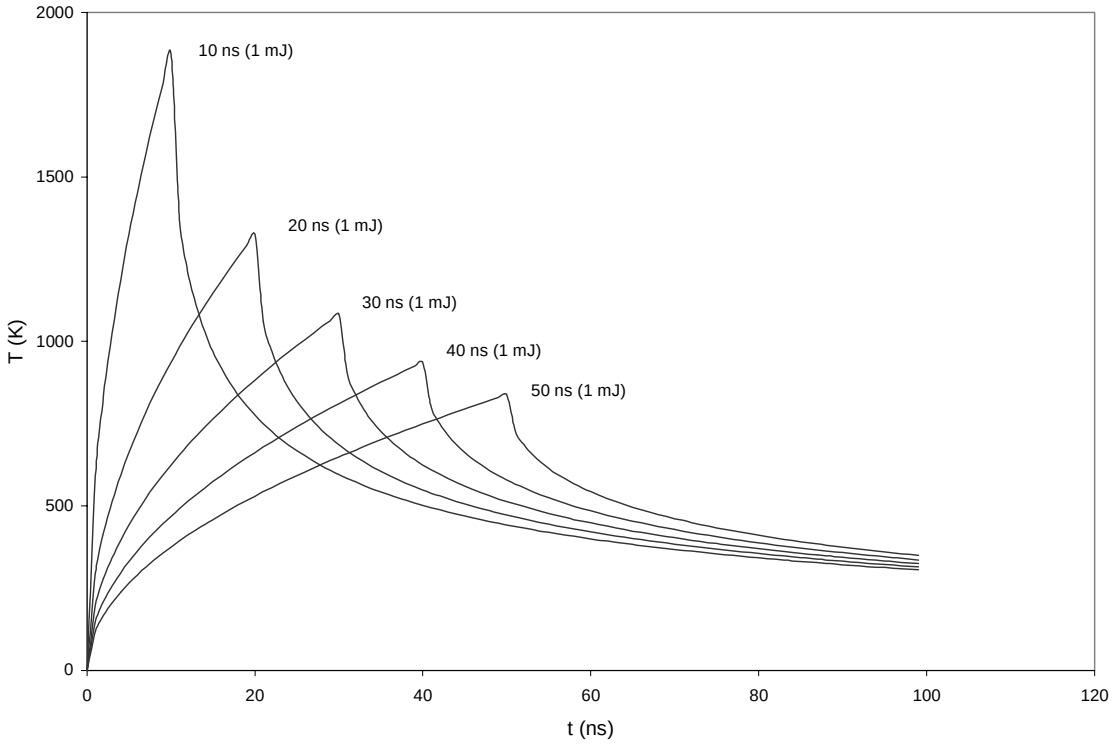

Figure 5.11. Front surface temperature profile of heat source in graphite/epoxy composite in response to an increase in incident laser pulse width with constant laser energy

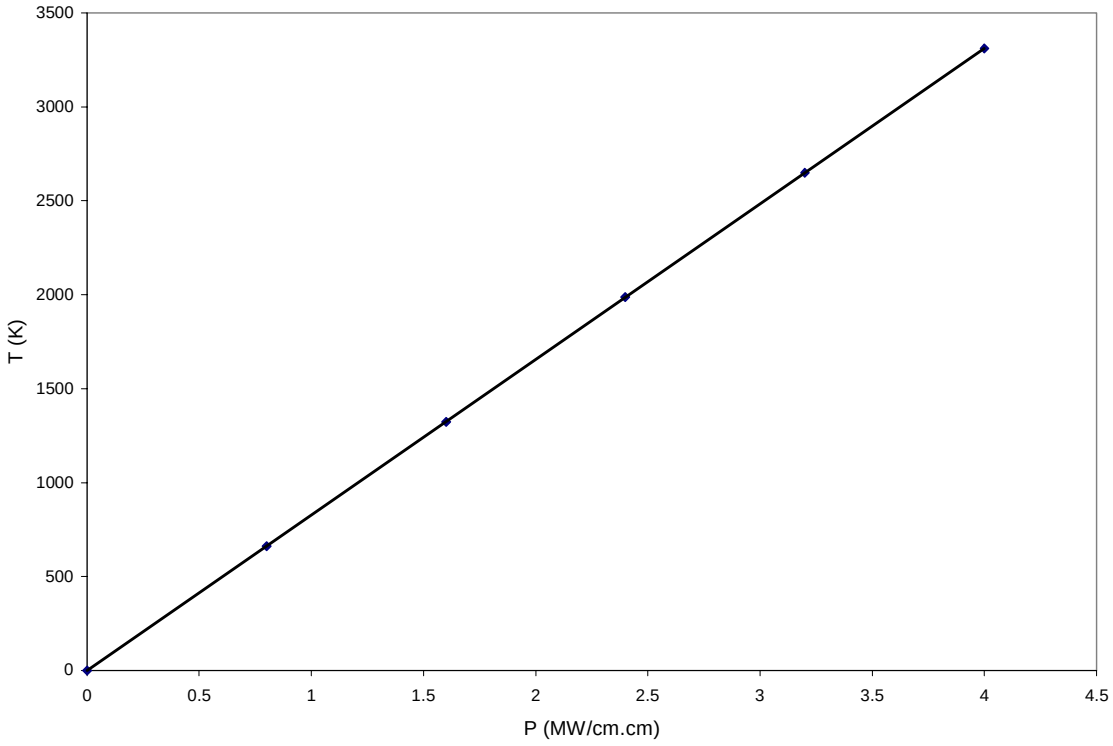

Figure 5.12. Relationship between maximum temperature rise of the front surface of the heat source and the incident laser power density in graphite/epoxy composite in response to an increase in incident laser energy with constant pulse width

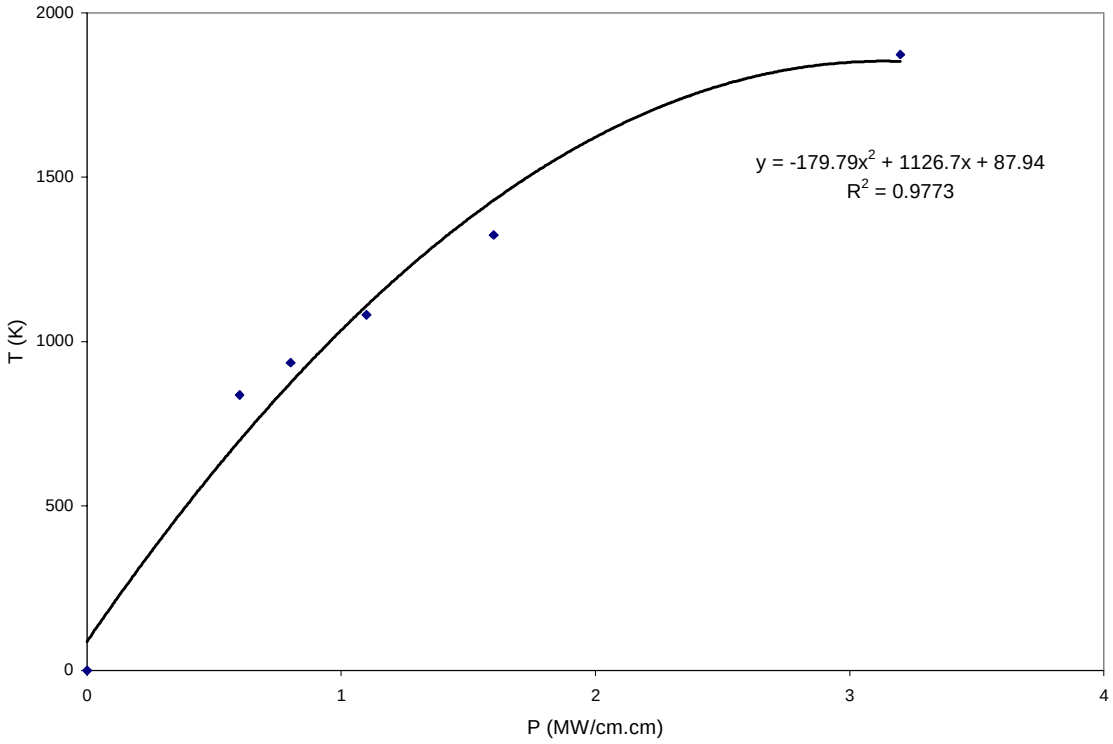

Figure 5.13. Relationship between maximum temperature rise of the front surface of the heat source and the incident laser power density in graphite/epoxy composite in response to an increase in pulse width with constant laser energy

CHAPTER 6

CONCLUSIONS

It has been demonstrated both experimentally and analytically that remotely generating ultrasonic waves in fiber reinforced graphite/epoxy composite material is feasible by PLUG from a Q-switched Nd:YAG laser pulse with a wave length of 1.06 μm. A practical analytical model for the PLUG in transversely isotropic fiber-reinforced composite material is derived using elastodynamics theories. The seismic reciprocity principle is invoked to determine a representation for the displacements in terms of the characteristics of the source strength known as the moment density tensor. The displacement at the epicenter are quite well predicted from a disk-like thermoelastic source model and elastodynamic calculations by Green's function. To obtain the Green's functions for a finite plate (transversely isotropic material), a finite difference program has been developed which simulates two dimensional ultrasonic wave propagation. The analysis confirms that the radially oriented dipolar forces are the predominant cause of disturbance in the interaction of the laser and the fiber reinforced graphite/epoxy composite material. Moreover we have been able to show and to conclude the following in fiber-reinforced composite material:

- the laser pulse is an ultrasonic source in composite material

- the radially oriented dipolar forces are the predominant cause of disturbance in the fiber-reinforced graphite/epoxy composite material
- thermoelastic generation mechanism is the dominant source of generating strong longitudinal waves
- the experimentally generated ultrasonic waveforms were found to be highly reproducible in shape, amplitude and wave speed measurements
- there exist a parabolic relationship between the incident laser energy and the amplitude of ultrasonic waves
- the predicted and the measured result are in agreement
- PLUG is essentially a nondestructive technique and it is applicable to metals and nonmetals.

The present study needs to be extended to a more general anisotropic, non-homogeneous materials. There is a need for more rigorous theoretical analysis and experimental investigation to be conducted to better understand both the interaction of electromagnetic radiation with non-metallic and the conversion of heat transfer into the mechanical energy to be able to knowledgeably exploit the capabilities of this method for nondestructive evaluation of fiber-reinforced composite materials.

BIBLIOGRAPHY

1. Bell, A. G., Philosophical Magazine, Vol. 11, 1881, pp. 510-528.

2. White, R. M., Journal of Applied Physics, Vol. 34, 1963, pp. 3559-3567.

3. Askar'yan, A., A. M. Prokhorov, G. F. Chanturiya, and M.P. Shipulo, Soviet Physics, JETP 17, 1963, pp. 1463-1465.

4. Ready, J. F., Journal of Applied Physics, Vol. 36, 1965, pp. 462-468.

5. Gournay, L. S., Journal of the Acoustical Society of America, Vol. 40, 1966, pp. 1322-1330.

6. Jones, E. D., Applied Physics Letter, Vol. 18, 1971, pp. 33-35.

7. O'Keefe, J. D., and C. H. Skeen, Applied Physics Letter, Vol. 21, 1972, pp. 464-466.

8. Lee, R. E., and R. M. White, Applied Physics Letter, Vol. 12, 1968, pp. 12-15.

9. Ledbetter, H. M., and J. C. Moulder, Journal of the Acoustical Society of America, Vol. 65, 1979, pp. 840-842.

10. Calder, C. A., and W. W. Wilcox, Materials Evaluation, January 1980, pp. 86-91.

11. Calder, C. A., and W. W. Wilcox, in Characterization of Materials for Service at Elevated Temperatures, ed. G. V. Smith, ASME, MPC-7, 1978, pp.169-181.

12. Scruby, C. B., R. J. Dewhurst, D. A. Hutchins, and S. B. Palmer, in Research Techniques in Nondestructive Testing, ed. R. S. Sharpe, Vol. 5, 1982, Academic Press, New York, NY.

13. Hutchins, D. A., Canadian Journal of Physics, Vol. 64, 1986, pp. 1247-1264.

14. Hutchins, D. A., in Physical Acoustics, ed. W. P. Mason, Vol. 18, 1987, pp. 21-118.

15. Scruby, C. B., and L. E. Drain, Laser Ultrasonics, 1990, Adam Hilger, Bristol, England.

16. Aindow, A. M., R. J. Dewhurst, D. A. Hutchins, and S. B. Palmer, Journal of the Acoustical Society of America, Vol. 69, No. 2, February 1981, pp. 449-455.

17. Fairand, B. P., and A.H. Clauer, Optical Communications, Vol. 18, No. 4, 1976, pp. 588-591.

18. Gutfeld Von, R. J., and R. L. Melcher, Applied Physics Letter, Vol. 30, No. 6, 1977, pp.257-259.

19. Dewhurst, R. J., D. A. Hutchins, S. B. Palmer, and C. B. Scruby, Journal of Applied Physics, Vol. 53, No. 6, 1982, pp. 4064-4071.

20. Scruby, C. B., R. J. Dewhurst, D. A. Hutchins, and S. B. Palmer, Journal of Applied Physics, Vol. 51, No. 12, 1980.

21. Sinclair, J. E., Journal of Physics D:, Vol. 12, 1979, pp. 1309-1315.

22. Rose, L. R. F., Journal of the Acoustical Society of America, Vol. 75, No. 3, 1984, pp. 723-732.

23. Wadley, H. N. G., J. A. Simmons, and C. Turner, in Review of Progress in Quantitative Nondestructive Evaluation, ed. D. O. Thompson and D. E. Chimenti, Vol. 3B, 1984, pp. 683-697, Plenum Press, New York, NY.

24. Doyle, P. A., Journal of Physics D:, Vol. 19, 1986, pp. 1613-1623.

25. Aussel, J. D., A. LeBrun, and J. C. Baboux, Ultrasonics, Vol.26, 1988, pp. 245-255.

26. Keck, R., and K. H. Mommertz, Japan Journal of Applied Physics, 1986, pp. 385-394.

27. Bar-Cohen, Y., British Journal of Nondestructive Testing, March 1979, pp. 76-78.

28. Calder, C. A., and W. W. Wilcox, Review of Scientific Instruments, Vol. 45, No. 12, December 1974, pp. 1557-1559.

29. Wilcox, W. W., and C. A. Calder, Instrumentation Technology, Vol. 25, No. 8, August 1978, pp. 63-68.

30. Aharoni, A., K. M. Jassby, and M. Tur, Journal of the Acoustical Society of America, Vol. 92, No. 6, 1992, pp.3249-3258.

31. Jen, C., P. Cielo, and X. Maldague, Journal of the American Ceramic Society, Vol. 68, No. 6, 1985, pp. 146- 148.

32. McKie, A. D. W., and R. C. Addison, Jr., Nondestructive Characterization for Advanced Technologies, ASNT Spring Conference, March 18-22, 1991, pp. 39-41.

33. Cielo, P., International Advances in Nondestructive Testing, Vol. 11, 1985, pp. 175-217.

34. Cielo, P., G. Rouset, L. Bertrand, and E. P. Pardinson, Canadian Aeronautics and Space Journal, Vol. 33, No. 3,1987, pp. 125.

35. Sarrafzadeh, A., R. J. Churchill, and M. G. Niimura, in Acousto-Ultrasonics: Theory and Application, ed. J. C. Duke, Jr., 1988, pp. 201-207, Plenum Press, New York, NY.

36. Burger, C. P., T. D. Dudderar, J. A. Gilbert, B. R. Peters, and J. A. Smith, Journal of Nondestructive Evaluation, Vol. 6, 1987, pp. 57-64.

37. Boyd, I. W., Laser Processing of Thin Films and Microstructures, 1987, Springer-Verlag, New York, NY.

38. Allmen, M. von, Laser-Beam Interactions with Materials, Physical Principles and Applications, 1987, Springer-Verlag, New York, NY.

39. Gorodetsky, G., T. G. Kazyaka, R. L. Melcher, and R. Srinivasan, Applied Physics Letter, Vol. 46, No. 9, 1985, pp. 828-830.

40. Garrison, B. J., and R. Srinivasan, Journal of Applied Physics, Vol. 57, No. 8, 1985, pp. 2909-2914.

41. Cozzens, R. F., and R. B. Fox, Polymer Engineering and Science, Vol. 18, No. 11, 1978, pp. 900-904.

42. Bauerle, D., Chemical Processing with Lasers, 1986, Springer-Verlag, New York, NY.

43. Duley, W. W., Laser Processing and Analysis of Materials, 1984, Plenum Press, New York, NY.

44. Charschan, S. S., Lasers in Industry, 1972, Van Nostrand Reinhold Company, New York, NY.

45. Plonus, M. A., Applied Electromagnetics, 1978, McGraw-Hill, New York, NY.

46. Bleaney, B. I., and B. Bleaney, Electricity and Magnetism, 1976, Oxford University Press, Ely House, London.

47. Eringen, A. C., Suhubi, E. S., Elastodynamics, 1975, Academic Press, New York, NY.

48. Aki, K., and G. Richards, Quantitative Seismology, 1980, Freeman, San Francisco, CA.

49. Ben-Menahem, A. and Singh, S. J., Seismic Waves and Sources, Springer-Verlag, New York, NY.

50. Lamb, Jr., G. L., Introductory Applications of Partial Differential Equations; with Emphasis on Waves Propagation and Diffusion, 1995, John Wiley & Sons, Inc., New York, NY.

51. Mei, C. C., Mathematical Analysis in Engineering; How to Use Basic Tools, 1995, Cambridge University Press, New York, NY.

52. Moller, K. D., Optics, University of Science Books, 1988, Mill Valley, CA.

53. Hirsch, C., Numerical Computation of Internal and External Flows, 1988, John Wiley & Sons, Inc., New York, NY.

54. Fukunaga, Y., Enoki, M., Kishi, T., Kihara, J., Journal of Vibrations and Acoustics, Vol. 112, 1990, pp. 45-52.

55. Fuyuki, M. and Matsumoto, Y., Bulletin of the Seismological Society of America, Vol. 70, pp. 1980, 2051-2069.

56. Wu, T. T., Kuo, C. L., Journal of Vibration and Acoustics, Vol. 113, October 1991, pp. 551-557.

57. Proctor, Jr., T. M., Journal of the Acoustic Society of America, Vol. 71, 1982, pp. 1163-1168.

58. Kautz, H. E., NASA Technical Memorandum TM-101299.

59. Carslaw, H. S., Jaeger, J. C., Conduction of Heat in Solids, 1959, Oxford University Press, London.

60. Ready, J. F., Effects of High-Power Laser Radiation, 1971, Academic Press, New York, NY.

61. Willis, J. R., Simmons, J.A. and Hsu, N. N., U.S. Department of Commerce, National Bureau of Standards.

62. Hsu, N. N., U.S. Department of Commerce, National Bureau of Standard, NBSIR 85-3234, November 1985.

63. Eitzen, D. G., Breckenridge, F. R., Clough, R. B., Fuller, E. R., Hsu, N. N. and Simmons, J. A., Department of Commerce, National Bureau of Standard, EPRI-NP-2089.

64. Page, J. D., The Industrial Graphite Engineering Handbook, 1991, UCAR Carbon Company Inc., Danbury, CT.

65. Kline, R. A., Nondestructive Characterization of Composite Media, 1992, Technomic Publishing Company, Inc., Lancaster, PA.

66. Lai, W. M., Rubin, D., Krempl, E., Introduction to Continuum Mechanics, 3rd Edition, 1993, Pergamon Press Inc., Tarrytown, NY.

67. Payton, R. G., Elastic Wave Propagation in Transversely Isotropic Media, 1983, Martinus Nijhoff Publishers.

68. Achenbach, J. D., Wave Propagation in Elastic Solids, 1973, North-Holland, New York, NY.

69. ASM International, Metals Handbook, Nondestructive Evaluation and Quality Control 9th Edition, Volume 17.

APPENDIX

```
C.. _____________________________________________________________
C.. This FORTRAN program computes the epicenter displacement as a
C.. function of time in linear, elastic, homogeneous both isotropic and
C.. transversely isotropic materials with axisymmetry.
C.. _____________________________________________________________

      PROGRAM PLUG
      COMMON /BLOCK1/ MATERIAL
      COMMON /BLOCK2/ C11, C12, C13, C33, C44
      COMMON /BLOCK3/ RO, TEXPR, TEXPZ, TDIF, TCONRR, SPHEAT
      COMMON /BLOCK4/ VL, VT
C.. ~~~~~~~~~~~~~~~~~~~~~~~~~~~~~~~~~~~~~~~~~~~~~~~~~~~~~~~~~~~~
C.. Sample = 1 (Isotropic), Sample = 2 (Composite)
      PARAMETER(Isample = 2)
C.. ~~~~~~~~~~~~~~~~~~~~~~~~~~~~~~~~~~~~~~~~~~~~~~~~~~~~~~~~~~~~
C.. THICK: Thickness, Q: Laser energy, DIAM: Beam aperture, ITRCO:Rise-time
C.. PULSDUR: Pulse-duration
      PARAMETER(THICK= 10., Q= 0.9, DIAM= 2., PULSDUR=20.E-09)
C.. ~~~~~~~~~~~~~~~~~~~~~~~~~~~~~~~~~~~~~~~~~~~~~~~~~~~~~~~~~~~~
C.. IROW=M=NRR*ICOL,  ICOL=N=NELZ+1,  ITIME=ITS, ITRCO=Force Rise Time
      PARAMETER(IROW = 202, ICOL = 101, ITIME = 800, ITRCO = 10)
      PARAMETER(LASER= 3, LOCR= 100, NRR= 2, NELZ= 100, ITS= 800)
C.. ~~~~~~~~~~~~~~~~~~~~~~~~~~~~~~~~~~~~~~~~~~~~~~~~~~~~~~~~~~~~
      PARAMETER(PICA = 1.0E-12, ONANO = 1.0E-09, OMICRO = 1.0E-06
     &, OMILI = 1.0E-03, PI= 3.1415926)
      CHARACTER*30 MATERIAL
C
      INTEGER*2 TMPYEAR, TMPMONTH, TMPDAY
      INTEGER*2 TMPHOUR, TMPMINUTE, TMPSECOND, TMPHUND
C
      DIMENSION A(0:IROW, -1:ICOL, -1:1)
      DIMENSION B(0:IROW, -1:ICOL, -1:1)

      IF(ISAMPLE .EQ. 2) THEN
C.. Composite Outputs Files
       OPEN (30, FILE = 'Comp.out')
       OPEN (31, FILE = 'Comp.stt')
       OPEN (33, FILE = 'CompEp.out')
       OPEN (39, FILE = 'CompSu.out')
C.. Call input data
```

```
      CALL TRANS(NRR, THICK, Q)
      ELSE
C.. Isotropic Outputs Files
      OPEN (30, FILE = 'Iso.out')
      OPEN (31, FILE = 'Iso.stt')
      OPEN (33, FILE = 'IsoEp.out')
      OPEN (39, FILE = 'IsoSu.out')
C.. Call input data
      CALL ISO1(NRR, THICK, Q)
      ENDIF

      NODZ = NELZ + 1
      NODR = NRR*NODZ
      NODTOT = (NODZ+2)*(NODR+1)
      ISIZE = NODTOT*3
      H = THICK*1.0E-03
      MEP = 0
      NEP = NODZ-1
      MSU = LOCR
      NSU = 0
      DELZ = H/NELZ
      NODERF = LASER
      NODEZF = 0
      DD = DIAM/10.
      AREA = 0.25*PI*DD**2
      DELT = DELZ / ((C33+C44)/RO)**0.5
      STCO = 9./10.
      TSTEP = STCO*DELT
      TRISE = ITRCO*TSTEP
      DZ = DELZ / H
      CTN = (C33/RO)**0.5/H
      DT = CTN*TSTEP
      ATD = TCONRR/(RO*SPHEAT)
      CMRR = ((C11+C12)*TEXPR+C13*TEXPZ)*(ATD/TCONRR)*Q*1.0E-03
      FR = CMRR/DD
      PO = Q*OMILI/PULSDUR
      ED = Q*1.0E-03/(AREA)
      PD = (ED/PULSDUR)/1.E06
      CNON = 1./(C33*H*H)
      TOT = CMRR*CNON
      STBLEF = VL*TSTEP/DELZ
      STBRIG = 1./((1.+(VT/VL)**2)**0.5)

      WRITE (30, 110) PO, DD, AREA, ED, PD, NODERF, NODEZF,THICK
     &,LOCR*DELZ*1000., NELZ, NODZ, NODR ,NODTOT, ISIZE, ITS, DELZ
```

```
     &, DELT, TSTEP, TRISE, DZ, DT, CMRR, FR, CNON, TOT, STBLEF
     &, STBRIG, STCO, ITRCO
  110  FORMAT (8X, 'Laser Power =', 10X, F15.2, 4X, '(W)' /
     &8X, 'Target Dia. =', 15X, F10.2, 4X, '(cm)' /
     &8X, 'Target Area =', 15X, F10.5, 4X, '(cm.cm)' /
     &8X, 'Energy Density =', 7X, F15.4, 4X, '(J/cm.cm)' /
     &8X, 'Power Density =', 8X, F15.2, 4X, '(MW/cm.cm)' /
     &8X, 'Source Node =', 17X, '(',I3,',',I3,')' //
     &8X, 'Long. & Trans. Wave Loc., z =', 2X, F5.2, 2X, '(mm)' /
     &8X, 'Rayleigh Surf. Wave Loc., r =', 2X, F5.2, 2X, '(mm)' //
     &8X, 'No. of Elements in Thickness =', I5 /
     &8X, 'No. of Nodes in Thickness =', 3X, I5 /
     &8X, 'No. of Nodes in Length =', 6X, I5 /
     &8X, 'Total Nodes =', 13X, I10 /
     &8X, 'Array Size =', 12X, I12, 4X, 'each,(2-arrays)' /
     &8X, 'No. of Time Steps =', 4X, I12 //
     &8X, 'Space Increment (DELZ) =', 5X, E15.5, 2X, '(m)' /
     &8X, 'DELT =', 23X, E15.5 , 2X, '(Sec.)' /
     &8X, 'Time Increment (TSTEP<DELT) =', E15.5 ,2X, '(Sec.)' /
     &8X, 'Rise Time (TRISE) =', 10X, E15.5, 2X, '(Sec.)' //
     &8X, 'Space Increment; (DZ, Non) =', 1X, E15.5 /
     &8X, 'Time Increment; (DT, Non) =', 2X, E15.5 //
     &8X, 'Mrr(CMrr) =', 18X, F15.5, 2X, '(N.m)' /
     &8X, 'Fr =', 25X, F15.5, 2X, '(N)' /
     &8X, 'Cnon =', 23X, E15.5, 2X, '(1/N)' /
     &8X, 'CMrr.Cnon =', 18X, E15.5, 2X, '(m)' //
     &8X, 'STBLEF =', 21X, E15.5 / 8X, 'STBRIG =', 21X, E15.5 //
     &8X, 'Stability Coef(STCO) =', 11X, F8.5 /
     &8X, 'Rise Time(ITRCO) =', 16X, I5, 4X, 'Time Step(TSTEP)' //)

      IF(STBLEF .GT. STBRIG) GO TO 8500

      TZ = (DT / DZ)**2
      CK1 = C11 / C33
      CK2 = C44 / C33
      CK3 = (C13 + C44) / C33
      CK4 = C13 / C33
      CK5 = C12 / C11
      CK6 = C13 / C11
      Y1 = CK1*TZ
      Y2 = CK2*TZ
      Y3 = CK3*TZ

C.. Set starting date & time
      KTMP = 0
```

```
      TMPHUND = 0
      WRITE(*,*) 'Program starting date & time'
      WRITE(30,*) 'Program starting date & time'
      WRITE(31,*) 'Program starting date & time'
      CALL GETDAT (TMPYEAR, TMPMONTH, TMPDAY)
      CALL GETTIM (TMPHOUR, TMPMINUTE, TMPSECOND, TMPHUND)
      CALL SHOWDATE (KTMP, TMPYEAR, TMPMONTH, TMPDAY)
      CALL SHOWTIME (KTMP, TMPHOUR, TMPMINUTE, TMPSECOND, TMPHUND)

      DO 1100 K = -1, 1
      DO 1100 I = 0, NODR
      DO 1100 J = -1, NODZ
       A(I,J,K) = 0.
       B(I,J,K) = 0.
 1100 CONTINUE

      TT = 0.
      BEP = 0.
      BSU = 0.
      WRITE(33, 121) TT, BEP
  121   FORMAT(2E20.8)
      WRITE(39, 122) TT, BSU
  122   FORMAT(2E20.8)

      KCOUNT = 0
      DO 2000 KI = 1, ITS

      IF(KI .EQ. KCOUNT+1) THEN
       KTMP = 1
       WRITE(*,*) 'KI =', KI
       WRITE(31,*) 'KI =', KI
       CALL GETDAT (TMPYEAR, TMPMONTH, TMPDAY)
       CALL GETTIM (TMPHOUR, TMPMINUTE, TMPSECOND, TMPHUND)
       CALL SHOWDATE (KTMP, TMPYEAR, TMPMONTH, TMPDAY)
       CALL SHOWTIME (KTMP, TMPHOUR, TMPMINUTE, TMPSECOND, TMPHUND)
       KCOUNT = KCOUNT+200
      ENDIF

      K = 0
      KP = K+1
      KN = K-1
      DO 2600 M = 0, NODR-1
      DO 2500 N = 0, NODZ-1
      IF(M .EQ. NODR-1 .AND. N .EQ. 0) GO TO 2700
      IF(M .EQ. NODR-1 .AND. N .EQ. NODZ-1) GO TO 2800
```

```
      IF (M .GT. 0) GO TO 2100

      A(M,N,KP) = 0.
      B(M,N,KP) = - B(M,N,KN)
     &+ 2.*(1. - 2*Y2 - TZ)*B(M,N,K)
     &+ 4.*Y2*B(M+1,N,K) + TZ*( B(M,N+1,K)+B(M,N-1,K) )
     &+ Y3*( A(M+1,N+1,K)-A(M+1,N-1,K) )

      IF(N .EQ. NEP) THEN
       TTE = KI*TSTEP
       BEP = B(M,N,KP)*TOT
       TTEO = TTE/OMICRO
       BEPP = BEP/PICA
       WRITE(33, 115) TTEO, BEPP
115    FORMAT(2E20.8)
      ENDIF
      GO TO 2500

2100  A(M,N,KP) = - A(M,N,KN)
     &+ ( 2.-(2.+(1./M**2))*Y1-2.*Y2 )*A(M,N,K)
     &+ (1.+0.5/M)*Y1*A(M+1,N,K) + (1.-0.5/M)*Y1*A(M-1,N,K)
     &+ Y2*( A(M,N+1,K)+A(M,N-1,K) ) + 0.25*Y3
     &* ( B(M+1,N+1,K)-B(M-1,N+1,K)-B(M+1,N-1,K)+B(M-1,N-1,K) )
      B(M,N,KP) = - B(M,N,KN)
     &+ 2.*(1.-Y2-TZ)*B(M,N,K) + (1.+0.5/M)*Y2*B(M+1,N,K)
     &+ (1.-0.5/M)*Y2*B(M-1,N,K) + TZ*( B(M,N+1,K)+B(M,N-1,K) )
     &+ (0.5/M)*Y3*( A(M,N+1,K)-A(M,N-1,K) ) + 0.25*Y3
     &* ( A(M+1,N+1,K)-A(M-1,N+1,K)-A(M+1,N-1,K)+A(M-1,N-1,K) )

      IF(M .EQ. NODERF .AND. N .EQ. NODEZF) THEN
       CD = (KI)*TSTEP
       H1 = CD - TRISE
       H2 = CD - 2.*TRISE
       IF (H2 .GT. 0.) GO TO 5500
       IF (H1 .GT. 0.) GO TO 5600
       F = (1./TRISE**2)*0.5*CD**2
       GO TO 1700
5500   F = (1./TRISE**2)*( 0.5*CD**2 - H1**2 + 0.5*H2**2 )
       GO TO 1700
5600   F = (1./TRISE**2)*( 0.5*CD**2 - H1**2 )
1700   A(M,N,KP) = A(M,N,KP) + H*F/(DIAM*OMILI)
      ENDIF

      IF(M .EQ. MSU .AND. N .EQ. NSU) THEN
       TTS = KI*TSTEP
```

```
      BSU = B(M,N,KP)*TOT
      TTSO = TTS/OMICRO
      BSUP = BSU/PICA
      WRITE(39, 117) TTSO, BSUP
117    FORMAT(2E20.8)
     ENDIF
     GO TO 2500

2700  A(M,N,KP) = - A(M,N,KN)
    &+ ( 2.-(2.+(1./M**2))*Y1-2.*Y2 )*A(M,N,K)
    &+ (1.+0.5/M)*Y1*A(M+1,N,K) + (1.-0.5/M)*Y1*A(M-1,N,K)
    &+ Y2*( A(M,N+1,K)+A(M,N-1,K) ) + 0.5*Y3
    &* ( B(M+1,N+1,K)-B(M+1,N,K)-B(M,N+1,K)+B(M-1,N-1,K)-B(M-1,N,K)
    &-B(M,N-1,K)+2.*B(M,N,K) )
     B(M,N,KP) = - B(M,N,KN)
    &+ 2.*(1.-Y2-TZ)*B(M,N,K) + (1.+0.5/M)*Y2*B(M+1,N,K)
    &+ (1.-0.5/M)*Y2*B(M-1,N,K) + TZ*( B(M,N+1,K)+B(M,N-1,K) )
    &+ (0.5/M)*Y3*( A(M,N+1,K)-A(M,N-1,K) ) + 0.5*Y3
    &* ( A(M+1,N+1,K)-A(M+1,N,K)-A(M,N+1,K)+A(M-1,N-1,K)-A(M-1,N,K)
    &-A(M,N-1,K)+2.*A(M,N,K) )
     GO TO 2500

2800  A(M,N,KP) = - A(M,N,KN)
    &+ ( 2.-(2.+(1./M**2))*Y1-2.*Y2 )*A(M,N,K)
    &+ (1.+0.5/M)*Y1*A(M+1,N,K) + (1.-0.5/M)*Y1*A(M-1,N,K)
    &+ Y2*( A(M,N+1,K)+A(M,N-1,K) ) + 0.5*Y3
    &* ( B(M+1,N-1,K)-B(M+1,N,K)-B(M,N-1,K)+B(M-1,N+1,K)-B(M-1,N,K)
    &-B(M,N+1,K)+2.*B(M,N,K) )
     B(M,N,KP) = - B(M,N,KN)
    &+ 2.*(1.-Y2-TZ)*B(M,N,K) + (1.+0.5/M)*Y2*B(M+1,N,K)
    &+ (1.-0.5/M)*Y2*B(M-1,N,K) + TZ*( B(M,N+1,K)+B(M,N-1,K) )
    &+ (0.5/M)*Y3*( A(M,N+1,K)-A(M,N-1,K) ) + 0.5*Y3
    &* ( A(M+1,N-1,K)-A(M,N-1,K)-A(M,N-1,K)+A(M-1,N+1,K)-A(M-1,N,K)
    &-A(M,N+1,K)+2.*A(M,N,K) )
2500  CONTINUE
2600  CONTINUE

     DO 4000 I = 0, NODR-2
      IF(I .EQ. 0) GO TO 4100

      J = 0
      A(I,J-1,KP) = A(I,J+1,KP) + B(I+1,J,KP) - B(I-1,J,KP)
      B(I,J-1,KP) = B(I,J+1,KP)
    & + CK4*( A(I+1,J,KP)-A(I-1,J,KP)+(2./I)*A(I,J,KP) )
```

```
      J = NODZ-1
      A(I,J+1,KP) = A(I,J-1,KP) - B(I+1,J,KP) + B(I-1,J,KP)
      B(I,J+1,KP) = B(I,J-1,KP)
     & - CK4*( A(I+1,J,KP)-A(I-1,J,KP)+(2./I)*A(I,J,KP) )
      GO TO 4000

4100   J = 0
      A(I,J-1,KP) = 0.
      B(I,J-1,KP) = B(I,J+1,KP) + 4.*CK4*A(I+1,J,KP)

      J = NODZ-1
      A(I,J+1,KP) = 0.
      B(I,J+1,KP) = B(I,J-1,KP) - 4.*CK4*A(I+1,J,KP)
4000  CONTINUE

     I = NODR-1
     DO 4200 J = 1, NODZ-2
      A(I+1,J,KP) = A(I-1,J,KP) - CK5*(2./I)*A(I,J,KP)
     & - CK6*( B(I,J+1,KP)-B(I,J-1,KP) )
      B(I+1,J,KP) = B(I-1,J,KP) - A(I,J+1,KP) + A(I,J-1,KP)
4200  CONTINUE

     I = NODR-1
     J = 0

     A(I,J-1,KP) = A(I,J+1,KP) + A(I-2,J+1,KP) - A(I-2,J-1,KP)
     &+ 2.*( B(I,J,KP)-B(I-2,J,KP) )
     B(I,J-1,KP) = B(I,J+1,KP) + B(I-2,J+1,KP) - B(I-2,J-1,KP)
     &+ CK4*2.*( (1.+2./I)*A(I,J,KP) - A(I-2,J,KP) )

     A(I+1,J,KP) = A(I-1,J,KP) - A(I+1,J+2,KP) + A(I-1,J+2,KP)
     &- CK6*2.*( B(I,J+2,KP)-B(I,J,KP) ) - CK5*(4./I)*A(I,J,KP)
     B(I+1,J,KP) = B(I-1,J,KP) - B(I+1,J+2,KP) + B(I-1,J+2,KP)
     &- 2.*( A(I,J+2,KP) - A(I,J,KP) )

     I = NODR-1
     J = NODZ-1

     A(I,J+1,KP) = A(I,J-1,KP) - A(I-2,J+1,KP) + A(I-2,J-1,KP)
     &- 2.*( B(I,J,KP)-B(I-2,J,KP) )
     B(I,J+1,KP) = B(I,J-1,KP) - B(I-2,J+1,KP) + B(I-2,J-1,KP)
     &- CK4*2.*( (1.+2./I)*A(I,J,KP) - A(I-2,J,KP) )

     A(I+1,J,KP) = A(I-1,J,KP) - A(I+1,J-2,KP) + A(I-1,J-2,KP)
     &- CK6*2.*( B(I,J-2,KP)-B(I,J,KP) ) - CK5*(4./I)*A(I,J,KP)
```

```
      B(I+1,J,KP) = B(I-1,J,KP) - B(I+1,J-2,KP) + B(I-1,J-2,KP)
     &- 2.*( A(I,J-2,KP)-A(I,J,KP) )

      DO 2900 M = 0,NODR-1
      DO 2900 N = 0,NODZ-1
       A(M,N,KN) = A(M,N,K)
       B(M,N,KN) = B(M,N,K)
       A(M,N,K) = A(M,N,KP)
       B(M,N,K) = B(M,N,KP)
       A(M,N,KP) = 0.
       B(M,N,KP) = 0.
2900  CONTINUE
      DO 2910 M = 0,NODR-1
       A(M,-1,K) = A(M,-1,KP)
       B(M,-1,K) = B(M,-1,KP)
       A(M,NODZ,K) = A(M,NODZ,KP)
       B(M,NODZ,K) = B(M,NODZ,KP)
       A(M,-1,KP) = 0.
       B(M,-1,KP) = 0.
       A(M,NODZ,KP) = 0.
       B(M,NODZ,KP) = 0.
2910  CONTINUE
      DO 2920 N = 0,NODZ-1
       A(NODR,N,K) = A(NODR,N,KP)
       B(NODR,N,K) = B(NODR,N,KP)
       A(NODR,N,KP) = 0.
       B(NODR,N,KP) = 0.
2920  CONTINUE
2000  CONTINUE
      GO TO 8502
8500  WRITE(30,8501)
8501  FORMAT('Error, Unstable')
8502  CONTINUE

C.. Program termination date & time
      KTMP = 0
      WRITE(*,*) 'Program termination date & time'
      WRITE(30,*) 'Program termination date & time'
      WRITE(31,*) 'Program termination date & time'
      CALL GETDAT (TMPYEAR, TMPMONTH, TMPDAY)
      CALL GETTIM (TMPHOUR, TMPMINUTE, TMPSECOND, TMPHUND)
      CALL SHOWDATE (KTMP, TMPYEAR, TMPMONTH, TMPDAY)
      CALL SHOWTIME (KTMP, TMPHOUR, TMPMINUTE, TMPSECOND, TMPHUND)

      END
```

```
C... MATERIAL PROPERTIES (Composite)
      SUBROUTINE TRANS(NRR, THICK, Q)

      COMMON /BLOCK1/ MATERIAL
      COMMON /BLOCK2/ C11, C12, C13, C33, C44
      COMMON /BLOCK3/ RO, TEXPR, TEXPZ, TDIF, TCONRR, SPHEAT
      COMMON /BLOCK4/ VL, VT
      CHARACTER*30 MATERIAL
      CHARACTER*30 FIBERE3, TRANSE1, SHEARG31
     &, POISSONV13, POISSONV12 , DENSITY, EXPANSIONR, EXPANSIONZ
     &, DIFFUSIVITY, CONDUCTIVITYR, SPECIFIC, UNIT

      OPEN (13, FILE = 'rgee.dat')
      READ (13,*)  MATERIAL, FIBERE3, EP, UNIT, TRANSE1, E, SHEARG31
     &, GP, POISSONV13, VP, POISSONV12, V, DENSITY, RO
     &, EXPANSIONR, TEXPR, EXPANSIONZ, TEXPZ, DIFFUSIVITY, TDIF
     &, CONDUCTIVITYR, TCONRR , SPECIFIC, SPHEAT
      CLOSE (13)

      G = E/(2.*(1.+V))
      S11 = 1./E
      S22 = S11
      S33 = 1./EP
      S12 = -V/E
      S13 = -VP/EP
      S23 = S13
      S44 = 1./GP
      S55 = S44
      S66 = 1./G

      SS= S11*S22*S33-S11*S23**2-S22*S13**2-S33*S12**2+2.*S12*S23*S13
      C11 = (S22*S33-S23**2)/SS
      C22 = (S33*S11-S13**2)/SS
      C33 = (S11*S22-S12**2)/SS
      C12 = (S13*S23-S12*S33)/SS
      C13 = (S12*S23-S13*S22)/SS
      C23 = (S12*S13-S23*S11)/SS
      C44 = 1./S44
      C55 = C44
      C66 = 1./S66

      VL = (C33/RO)**0.5
      VT = (C44/RO)**0.5
```

```
      VQL = (C11/RO)**0.5
      VQT1 = (C66/RO)**0.5
      VQT2 = (C44/RO)**0.5
      WIDTH = NRR*THICK

      WRITE(30, 105) MATERIAL, FIBERE3, EP, UNIT, TRANSE1, E
     &, SHEARG31, GP, POISSONV13, VP, POISSONV12, V
105   FORMAT(// 10X, A30 // 6X, A20, E15.5, 2X, A10 / 6X, A20, E15.5 /
     &6X, A20, E15.5 / 6X, A20, F10.3 / 6X, A20, F10.3 /)
      WRITE(30, 106) S11, S12, S13, S33, S44, S66
106   FORMAT (6X, 'S11 =', E15.5 /
     &6X, 'S12 =', E15.5 / 6X, 'S13 =', E15.5 /
     &6X, 'S33 =', E15.5 / 6X, 'S44 =', E15.5 /
     &6X, 'S66 =', E15.5 /)
      WRITE(30, 107) C11, C12, C13, C33, C44
     &, RO, THICK, WIDTH, EXPANSIONR, TEXPR, EXPANSIONZ, TEXPZ
     &, DIFFUSIVITY, TDIF, CONDUCTIVITYR, TCONRR, SPECIFIC, SPHEAT
     &, VL, VT, VQL, VQT1, VQT2, Q
107   FORMAT (6X, 'C11 =', E15.5, 2X, '(Pa)' /
     &6X, 'C12 =', E15.5 / 6X, 'C13 =', E15.5 /
     &6X, 'C33 =', E15.5 / 6X, 'C44 =', E15.5 //
     &8X, 'Density =', 20X, F10.2, 4X, '(Kg/m.m.m)' /
     &8X, 'Thickness =', 18X, F10.2, 4X, '(mm)' /
     &8X, 'Width =', 22X, F10.2, 4X, '(mm)' //
     &8X, A25, E15.5, 4X, '(1/F)'  /
     &8X, A25, E15.5, 4X, '(1/F)' /
     &8X, A25, E15.5, 4X, '(m.m/Sec)' /
     &8X, A25, F10.2, 9X, '(W/m.F)' /
     &8X, A25, F15.2, 4X, '(J/Kg.F)'  //
     &8X, 'Velocity(Long,z) =', 9X, F12.2, 4X, '(m/s)' /
     &8X, 'Velocity(Trans,z) =', 8X, F12.2, 4X, '(m/s)' //
     &8X, 'Velocity(Quasi-Long,r) =', 3X, F12.2, 4X, '(m/s)' /
     &8X, 'Velocity(Quasi-Trans-1,r) =', F12.2, 4X, '(m/s)' /
     &8X, 'Velocity(Quasi-Trans-2,r) =', F12.2, 4X, '(m/s)' //
     &8X, 'Laser Energy =', 12X, F12.2, 4X, '(mJ)' )
      END

      SUBROUTINE SHOWDATE(K, YEAR, MONTH, DAY)
      INTEGER*2 YEAR, MONTH, DAY
      IF(K .EQ. 1) THEN
       WRITE(31, 9001) MONTH, DAY, YEAR
       WRITE(*, 9001) MONTH, DAY, YEAR
      ELSE
       WRITE(30, 9001) MONTH, DAY, YEAR
       WRITE(31, 9001) MONTH, DAY, YEAR
```

```
      WRITE(*, 9001) MONTH, DAY, YEAR
     ENDIF
9001  FORMAT(4X, I2, '/', I2.2, '/', I4.4)
     END

     SUBROUTINE SHOWTIME(K, HOUR, MINUTE, SECOND, HUND)
     INTEGER*2 HOUR, THOUR, MINUTE, SECOND, HUND
     CHARACTER*2 AP
     IF (HOUR .GT. 12) THEN
      AP = 'PM'
      THOUR = HOUR - 12
     ELSE
      THOUR = HOUR
      AP = 'AM'
     ENDIF
     IF(K .EQ. 1) THEN
      WRITE(31, 9002) THOUR, MINUTE, SECOND, HUND, AP
      WRITE(*, 9002) THOUR, MINUTE, SECOND, HUND, AP
     ELSE
      WRITE(30, 9002) THOUR, MINUTE, SECOND, HUND, AP
      WRITE(31, 9002) THOUR, MINUTE, SECOND, HUND, AP
      WRITE(*, 9002) THOUR, MINUTE, SECOND, HUND, AP
     ENDIF
9002  FORMAT(4X, I2,':', I2.2, ':', I2.2, ':', I2.2, ' ', A5)
     END

C.. MATERIAL PROPERTIES (ISOTROPIC)
     SUBROUTINE ISO1(NRR, THICK, Q)
     COMMON /BLOCK1/ MATERIAL
     COMMON /BLOCK2/ C11, C12, C13, C33, C44
     COMMON /BLOCK3/ RO, TEXPR, TEXPZ, TDIF, TCONRR, SPHEAT
     COMMON /BLOCK4/ VL, VT
     CHARACTER*30 MATERIAL
     CHARACTER*30 DENSITY, EXPANSION, DIFFUSIVITY, CONDUCTIVITY
    &, SPECIFIC, YOUNG, POISSON, UNIT

     OPEN (11, FILE = 'al1e.dat')
     READ (11,*)  MATERIAL, YOUNG, E, UNIT, POISSON, V
    &, DENSITY, RO, EXPANSION, TEXP, DIFFUSIVITY, TDIF
    &, CONDUCTIVITY, TCON ,SPECIFIC, SPHEAT
     CLOSE (11)

     G = E/(2.*(1.+V))
     TEXPR = TEXP
     TEXPZ = TEXP
```

```
      TCONRR =TCON
      WIDTH = NRR*THICK

      C11 = ((1.-V)*E)/((1.+V)*(1.-2.*V))
      C12 = (V*E)/((1.+V)*(1.-2.*V))
      C44 = G
      C13 = C12
      C33 = C11

      VL = (C33/RO)**0.5
      VT = (C44/RO)**0.5

      WRITE(30,101) MATERIAL, YOUNG, E, UNIT, POISSON, V
101   FORMAT(// 14X, A30 // 8X, A5, E15.5, 4X, A10 / 8X, A5, F10.4 /)
      WRITE(30, 102) C11, C12, C13, C33, C44
     &, RO, THICK, WIDTH, TEXPR, TEXPZ, TDIF, TCONRR, SPHEAT
     &, VL, VT, Q
 102  FORMAT (12X, 'C11 =', E15.5, 2X, '(Pa)' /
     &12X, 'C12 =', E15.5 / 12X, 'C13 =', E15.5 /
     &12X, 'C33 =', E15.5 / 12X, 'C44 =', E15.5 //
     &8X, 'Density =', 19X, F10.2, 4X, '(Kg/m.m.m)' /
     &8X, 'Thickness =', 17X, F10.2, 4X, '(mm)' /
     &8X, 'Width =', 21X, F10.2, 4X, '(mm)' //
     &8X, 'Thermal Expansion(R) =', E15.5, 2X, '(1/F)'  /
     &8X, 'Thermal Expansion(Z) =', E15.5, 2X, '(1/F)' /
     &8X, 'Thermal Diffusivity =', E15.5, 3X, '(m.m/Sec)' /
     &8X, 'Thermal Conductivity(R) =', F10.2, 4X, '(W/m.F)' /
     &8X, 'Sp. Heat Capacity =', F15.2, 5X, '(J/Kg.F)'  //
     &8X, 'Velocity (Long.) =', 8X, F12.2, 2X, '(m/s)' /
     &8X, 'Velocity (Trans.) =', 7X, F12.2, 2X, '(m/s)' //
     &8X, 'Laser Energy =', 17X, F7.2, 4X, '(mJ)' )
      END
```

VITA

Mohammad Ali Rezaizadeh

The author was born in 1958 and grew up in Tabriz, Iran. After graduating from high school, he continued his education in the U.S.A. He received B.S. in Mechanical Engineering from the University of Missouri-Columbia and subsequently M.S. in Engineering Mechanics from the University of Missouri-Rolla. For few years he was employed as an instructor in the Engineering Mechanics department at the University of Missouri-Rolla. Later he moved to Blacksburg and pursued Ph.D. in Engineering Mechanics at Virginia Tech. During his Ph.D. residency at Virginia Tech he was constantly employed by Dr. John C. Duke, Jr. as a research assistant and/or by the ESM department as an instructor.